

Waterflood Efficiency and Single-Phase Flow Properties of Carbonate Porous Media

Shahram Pourmohammadi



University of Bergen

2009

Shahram Pourmohammadi

Centre for Integrated Petroleum Research

Department of Physics and Technology

University of Bergen

Alégaten 41, N-5007 Bergen

Norway

Thesis submitted for the degree Philosophiae Doctor

University of Bergen, June 2009

*To my dear wife Nikou, and my parents
who were my first teachers.*

PREFACE

This thesis submitted for the degree Philosophiae Doctor at the University of Bergen .The dissertation consists an introduction to the subject including theoretical background, four papers, and additional analysis beyond what was obtained in the papers. The research work has been done at the Center of Integrated Petroleum Research (CIPR) at the University of Bergen in the period of 2005-2008.

The thesis concerns experimental results on water flooding and single-phase flow properties for different carbonate materials. The results are compared to a new carbonate pore class system. The validity of the pore class system for single-phase and two-phase flow properties has been evaluated.

The first paper addresses the miscible displacement in carbonates with different pore classes and its influence on the waterflood efficiency of selected samples. The second paper explores variations in different single-phase flow properties of carbonate rocks with more measurements and more pore classes. The third paper discusses the influence of single-phase flow properties on waterflood efficiency. The last paper presents the effect of the wettability alteration from water-wet to mixed-wet state together with single-phase flow properties on waterflood efficiency for chalk materials.

ACKNOWLEDGMENTS

I would like to express my gratitude to my supervisors Professor Arne Skauge, Dr. Kristine Spildo, and senior researcher Sverre Hetland for giving me the opportunity to undertake this study and for excellent academic and professional guidance, advice, and support throughout the course of this work.

I wish to thank Dr. Ketil Djurhuus as a fellow during PhD studies at CIPR, and more importantly for NMR experiments, which strongly improved my study of carbonates. I would like to thank Per Arne Ormehaug and Asbjørn Spilde for help with different challenges in laboratory during this study.

I wish to acknowledge Norsk Hydro ASA (now StatoilHydro ASA) for financial support during this work. I would like to give my sincerely thanks to Arve Lønøy, who brought new insight and better understanding of carbonate pore classification. The research by Lønøy was the background for initialisation of the carbonate core analysis studies at CIPR and also this thesis.

Thanks to my fellow students and colleagues at the CIPR particularly in the administration section to provide a social environment and a friendly workplace. I specially thank the Almighty General, Bartek, and Edin who socialised with me the most during three years study in CIPR and also thanks to Iranian friends.

Finally, but not least, I would like to thank my dear wife Nikou for putting up with me during this work by encouragement and unconditional support.

15th June 2009

Shahram Pourmohammadi

LIST of PAPERS

I. Dispersion Measurements Used in Special Core Analysis of Carbonates

Skauge, A., Vik, B., Pourmohammadi, S., and Spildo, K.

Reviewed Proceedings from International Society of Core Analysts, Trondheim, Norway 12-16 September 2006. SCA 2006-14

II. Fluid Flow Properties of Different Carbonate Pore Classes

Pourmohammadi, S., Hetland, S., Spildo, K., and Skauge, A.

Proceedings from 2007 SPE/EAGE Reservoir Characterization and Simulation Symposium, SPE 111433

III. Does the Pore Class Concept for Carbonates Make Sense for Multi-Phase Flow?

Pourmohammadi, S., Hetland, S., Spildo, K. and Skauge, A.

Reviewed Proceedings from International Symposium of the Society of Core Analysts, Abu Dhabi, UAE 29 October-2 November 2008. SCA 2008-29

IV. Impact of Petrophysical Properties on Water Flooding in Cretaceous and Tertiary Chalk

Pourmohammadi, S., Hetland, S., Spildo, K. and Skauge, A.

Reviewed Proceedings from International Symposium of the Society of Core Analysts, Abu Dhabi, UAE 29 October-2 November 2008. SCA 2008-28

NOMENCLATURE

A: area [cm²]
a: shape factor, Humble factor, actual term
B: magnetic field [Tesla]
BVI: bulk volume of irreducible fluid [cm³]
BVM: bulk volume of movable fluid [cm³]
C: concentration [mol/cm³]
CDE: convection-diffusion equation
CT: computer technology
c: threshold pressure
c*: concentration in the stagnant volume [mol/cm³]
D: diffusion coefficient [cm²/s], diameter [cm]
d: differential term
E: energy level [J]
erf: error function
F: formation factor [dimensionless]
FW: Fractional wet
f: **flowing** fraction, frequency [Hz]
G: internal geometry parameter
h: Plank's constant [J's]
HCIP: hydrocarbon in-place [cm³]
I: spin quantum number of the nucleus, resistivity index [dimensionless], wettability index, inaccessible fraction
J: diffusive flux [mol/cm²s]
JBN: Johnson, Bossler, and. Naumann method
K: Boltzmann's constant [J/K], longitudinal dispersion coefficient [cm²/s], absolute permeability [cm²]
L: length of rock or permeable medium [cm]
M: magnetic momentum [Ampere/Meter (A/M)], mass constant [s⁻¹], macroscopic
m: cementation factor
MCIP: mercury capillary injection pressure
MWL: mixed-wet large
MWS: mixed-wet small
NMR: Nuclear Magnetic Resonance
N: number of nuclei per unit volume, number
n: saturation exponent
P: pressure [Pa]
PSDI: pore size distribution index
q: rate [cm³/s]
REV: The representative elementary volume

R: resistivity [Ω m], radius curvature [cm], recovery
r: distances from the end-faces [cm], resistance [Ω] [frac. HCIP]
S: surface layer [cm²], saturation [fraction]
SSW: Synthetic Sea Water
S*: normalized saturation [fraction]
T: absolute temperature [K], relaxation-time[s]
t: time[s]
u: Darcy velocity [cm/s]
V: bulk volume [cm³]
x: distance, length

Greek Letters

σ: interfacial tension [N/m]
α: dispersivity [cm], fraction
γ: gyromagnetic ratio, [rad/Tesla]
β: exponent
Δτ: time intervals[s]
δ: Width [cm]
ρ: surface-relaxivity [cm/s], density [g/cm³]
ξ: Volume fraction of the pores

Φ: porosity [fraction]
τ: tortuosity factor
v: interstitial velocity [cm/s]
Δ: difference
θ: contact angle [rad]
λ: pore size distribution factor
ω: rotational speed [rad/s]
μ: viscosity [Pa's]

Indices

AH: Amott-Harvey
b: bulk
c: capillary
cd: entry or threshold
D: Dimensionless
F: factor
f: flowing, forced
g: gas

I: Index, initial, inaccessible
i: initial
J: Injection
L: Larmor, length
l: longitudinal
max: maximum
min: minimum
nw: non-wetting
o: original, bulk, oil
orw: remaining oil after waterflood
or: residual oil
P: particle
Pe: Peclet
R: resistivity
Ra: apparent resistivity
RL: Rapoport and Leas
r: relative
rec: receding angle
s: stagnant, surface
sp spontaneous
T: total
USBM: United States Bureau of Mines
w: water, wetting

WF: water flooding
X: horizontal dissection
Y: lateral direction
Z: vertical direction
1: longitudinal, inlet
2: transverse, outlet

Pore Class Codes:

CC: Cretaceous Chalk
IC-UMa: Intercrystalline Uniform Macro-Porosity
IC-UMi: Intercrystalline Uniform Micro-Porosity
IC-PMe: Intercrystalline Patchy Meso-Porosity
IC-PMi: Intercrystalline Patchy Micro-Porosity
IC-PMe&IP-PMe: Mixed of Intercrystalline Patchy Meso- and Interparticle Patchy Meso- Porosities
IP-UMa: Interparticle Uniform Macro Porosity
IP-UMa&M-Ma: Mixed of Interparticle Uniform Macro-and Macro-Moldic Porosities
M-Ma: Macro-Moldic Porosity
M-Mi: Micro-Moldic Porosity
TC: Tertiary Chalk

CONTENTS

PREFACE.....	iv
ACKNOWLEDGMENTS.....	v
LIST of PAPERS.....	vi
NOMENCLATURE.....	vii
CONTENTS.....	ix
CHAPTER 1:Introduction.....	1
1.1. Background and Motivation.....	1
1.2.Objective and Work Description.....	2
CHAPTER 2: Carbonate Pore System Classification.....	4
2.1.Carbonate Rock Classifications.....	4
2.1.1.Lithologic and Textural Schemes for Carbonate Rock Classification	4
2.1.2.Classification of Carbonate Rocks based on their Pore Types.....	9
2.2.Summary.....	18
CHAPTER3: Single-Phase Flow Properties.....	20
3.1.Definition of Single-Phase Flow Properties.....	20
3.2.NMR Techniques and Applications.....	20
3.3.Electrical Properties of Porous Media.....	29
3.4.Miscible Displacement in Porous Media.....	37
3.5.Summary.....	48
CHAPTER 4: Two-Phase Fluid Flow Properties in Porous Media.....	49
4.1.Capillary Pressure.....	49
4.2.Relative Permeability.....	56
4.3.Wettability, its Measurements and Effect on Fluid Transport Properties	60
CHAPTER 5: Experimental Procedures and Workflow.....	71
5.1.Procedures and Workflow.....	71
5.2.Pore Class Determination.....	72
5.3.Pore size Distribution from Mercury Injection Capillary Pressure and NMR.....	74
5.4.Single-Phase Dispersion Experiments and Simulation Analysis.....	76
5.5.Conductivity Experiments.....	81

5.6. Wettability Assessment of Core Samples in Cleaned State.....	82
5.7. Unsteady-State Water Flooding Experiments, Simulation Analysis, and End-Effect Investigations.....	83
5.7.1. Simulations of Water Flooding Experiments	86
5.7.2. Evaluation of Factors Controlling Water Flooding	89
5.8. Dispersion Experiments at Remaining Oil Saturation after Water Flooding and Analysis.....	98
5.9. Restoration of Wettability by Aging Process and Evaluation of Wettability Alteration.....	101
5.10. Water Flooding of Restored Samples and Simulations.....	103
5.11. Summary.....	105
CHAPTER 6: Main Results and Discussions.....	107
6.1. Pore Structure Variations in Selected Carbonates	107
6.2. Single-Phase Flow for Different Carbonate Pore Classes	109
6.2.1. Variations in Single-Phase	109
6.2.2. Miscible Displacement in Carbonates Containing Different Pore Classes	115
6.2.3. Relationship for Single-Phase Flow Properties.....	117
6.3. Link between Initial Water Saturations and Flow Properties.....	121
6.4. Main Factors Influencing Remaining Oil Saturation.....	125
6.5. Relative Permeability by Water Flooding of Carbonates.....	127
6.5.1. Correlations between Recovery Efficiency and Single-Phase Flow Properties..	128
6.5.2. Wettability Effect on Recovery Efficiency.....	133
CHAPTER 7: Concluding Remarks and Further Work.....	137
7.1. Main Conclusions.....	137
7.2. Further Work.....	139
REFERENCES.....	141
APPENDIX.....	153
PAPERS.....	157

CHAPTER 1

Introduction

1.1. Background and Motivation

For decades, oil recovery from carbonate reservoirs, which constitute almost half of hydrocarbon reserves, has been a challenge to the oil industry. This is because fluid flow properties in these reservoirs compared to siliciclastic sandstone reservoirs is unpredictable due to more heterogeneity.

In the earlier stages of exploration and oil production from an oil field, it is often interesting to predict the initial oil in place and also the amount of extractable oil. The potentially complex nature of carbonates makes it difficult to predict the reservoir qualities such as porosity, permeability and hydrocarbon saturation. Variation in petrophysical properties makes reservoir characterization and reserve estimation difficult.

Variations in pore size, pore size distribution, pore geometry, and pore connectivity influence reservoir rock properties and flow properties. In addition, multi-phase flow properties such as wettability, capillary pressure and relative permeability are related to these parameters. As a result, correlation between petrophysical properties and oil recovery is not simple and modeling fluid flow for carbonate reservoirs is a difficult task.

Classification of pore types in carbonates is the first stage towards simplifying the complexity of carbonates and provides a mechanism for comparison, a reference to think and finally contributes to better prediction. It is based on geological characterization; sedimentology; thin sections and porosity-permeability relationships. However, improvement in carbonate

reservoir characterization by rock-typing depends on the selection of a proper scheme to classify carbonate rocks.

The improvement of single-phase and two-phase flow rock-typing by employment porosity classification for carbonate rocks has not been tested elsewhere and therefore, it was motivating to be investigated.

1.2. Objective and Work Description

The foundation of this research is based on Lønøy's (2006) comprehensive work towards improving correlation between porosity and permeability in carbonates with a new approach to pore type definition. By employing Lønøy's pore type classification at the start, the main objective is to find important single-phase flow properties that influence oil recovery from carbonate rocks and also evaluation Lønøy's (2006) pore class system for multi-phase flow rock-typing.

This work is limited to the study of carbonates on a macroscopic scale using special core analysis where the pore system can affect flow properties.

At the first step, the impact of different carbonate pore types on petrophysical properties was subject to investigation. The main objective was to find variation in petrophysical properties of different carbonate pore classes.

After characterization of the carbonate pore types by measurement of petrophysical properties, unsteady state water flooding was performed and oil recovery was measured for the samples under study. An attempt was made to find the possible correlations between waterflood efficiency and derived petrophysical properties while the pore class concept was used as the reference for comparison.

This work is presented and described in seven chapters and an appendix which also contains four papers. A short summary for each paper was provided in the preface, thus they are not repeated and only a short summary of chapters are presented.

Chapter one is an introduction to the background and motivation for the research on carbonates followed by a summary of the work description.

Chapter two starts with an introduction to carbonate reservoirs, reviews some important geological aspects of carbonates and mainly focuses on the state of the art in the carbonate pore classification.

Chapter three provides theories and background for single-phase flow properties that are later interrelated with two-phase flow properties. Single-phase flow properties include: a short introduction to NMR and its application for estimation of pore size distribution and comparison with the Mercury Injection Capillary Pressure (MICP) approach, a brief discussion on electrical properties, and discussion of mixing phenomena in porous media associated with the available models and its application to characterize the porous media follows. Earlier studies of dispersion and mixing properties in carbonates are also reviewed.

Chapter four summarizes two-phase flow in the porous media and the impact of the rock and fluid interaction parameters on two phase flow. The two-phase flow properties are limited to water displacing oil by unsteady-state process and relevant equations.

Chapter five presents the experimental procedures and shows the workflow of this research study. It gives the SCAL methods and describes set ups used for the acquired data and result analysis.

Chapter six synthesizes all results and leads to an understanding of some new facts about carbonates and the contribution of the carbonate pore class concept. Most of the results and discussions in this section were presented in four papers and therefore details are not repeated in this chapter. The emphasis is to add analysis beyond what was obtained in the papers.

Finally, in chapter seven, concluding remarks are made according to results presented in chapter six. Recommendations for further work are also presented at the end.

CHAPTER 2

Carbonate Pore System Classification

This chapter reviews the main important aspects of carbonate rock-typing. The employment of rock-typing to improve understanding the multi-phase flow in porous media is a debate. This is because none of the rock-typing approaches uniquely fits requirement for description or characterization of flow properties. The objective is to provide guidance toward the selection of the best carbonate rock classification approach that can relate complex carbonate rock materials and petrophysical properties on the one hand, and to characterize flow properties on the other hand. At first, the most reported schemes for classifying carbonate rock materials are discussed. Then, at the end of the chapter, the selected carbonate rock-typing approach that will be used for the rest of this study is introduced.

2.1. Carbonate Rock Classifications

Depending on their specific interests, geologists, petrophysicists, sedimentologists and reservoir engineers have employed different schemes to classify carbonate rocks (Bissell and Chilingar, 1967; Archie, 1952; Lucia; 1983, 1995, 1999). The literature on carbonate rocks contains only two fundamental schemes for carbonate rock-typing: 1) Lithology and texture 2) Pore type.

2.1.1. Lithologic and Textural Schemes for Carbonate Rock Classification

Lithology and texture schemes are typically based on compositional mineralogy, grain type, grain size, and the portion of each component (grain type) in the carbonate matrix.

Carbonate Rocks and Mineralogy

Discussion of the mineralogy of carbonate rocks, one must necessarily consider age and degree of mineralogical stability or maturity. Although ancient limestones and dolomites are

composed of calcite and dolomite, respectively, other calcite group minerals such as magnesite ($MgCO_3$), rhodochrosite ($MnCO_3$), and siderite ($FeCO_3$) occur in limited amounts in depositional environments. Modern carbonate sediments are composed almost entirely of metastable aragonite ($CaCO_3$) and magnesium-rich calcite, both of which readily recrystallize during diagenesis to form calcite. Diagenesis is defined as any chemical, physical, and biological process or combination of all that alter the primary deposited porosity.

Pure limestone is regarded by many workers as the rock containing 90 % or more of calcite, whereas dolomitic limestone contains between 10 and 50 % dolomite; calcitic dolomite is that carbonate rock containing from 50 to 90 % dolomite and the end member dolomite contains more than 90% of mineral dolomite (Bissell and Chillingar, 1967; Pettijohn, 1975, p.360). Figure 2.1 shows a ternary diagram that summarizes terminologies for carbonate rocks with different compositions.

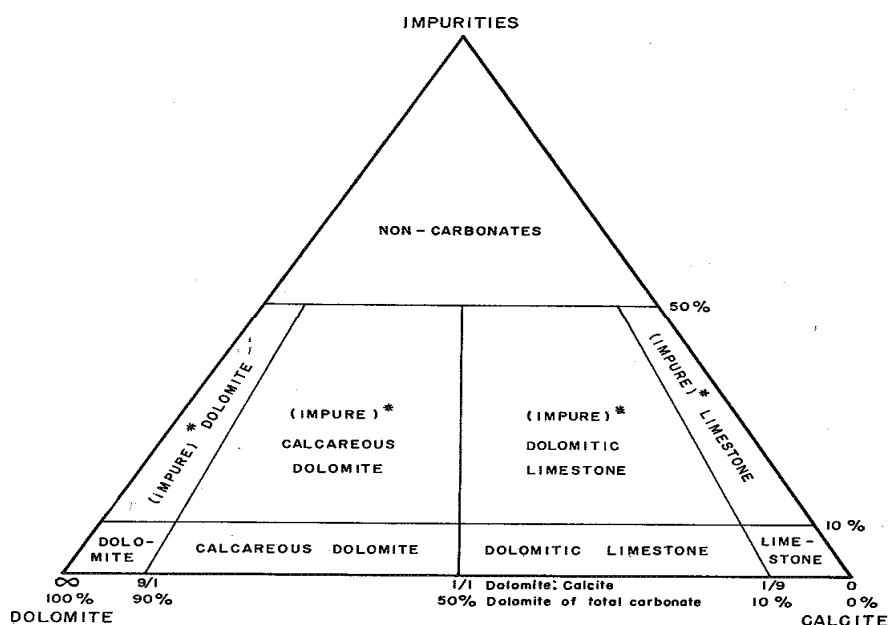


Figure 2.1: Compositional terminology for carbonate rocks. Percentage of impurities and the ratio of dolomite: Calcite is used to define compositional groups for carbonate rocks, that is, those rocks containing more than 50 per cent carbonate minerals. (Adapted from Leighton and Pendexter, 1962.)

Non-carbonate minerals can also be presented in carbonate rocks such as clay minerals; detrital quartz; siderite (FeCO_3); ankerite ($\text{CaFe}(\text{CO}_3)_2$); feldspar; pyrite, and evaporate minerals such as gypsum, anhydrite and halite. Dissolution and removal of evaporates leaves a characteristics mineralogy in carbonate rocks. The classification of carbonates based on the amount of these mineral and terminologies applied for them is out of the scope of this work and readers are recommended to review the papers by Bissell and Chilingar (1967) and also Mount (1985).

Folk Limestone Classification

Rock-typing schemes based on texture for carbonate rocks are mainly grainsize and graintype. Classification of carbonates based on their grainsize depends on whether they are originally limestone or dolomite. A summary of the main classification systems is given here, focusing on widely used classifications, Folk (1959, 1962) and Dunham (1962). Both classifications subdivide limestones primarily on the basis of matrix content. Figure 2.2 shows the classification by Folk (1959, 1962) based on the textural scheme.

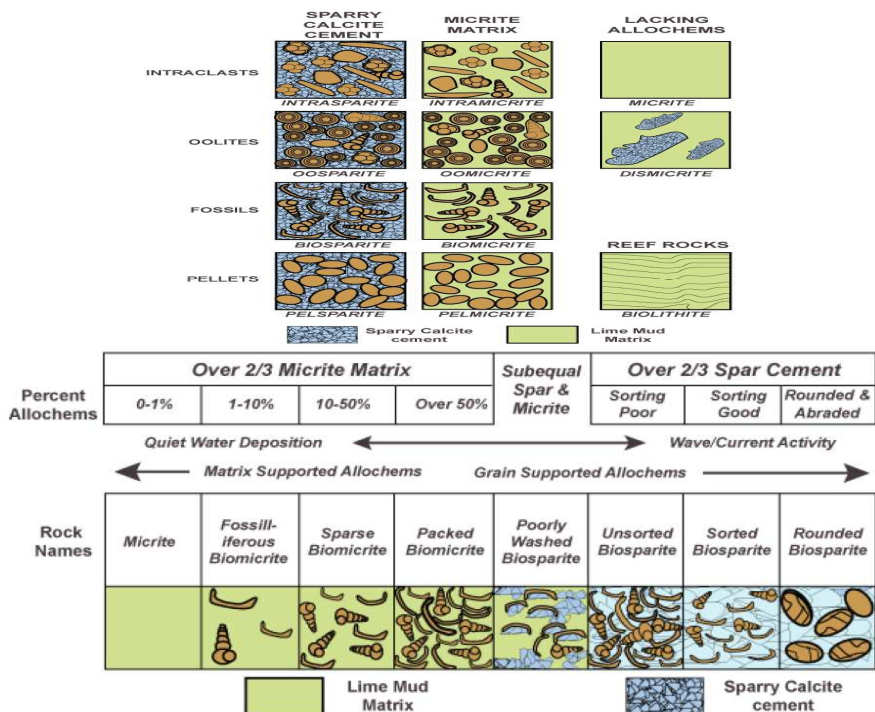


Figure 2.2: Classification of carbonate rocks and carbonate textures. (After Folk, 1959, 1962.)

Folk (1962) recognized four diagenetic materials: the allochems (particles), microcrystalline ooze, called *micrite*; crystalline calcite, called *spar* or *sparite*; and intergrown, fossiliferous reef rock, called *biolithite*. In addition, *dismicrite*, which is *micrite* containing local areas of sparry calcite, and crystalline carbonate, are recognized. Folk's scheme consists of five classes of carbonate rocks which are designated in geologic shorthand by the Roman numerals I, II, III, IV, V. Class I and II are limestones (calcite and aragonite rocks), partially dolomitized limestones (dolomite less than 50%), and primary dolomites (their existence is of debate) which have greater than 10% by volume carbonate allochems.

Class I rocks have mesocrystalline *spar* between the allochems. The Class II rocks have *micrite* filling the space between the allochems. Class III rocks all have less than 10% by volume carbonate allochems. Class IV rocks are all "undisturbed bioherm rocks" which are almost synonymous with Boundstone rocks defined by Dunham (1962). The 'Bafflestone' of Kloven and Emory's (1971) modified Dunham (1962) classification does not fit well in this class. Class V rocks consist entirely of replacement dolomite.

The classification of carbonates using the allochem/interstitial material system (the Folk system) is very systematic and straight forward. The allochem name is combined with the interstitial name (*micrite* or *spar*). Table 2.1 shows the major categories of carbonate rocks based on their allochems and interstitial material.

Table 2.1: Categories of carbonate rocks and their allochems with interstitial materials.

		Interstitial Material	
		Micrite Matrix	Spar Matrix
Allochems	Fossils	Biomicrite	Biosparite
	Oolites	Oomicrite	Oosparite
	Pellets	Pelmicrite	Pelsparite
	Intraclasts	Intramicroite	Interasparite

But what happens if there is more than one allochem in the rock, or there is a mixture of *micrite* and *spar*? This classification system has great flexibility and creativity and one can easily build one's own descriptive rock names. The name is built up by stringing together all

the allochem names in order from least to most abundant, and then adding the interstitial material names. (see Table 2.2)

Table 2.2: Building up the limestone name according to the name of allochem.

The stringing name of the allochem	The name of the limestone
<i>Oolites+Fossils+SparMatrix=Oo+bio+sparite</i>	<i>Oobiosparite</i>
<i>Pellets+Oolites+Fossils+MicriteMatrix=Pel+oo+bio+micrite</i>	<i>Peloobiomicrite</i>
<i>Matrix+Micrite Matrix=Bio+spar+icrite</i>	<i>Biosparicrite</i>

Image thin-sections of limestone classification introduced by Folk (1959, 1962), were given by Scholle *et al.* (1978) and readers can see examples in this reference.

Dunham Classification

In the Dunham (1962) classification, the relative amounts of mud (equivalent to the term

<i>Depositional texture by Dunham (1962)</i>				<i>Modified Dunham (1962) by Embry and Klovan (1971)</i>				
Original components not bound together during deposition				Original components were bound together during deposition			Original components not bound together during deposition	
Generally <i>smaller</i> grains (arenite and silt size)				Organisms act as sediment bafflers (e.g. dendroid corals)	Organisms act as sediment binders (e.g. algal mats)	Organisms act as frame builders (e.g. intergrown reef corals)	More than 10 percent <i>larger</i> grains (rudite size)	
Contains mud (micritic matrix)		Lacks mud (sparite matrix)					Contains mud (micrite matrix)	Lacks mud (sparite matrix)
Less than 10 percent grains	More than 10 percent grains							
Mud supported		Grain supported		Boundstone			Matrix supported	Grain supported
<i>Mudstone</i>	<i>Wackestone</i>	<i>Packstone</i>	<i>Grainstone</i>	<i>Bafflestone</i>	<i>Bindstone</i>	<i>Framestone</i>	<i>Floatstone</i>	<i>Rudstone</i>

Figure 2.3: Classification of limestones according to the depositional texture by Dunham (1962) and modified by Embry and Klovan (1971). Thin-section images from the left the right are respectively: lime mudstone; fossiliferous lime wackestone; crinoidal packstone; lime rudist floatstone;lime rudist mud-rich rudstone; lime coral framestone; algal stromatolite dolobindstone;algal-plate lime bafflestone.(Adapted from Scholle *et al.* ,1978.)

micrite used by Folk (1962)) versus carbonate grains is used to define four major allochemical limestone types (Figure 2.3).

The major pore classes in the Dunham (1962) classification are defined based on the presence of organic binding, presence or absence of carbonate mud, and the concept of grain versus matrix support. Dunham (1962) classified limestones as *Mudstone*, *Wackestone*, *Packstone*, and *Grainstone*. Embry and Kolvan (1971) subdivided the limestone-biolithite category of Dunham (1962) into those organic buildups composed of in-place and transported limestone textural types. In-place reef limestones were further divided into *Bafflestones*, *Bindstones*, and *Framestones*. The textures of transported reef limestones include *Floatstones* and *Rudstones*.

Dolomites Carbonate Rocks

Dolomites have been classified on the basis of several criteria, among them being: Calcium-magnesium ratio; mineralogic composition; presence of relict textures; crystal texture and fabric, including crystal size; the environment of deposition of dolomitized rocks; and geological evolution (Chilingarian *et al.*, 1992). Study in dolomite carbonate rocks is not the major concern in this study, thus dolomite classification schemes are not reviewed here.

2.1.2. Classification of Carbonate Rocks based on their Pore Types

Pore systems in carbonates are more complex than siliciclastic. As mentioned before, this is because of high varieties in elements that form carbonate rocks and secondary porosities that are developed by diagenesis processes. Table 2.3 compares various aspects of carbonate and siliciclastic porosities given by Choquette and Pray (1970).

As the table shows, the secondary porosity is more important in carbonates than sandstones. The comparison shows that elements which characterize pores in carbonates such as pore size, pore shape and pore size distribution are less related to sedimentary particle size and shape of depositional components for carbonates compared to sandstones.

Table 2.3: Comparison of carbonate and siliciclastic porosity. (Adapted from Choquette and Pray, 1970.)

Aspect	Sandstone	Carbonate
Amount of primary porosity in Sediments	Commonly 25-40%	Commonly 40-70%
Amount of ultimate porosity in rocks	Commonly half or more of initial porosity; 15-30% common	Commonly none or only small fraction of initial porosity; 5-15% common in reservoir facies
Type(s) of primary porosity	Almost exclusively interparticle	Interparticle commonly predominates, but intraparticle and other types are important
Type(s) of ultimate porosity	Almost exclusively primary Interparticle	Widely varied because of postdepositional Modifications
Sizes of pores	Diameter and throat sizes closely related to sedimentary particle size and sorting	Diameter and throat sizes commonly show little relation to sedimentary particle size or sorting
Shape of pores	Strong dependence on particle shape -- a "negative" of articles	Greatly varied, ranges from strongly dependent "positive" or "negative" of particles to form completely independent of shapes of depositional of diagenetic components
Uniformity of size, shape, and distribution	Commonly fairly uniform within homogeneous body	Variable, ranging from fairly uniform to extremely heterogeneous, even within body make up of single rock type
Influence of diagenesis	Minor; usually minor reduction of primary porosity by compaction and cementation	Major; can create, obliterate, or completely modify porosity; cementation and solution important
Influence of fracturing	Generally not of major importance in reservoir properties	Of major importance in reservoir properties if Present
Visual evaluation of porosity and permeability	Semiquantitative visual estimates commonly relatively easy	Variable; semiquantitative visual estimates range from easy to virtually impossible; instrument measurements of porosity, permeability and capillary pressure commonly needed
Adequacy of core analysis for reservoir evaluation	Core plugs if 1-in. diameter commonly adequate for matrix" Porosity	Core plugs commonly inadequate; even whole cores (~3-in. diameter) may be inadequate for large pores
Permeability porosity interrelations	Relatively consistent; commonly dependent on particle size and sorting	Greatly varied; commonly independent of particle size and sorting

In this section, the following four carbonate porosity classifications are discussed:

- 1) Archie (1952)
- 2) Choquette and Pray (1970)
- 3) Lucia (1983)
- 4) Lønøy (2006)

Figure 2.4 shows the main pore types present in carbonate rocks and a summary of the four pore classification approaches.

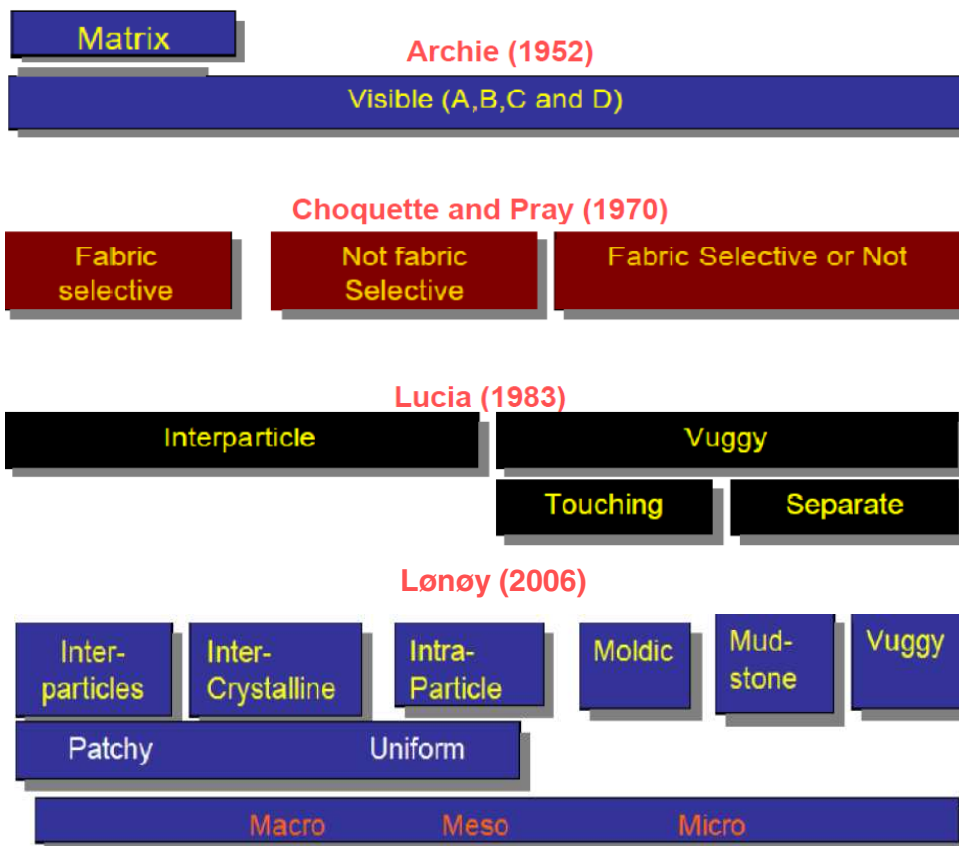


Figure 2.4: Summary and Comparison of different type of carbonate porosity classifications.

Archie Classification (1952)

Archie (1952) made the first attempt to integrate geological information to carbonate reservoir models by developing a porosity classification. This pore classification was aimed to relate rock texture to petrophysical properties such as porosity, permeability and capillarity.

Archie (1952) distinguished visible porosity from matrix porosity as shown in Table 2.4. He used the surface texture of broken rock to obtain matrix porosity, permeability and capillarity. He described visible porosity according to pore size greater than 0.01 mm under the microscope. These three main types of matrix were further described according to their macroscopic and microscopic appearances.

Table 2.4: Pore Classification of Archie (1952).

Texture of matrix	Macroscopic appearance	Microscopic appearance 10× to 15×
Type I Compact Crystalline	Crystalline, hard, dense, sharp edges and smooth faces on breaking Resinous	Matrix made up of tightly interlocking crystals; no visible pore space between crystals; commonly produced “feather edge” and thin flakes on breaking
Type II Chalky	Dull, earthy, siliceous, or argillaceous. Crystalline appearance absent because small crystals are less tightly interlocked thus reflecting light in different directions, or made up of extremely fine particles (skeletal or other)	Crystals joined at different angles Extremely fine texture may still appear “chalky” under this power, but others may begin to appear crystalline. Grain size < 0.05 mm generally. Coarser textures classed as Type III
Type III Granular or saccharoidal	Sandy or sugary appearance (sucrose). Size of crystals or particles classed as: Very fine = 0.05 mm Fine = 0.1 mm Medium = 0.2 mm Coarse = 0.4 mm	Crystals interlock at different angles, but considerable porosity between crystals. Oolitic and other granular textures fall in this class

Classification of visible pores

- Class A: No visible porosity under 10× microscope or where pore size is < 0.01 mm
 Class B: Visible porosity, 0.01 but < 0.1 mm
 Class C: Visible porosity, 0.1 mm but size of cuttings
 Class D: Visible porosity as shown by secondary crystal growth on faces of cuttings or “weathered-appearing” faces showing evidence of fracturing or solution channels; where pore size > size of cutting

Classification of visible-pore frequency

Description	Frequency – percentage of surface covered by pores
Excellent	20
Good	15
Fair	10
Poor	5

Choquette and Pray (1970)

The most widely used pore system classification for geological modeling is the one by Choquette and Pray (1970). This system consists of four elements: Basic porosity types, genetic modifiers, size modifiers and abundance modifiers (Figure 2.5). The solid depositional and diagenetic constituents of a sediment or rock are defined as its “fabric” (Moore, 2001). The term “fabric” has been used instead and replaced the term “rock texture” by Choquette and Pray (1970).

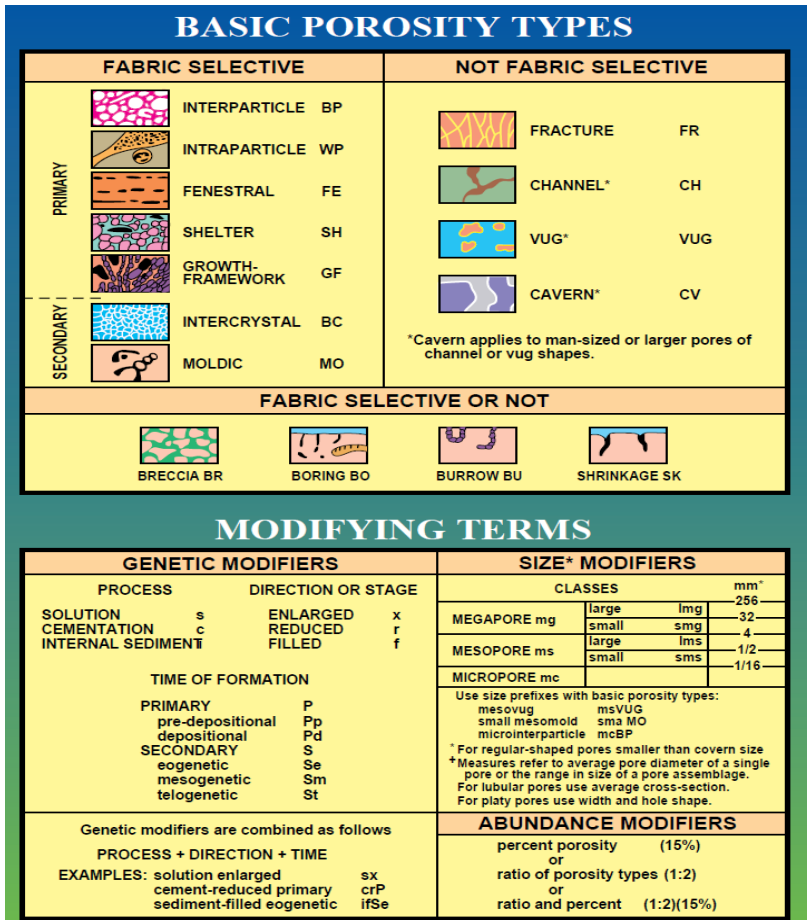


Figure 2.5: Classification of carbonate porosities according to the Choquette and Pray (1970). Classification includes the basic porosity types and modifying terms that represent their origin and the size.

In this classification, fifteen pore types in carbonates are recognized and classified into three main groups. The prime component of the classification is the “fabric selectivity”. According to Choquette and Pray (1970), if a dependent relationship between porosity and fabric elements can be found, that porosity is referred to as fabric-selective.

In other words, the pore shape, pore size and pore size distributions are controlled by textural elements that form the rock for fabric-selective porosities.

The rock fabric in carbonates consists of primary grains such as: ooids and bioclasts; later formed diagenetic products, such as calcite, dolomite and sulfate cements, and recrystallization or replacement components such as dolomites and sulfate crystals. Two factors are criteria to infer fabric selectivity; the configuration of the pore boundary and the position of the pore relative to the matrix elements.

Primary interparticle porosity is fabric-selective; this is because grain size and grain shape in addition to cement materials, effect on the size and shape of preserved pores between particles. Secondary moldic porosity is also commonly fabric-selective due to the preferential removal of some fabric elements by dissolution.

If no relationship between fabric and porosity can be established, the porosity is classed as “not-fabric selective”. Good examples of this pore class are fracture and vuggy porosities where the size of fractures and vugs cut across the rock fabric.

There are four classes that could be either fabric-selective or no fabric-selective like breccia porosity.

Classification by Lucia (1983)

Lucia (1983; 1995; 1999) established a carbonate pore system classification which is an improved version of the classification by Archie (1952). He incorporated rock fabric and petrophysical characteristics to define carbonate pore classes which are applicable in dynamic and engineering models. The Lucia (1983) classification emphasizes the petrophysical aspects of carbonate porosity as does the earlier Archie (1952) classification. Lucia’s (1983) classification divides carbonate porosity into two main groups: Interparticle and vuggy porosities. Figure 2.6 shows the classification by Lucia (1983). The Lucia (1983) classification includes Dunham’s (1962) textural scheme to integrate porosity elements from the rock fabric.

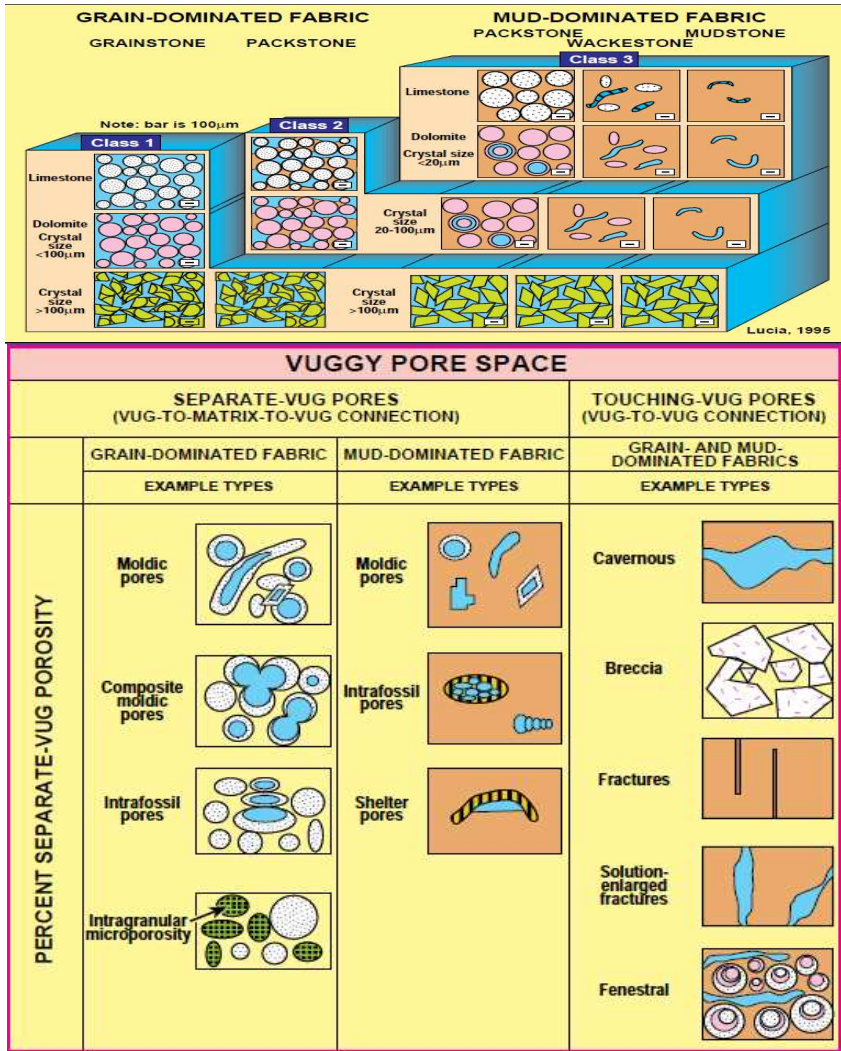


Figure 2.6: Petrophysical and rock fabric classes of Lucia (1995). Interparticle porosity (top) includes three main sub-pore classes based on size and sorting of grains and crystals. The vuggy porosity (bottom) is subdivided into separate or touching-vug pores. The rock fabric classification is based on the textural classification by Dunham (1962).

The interparticle porosity is further subdivided into three petrophysical classes. These classes are recognized by fields between permeability/porosity crossplots where the grain size determines the boundaries. Figure 2.7 shows the semi-log cross-plots of permeability and porosity. Three petrophysical classes show the three distinguishable permeability/porosity fields. Both Lucia (1983; 1995; 1999) and Archie (1952) emphasize that pore size

distribution controls permeability. They both also relate saturation and pore size distribution to the rock fabric.

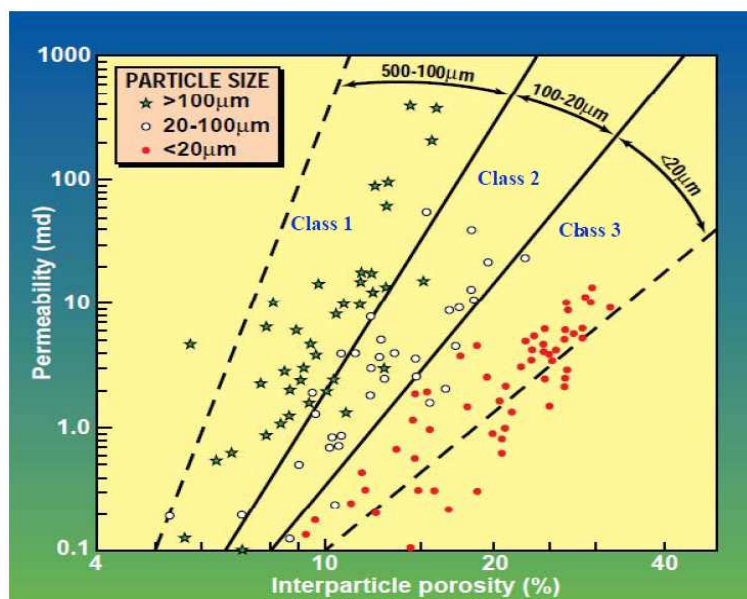


Figure 2.7: Cross-plot of permeability versus interparticle porosity for various particle-size groups in non-vuggy carbonate rocks. (Adapted from Lucia, 1995.)

Classification by Lønøy (2006)

Some weak aspects of Lucia's (1983) classification were discussed by Lønøy (2006) and a new pore system classification was therefore introduced. According to Lønøy (2006), there are two important elements that control porosity preservation in the Lucia (1983) classification which are missed:

1. The classification system does not consider the effect of allochem sorting on the pore size. Moderately to poorly sorted Grainstones and mud-lean Packstones have a wide range of grain sizes, even within the same grain size class; the closer packing of grains produces smaller pore sizes.
2. The effect of cement on pore size is not covered by the Lucia (1983, 1995, and 1999) classification system. Both particle size and sorting are unaffected by interparticle cement, but the cement will reduce pore size and pore throats. Samples with similar

particle size and sorting may thus have a significant spread in pore size and permeability/porosity relationship, depending on cement volume and morphology.

In order to improve the Lucia (1983) classification, Lønøy (2006) suggested a new pore system classification based on three main elements: Pore type, pore size, and pore distribution (Figure 2.8). Age is also an important factor for some of the mudstone micro-pore classes. This new pore classification includes some porosity examples defined by Choquette and Pray (1970) and the Lucia (1983) classifications.


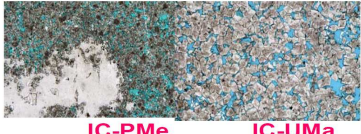
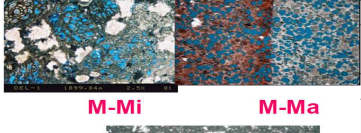
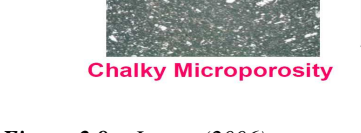
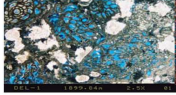
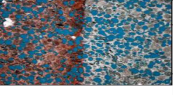

	Pore Type	Pore Size	Pore Distribution	Pore Fabric
 IP-UMa	Interparticle	Micropores (10-50 μm)	Uniform	Interparticle, uniform micropores
			Patchy	Interparticle, patchy micropores
		Mesopores (50-100 μm)	Uniform	Interparticle, uniform mesopores
			Patchy	Interparticle, patchy mesopores
 IP-PMe	Macropores (>100 μm)	Uniform	Interparticle, uniform macropores	
		Patchy	Interparticle, patchy macropores	
 IC-UMa	Intercrystalline	Micropores (10-20 μm)	Uniform	Intercrystalline, uniform micropores
			Patchy	Intercrystalline, patchy micropores
		Mesopores (20-60 μm)	Uniform	Intercrystalline, uniform mesopores
			Patchy	Intercrystalline, patchy mesopores
 IC-PMe	Macropores (>60 μm)	Uniform	Intercrystalline, uniform macropores	
		Patchy	Intercrystalline, patchy macropores	
 M-Mi	Intraparticle		Intraparticle	
		Moldic		Moldic micropores
 M-Ma	Moldic		Moldic macropores	
		Vuggy		Vuggy
 Chalky Microporosity	Mudstone microporosity	Micropores (<10 μm)		Tertiary chalk
				Cretaceous chalk
			Uniform	Chalky micropores, uniform
			Patchy	Chalky micropores, patchy

Figure 2.8: Lønøy (2006) pore system classification associated with thin section images of some sub-pore classes. The pore system classification includes 20 pore types according to the size and relative distribution of pores to the matrix. Patchy porosity distribution is due to incomplete diagenetic processes such as selective dissolution or partial cementation. Thin-sections include: interparticle uniform-macro porosity (IP-UMa); interparticle patchy-meso porosity (IP-PMe); intercrystalline uniform-macro porosity (IC-UMa); intercrystalline patchy-meso porosity (IC-PMe); micro and macro moldic porosities (M-Mi & M-Ma) and chalky microporosity.

However, because of insufficient data, Lønøy's pore classes do not include fenestral, shelter, boring, burrow, and shrinkage porosity, and/or analytical considerations for fracture, channel, cavern, growth framework, and breccia porosity, these pore types were not included

in this new system. The main differences between this system and those of Choquette & Pray (1970) and Lucia (1983) are as follows:

- Porosity distribution is a new element in the classification.
- Lucia's subdivision of interparticle porosity has been partly incorporated into the new classification system, but rather than based on grain size and sorting, it is now based on pore size.
- Lucia's three interparticle pore type classes and Choquette and Pray's interparticle and intercrystalline porosity types have been subdivided into twelve new classes (6 interparticle and 6 intercrystalline).
- Micro-moldic and macro-moldic pores are differentiated.
- A new pore-type category, consisting of four pore types, is introduced: Mudstone micro-porosity.

This new pore classification as shown by Lønøy (2006) improves correlation between porosity and permeability for selected pore classes. This improvement is most notable when intercrystalline porosity is differentiated from interparticle porosity and the pore size and pore distribution schemes are involved.

2.2. Summary

Carbonate rock materials have generally more complex pore systems than siliciclastics because of their wide variety of particles. Two main schemes have been developed to classify and characterize carbonate sediments and carbonate rock materials: 1) Lithology and texture, 2) Pore type.

The classification of carbonate porosity should provide the possibility to build up geological models, full prediction petrophysical parameters (porosity, permeability and saturation) and multi-phase flow properties (capillary pressure, relative permeability, etc.). Classification of carbonate rocks based on pore types is more useful to predict petrophysical and multi-phase flow properties than the textural carbonate classification.

Archie's classification (1952) is useful to predict with petrophysical properties but it is difficult to be use for building of a reservoir geological model for the field development. This is because Archie's classification (1952) does not include useful information to infer with carbonate depositional environment and diagenetic effects. Thus Archie's classification

(1952) was a breakthrough for well-bore scale modeling, but did not facilitate prediction of inter-well or field-scale prediction.

The complexity of Folk's (1959, 1962) classification makes it more applicable for petrographic and microscopic research rather than field application. Dunham's classification (1962), on the other hand, is primary textural in nature, is simple, and is easily used by geologists in the field.

The carbonate porosity classification by Choquette and Pray (1970) is well integrated with depositional environments and involves the time interval for diagenesis, thus it has been widely used for geological modeling. This system is closely linked to sedimentological fabric, and pore types can therefore, to some extent, be predicted based on depositional setting and/or diagenetic evolution. This classification system is particularly useful for porosity evolution studies that are important for exploration. However, this classification is not integrated with petrophysical parameters and dynamic and flow properties.

The Lønøy (2006) pore system classification, which employs the Lucia (1983) approach and Choquette and Pray (1970) scheme, is more useful to be examined in relationship to multi-phase flow properties. This is because it includes elements such as pore type, pore size and pore distribution. These rock elements are linked to multi-phase flow properties like capillary pressure and relative permeability. The Lønøy (2006) pore system classification was therefore used as the foundation for carbonate rock-typing for further work in this thesis.

CHAPTER 3

Single-Phase Flow Properties

In the second chapter, carbonate rock classification was reviewed. This chapter provides theories and background for single-phase flow properties that are later integrated with two-phase flow properties, as it is presented in the next chapter.

3.1. Definition of Single-Phase Flow Properties

The term “single-phase flow properties“, is used frequently in this chapter and therefore it is defined clearly to avoid confusion. Any property of a porous medium derived by occupying a single-phase that can influence the fluid flow is defined as a “single-phase flow property “. The single-phase flow property of the medium can be derived “statically“, like pore size distribution from NMR experiments or “dynamically“ like *dispersivity* from dispersion experiments . For the static measurements, it is not often necessary to measure a property of the effluent outside of the medium. For simplicity, all dynamic and static single-phase flow properties are referred to as “single-phase flow properties“, here and elsewhere.

3.2. NMR Techniques and Applications

NMR applications for porous media include: Pore size distribution; bulk of irreducible fluid (**BVI**) versus bulk volume of movable oil (**BVM**); permeability and wettability. Since, in this thesis, only derived pore size distribution by **NMR** techniques are employed to relate to other petrophysical properties, the discussion is thus limited to this field. In this section, the principles of **NMR** are shortly introduced and reviewed with focusing on application for deriving pore size distribution. All **NMR** data presented in this thesis is based on the method developed by Sorland *et al.* (2006).

Methods for Derivation of Pore Size Distribution

The most representative approach to determine pore size distribution involves measurements of the size of all the pores in a macroscopic sample. All other methods are indirect and the

results obtained by them depend on assumptions about the pore structure and pore accessibility (Dullien, 1992).

The widely used and traditional methods are mercury porosimetry, sorption isotherms and recently Nuclear Magnetic Resonance (NMR) techniques. As discussed by Dullien (1992), the mercury intrusion technique has some limitations because not all materials are wetting to mercury and not all pores are accessible to the mercury even under applied high pressure. Moreover, pore sizes are estimated based on the invaded volume on the pore scale model. The filling sequence by mercury injection is limited by pore accessibility. Therefore, derived pore size distribution from the mercury intrusion technique should always be evaluated together with the other methods.

Nuclear Magnetic Resonance (NMR)

Nuclei with an odd number of protons or neutrons possess spin. We will focus on the spins of the hydrogen nucleus since they exist in both hydrocarbons and water. In the absence of a magnetic field, B_0 , the nuclear magnetic axes distribute randomly (Figure 3.1). The spins can be polarized in two ways if they are exposed to the magnetic field, B_0 : 1) Along the magnetic field, B_0 2) Opposite to the magnetic field, B_0 . According to the Boltzmann statistics, there will be more spins along the magnetic field.

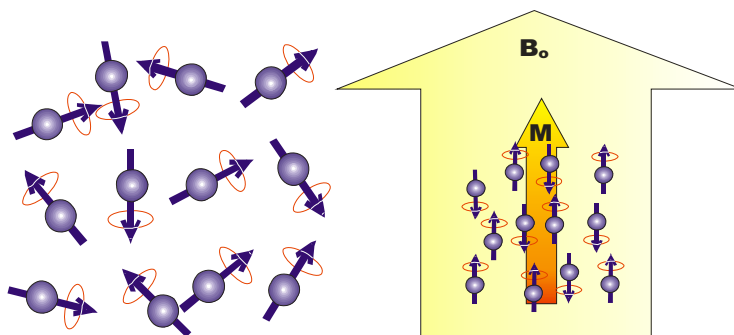


Figure 3.1: Protons in the absence of the magnetic field, B_0 (left) spin randomly while in the presence of a magnetic field they are frequently aligned with the magnetic field (right). Spinning protons can be looked upon as small magnets.

Furthermore, nuclei will precess around the field, \mathbf{B}_o . The precessing frequency is called the *Larmor frequency* and is given by following equation:

$$f_L = \frac{\gamma \mathbf{B}_o}{2\pi} \quad \text{Eq.3-1}$$

where γ is the gyromagnetic ratio, which has different values for different nuclei, for hydrogen γ is $2.6752 \cdot 10^8$ rad/sTesla. The spinning protons aligned with the magnetic field \mathbf{B}_o causes a net magnetization \mathbf{M}_o . The net macroscopic magnetization \mathbf{M}_o is defined as the net magnetic moment per unit volume. At equilibrium, the net macroscopic magnetization, which is the magnetic contribution of all the polarized nuclei, will provide a signal for NMR measurements and is given by Curie's law:

$$\mathbf{M}_o = N \frac{\gamma^2 \hbar^2 I(I+1)}{3(4\pi^2)kT} \mathbf{B}_o \quad \text{Eq.3-2}$$

where, N is number of nuclei per unit volume, k is Boltzmann's constant, T is absolute temperature, \hbar is Planck's constant and I is the spin quantum number of the nucleus.

In order to alter the energy of the system with precessing nuclei, radiofrequency pulses can be implemented. Some of the nuclei will be excited to the higher energy state and precess anti-parallel to the field, \mathbf{B}_o .

The frequency of the photons with the energy needed to excite a nucleus from energy level, E_α , to energy level; E_β has to be the same as the frequency of the precessing spins, i.e. the *Larmor frequency*. This is the resonance condition and it can be expressed by following equation:

$$\Delta E = \frac{h\gamma}{2\pi} \mathbf{B}_o = hf_l \quad \text{Eq.3-3}$$

Spins may be disturbed or flipped away from their preferred orientation in a magnetic field. The process of reorientation of spins is called relaxation. Relaxation is the process where disturbed or flipped magnetic momentum vector, \mathbf{M} returns to stable conditions aligned along the magnetic field vector, \mathbf{B}_0 .

The magnetization is proportional to the sum of magnetic momentums of spins. The sum of magnetizations from contributing spins depends on the number of hydrogen molecules available in the fluids which is related to the porosity. In other words, the amount of hydrogen reflects the total porosity of the rock.

When current with a carrier frequency equal to the *Larmor frequency* is applied through a coil, it generates a transverse magnetic field, \mathbf{B}_1 along the y-axis. The pulse can then be adjusted such that, \mathbf{M}_0 rotates by exactly 90° . If the pulse then terminates, the only field left is the fixed field, \mathbf{B}_0 in the z-direction (Figure 3.2).

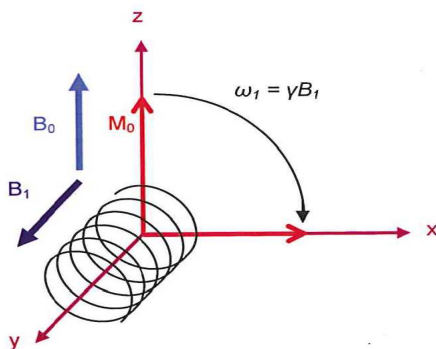


Figure 3.2: The net macroscopic magnetization, \mathbf{M}_0 is flipped 90° to align with the x-direction when a magnetic field \mathbf{B}_1 is generated. (Adapted from Dunn, 2002.)

Relaxation Time

Felix Bloch (1946) described T_1 and T_2 as longitudinal and transverse relaxation time constants respectively mathematically in a coupled set of differential equations collectively known as the Bloch equations. Each relaxation process decays with characteristic time constants. Solving the coupled set of differential equations yield:

$$M_z = M_o \left(1 - e^{-\frac{t}{T_1}} \right) \quad \text{Eq.3-4}$$

$$M_x = M_y = M_o e^{-\frac{t}{T_2}} \quad \text{Eq.3-5}$$

Relaxation time for fluids like water hydrocarbon within the porous media is shorter than the bulk of the fluid and relies on properties of the rock such as pore sizes, pore size distribution and surface properties as well as rock-fluid interactions like wettability (Dunn, 2002). Interaction between liquid and surface enhances the relaxation and this phenomenon is known as the surface relaxation and theoretically formulated by Korringa *et al.* (1962). Foley *et al.* (1996) verified experimentally the theory of Korringa *et al.* by measuring the relaxation time on idealized models of porous media. Their results showed a linear decrease in the relaxation time with increasing content of paramagnetic contaminants in the porous structure and Matteson *et al.* (2000) found a similar trend for the surface relaxivity of clay.

Surface Relaxivity

The usefulness of **NMR** as a tool for measuring pore size distributions was established in two papers by Brownstein and Tarr (1977, 1979). The pore volume in a single pore can be divided into surface volume and bulk volume. The surface volume is a thin layer, δ with a width of only a few molecular diameters (see Figure 3.3).

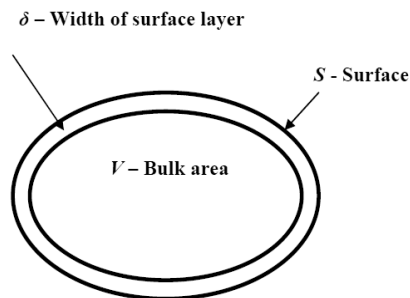


Figure 3.3: Schema of a pore which is divided into a surface layer S , with a width of δ , and a bulk volume V .

The inverted relaxation-time is a measurement of the relaxation-rate, and by combining the contribution from the surface layer and the bulk volume, it can be written:

$$\frac{1}{T_i} = \left(1 - \frac{\delta \cdot S}{V}\right) \frac{1}{T_{ib}} + \frac{\delta \cdot S}{V} \frac{1}{T_{is}} \quad i = 1,2 \quad \text{Eq.3-6}$$

where the subscripts 1 and 2 denote for longitudinal and transverse respectively. T_{ib} and T_{is} denote relaxation-times for the bulk and surface layer regions respectively. The first term can be neglected because the relaxation-rate will be substantially faster for a molecule in the surface layer than for a molecule in the bulk volume and moreover the thickness of the surface layer, δ is too small. This can be caused for instance by paramagnetic centres in the pore-walls that strongly speed up the relaxation-process. The formula is then given by:

$$\frac{1}{T_i} = \frac{1}{T_{ib}} + \frac{\delta \cdot S}{V} \frac{1}{T_{is}} \quad i = 1,2 \quad \text{Eq.3-7}$$

By definition, the ratio δ/T_{is} is called the surface-relaxivity, ρ , and it is the measurement of the strength of the relaxation-processes that take place on the pore-surface. Surface-relaxivity was shown by Kleinberg *et al.* (1994) to be almost independent of the pore size for given material such as carbonates and sandstones. If the fast diffusion is assumed during the relaxation process, Equation 3-7 can be written for a simple pore space as:

$$\frac{1}{T_i} = \rho \cdot \frac{S}{V} \quad i = 1,2 \quad \text{Eq.3-8}$$

Equation 3-8 then establishes the link between relaxation-rate and pore size. In a system consisting of identical sized pores, the relaxation is characterized by a single exponential decay under the fast diffusion approximation. As a result, for a system composed of different pore sizes, the measured signal is represented by a sum of exponentials with different time constants corresponding to the different pore sizes where the intensity of each exponential represents the population of the corresponding pore size and mathematically can be expressed as :

$$M(t) = M_0 \sum_j^n a_j (T_{2j}) \exp\left(-\frac{t}{T_{2j}}\right) \quad \text{Eq.3-9}$$

To solve Equation 3-9 for a_j when $M(t)$ is known, there is a so called inverse problem and the solution can be unstable. The coefficient distribution will then be proportional with the pore size distribution.

The link between relaxation time distributions and pore sizes were experimentally verified by Howard *et al.* (1993) and Ausbrooks *et al.* (2004). Straley *et al.* (1991) observed decreasing T_2 values in the relaxation time distribution as the centrifuge speed increased for water saturated core samples. Results showed consistency when pore size distribution derived from **NMR** was compared against pore size distribution from thin sections (Bowers *et al.*, 2004; Carr *et al.*, 1996). As further evidence of the correlation between relaxation time and pore size distribution, Lyne *et al.* (1996) and Ausbrooks *et al.* (2004) compared pore size distribution derived from **NMR** with the one from mercury-capillary pressure injection method (MCIP).

Effect of Pore Connectivity on Relaxation Rate

It should be noted that the analysis approach by Brownstein and Tarr (1977, 1979) is only valid for an isolated pore. However, for real porous media, it is not usually the case that pores are isolated, and coupling between pores can therefore pose a significant influence on the relaxation time distribution. McCall *et al.* (1991, 1993) provided a review of the impact of pore coupling (connectivity) on the magnetization evolution in connected porous media and they identified four reaction rates contributing to the magnetization evolution. Experimental evidence does however largely show that interpore coupling is not significant in many real porous systems. The experiments by Straley *et al.* (1991) on centrifuged cores did not show any evidence of pore coupling as this would have affected the shape of the distribution and not only exclude desaturated regions. The diffusion also can effect of the results as it is ignored for the interpretation results. One way to examine the significance of diffusion on measurements is to perform them in different temperatures because molecular diffusion is temperature dependent.

The Method by Sorland et al. (2006)

Restricted diffusion measurements have been used combined with spin-lattice relaxation time T_1 measurements (Kenyon *et al.*, 1988; Song *et al.*, 1992) and T_2 measurements (Sorland *et al.*, 2006) to measure the surface relaxivity.

The method developed by Sorland *et al.* (2006) is aimed to employ the diffusion to measure the surface relaxivity based on measurements at the short period of observation, and include two initial assumptions: 1) The surface relaxation strength is fairly independent of pore size; 2) The molecules rarely probe from one pore to adjacent pores.

In the analysis by Sorland *et al.* (2006), the derived restricted-diffusion coefficient by Mitra *et al.* (1993) as the following equation is employed:

$$\frac{D(t)}{D_o} \approx 1 - \frac{4}{9\sqrt{\pi}} \sqrt{D_o t} \frac{S}{V} + \varphi(\rho, R, t) \quad \text{Eq.3-10}$$

Where $D(t)$ is the time-dependent diffusion coefficient, D_o is the unrestricted-diffusion coefficient in bulk fluid, and t is the observation time. The higher order terms in t , $\varphi(\rho, R, t)$ holds the deviation due to finite surface relaxivity and curvature (R) of the surfaces. At the shortest observation times, these terms may be neglected such that the deviation from bulk diffusion depends on the surface to volume ratio alone.

In a porous system, a large span in pore sizes is usually assumed. Eq.3-10 must also be expected to be valid for a heterogeneous system. From Eq.3-8, Eq.3-11 can be written as:

$$\overline{\left(\frac{1}{T_2}\right)} = \rho \overline{\left(\frac{S}{V}\right)} \rightarrow \rho = \overline{\left(\frac{1}{T_2}\right)} \cdot \overline{\left(\frac{S}{V}\right)}^{-1} \quad \text{Eq.3-11}$$

and thereby the pore size independent relaxivity, ρ can be found, and then ρ can be used in Eq.3-8. This results in a linear relation between T_2 and the volume to surface ratio which is the measure for pore size. The T_2 distribution is multiplied with the calculated surface relaxivity and the distribution is then normalized to a pore size distribution in absolute length units. Figure 3.4 shows an example of a pore size distribution derived by the method

described above compared to pore size distribution derived by the mercury injection capillary method (MICP).

Mercury porosimetry is based on injecting mercury into the sample at successively higher pressures while recording the volume of fluid injected into the sample at each step. When the connectivity of the medium deviates from ideality, the technique tends to underestimate the larger cavities within the rock as the volumes of larger pores are assigned to smaller pores thus leaving a narrow distribution of pore sizes shifted towards smaller pore sizes.

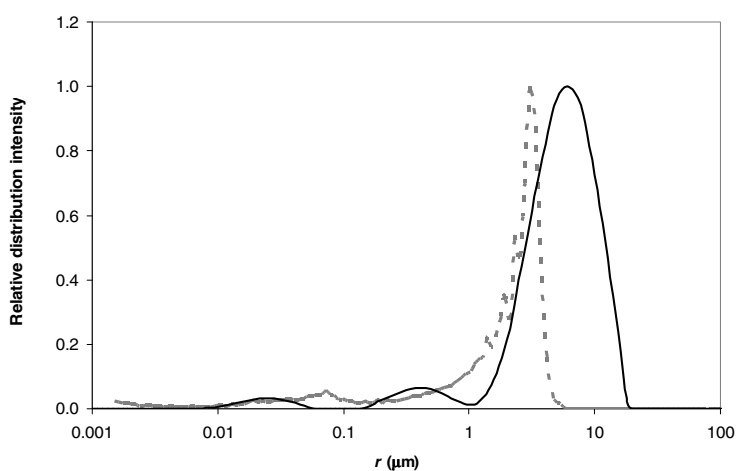


Figure 3.4: Pore size distributions of sample A from the NMR method (solid line) and from mercury intrusion (dashed line). (Adapted from Sorland et al., 2006.)

The limitation for NMR technique to estimate the pore size distribution is that it does not distinguish between throats.

More details of theories behind the **NMR** techniques are beyond the scope of this thesis. **NMR** techniques have been widely used in the oil industry in both laboratory and field scale for characterization of the porous media.

3.3. Electrical Properties of Porous Media

Sedimentary formations are capable of transmitting electric current only by means of the interstitial and absorbed water they contain. They would be non-conductive if they were entirely dry. The interstitial or connate water containing dissolved salts constitutes can act as electrolyte capable of conducting current, as these salts dissociate into positively charged cations such as **Na⁺** and **Ca⁺**, and negatively charged anions, such as **Cl⁻** and **SO₄⁻**. These ions move under the influence of an electrical field and carry electrical current through the solution; the greater the salt concentration, the greater the conductivity of connate water. Oil, gas, and fresh water are not conductive.

Formation Resistivity and Cementation Factor

The electrical resistivity (reciprocal of conductivity) of a fluid-saturated rock is its ability to impede the flow of electric current through that rock.

Archie (1942, 1950) defined the formation resistivity factor, **F_R** as:

$$F_R = \frac{R_o}{R_w} \tag{Eq.3-12}$$

where **R_o** is the resistivity of the rock when 100% saturated with brine in **Ωm**, **R_w** is the water resistivity in **Ωm**. Since **R_o** is greater than **R_w** then, **F_R** is always greater than unity. Figure 3.5 shows the qualitative effect of brine resistivity (assuming all other factors, such as porosity, cementation, and amount of shale remains constant) on *formation factor* for limestone and clean sand, and shaly (dirty) sand. As seen, the *formation factor* is constant for clean sand and limestone while for dirty or shaly sand, it decreases as brine resistivity increases. This is because by increase in brine resistivity (**R_w**); rock resistivity (**R_o**) does not increase proportionally due to existence of clay in water and clay acts as a conductor.

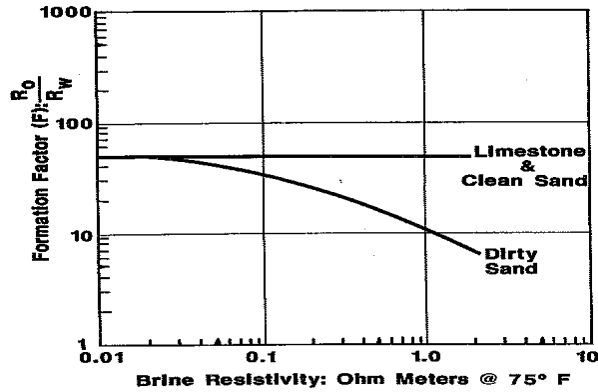


Figure 3.5: General relationship between formation factor and brine resistivity, R_w . (Courtesy of Core Laboratories.)

Wyllie (1950) proposed that the observed effect of clay minerals was similar to having two electrical circuits in parallel: the conducting clay minerals and the water-filled pores. Thus:

$$\frac{1}{R_{oa}} = \frac{1}{R_c} + \frac{1}{F_R R_w} \quad \text{Eq.3-13}$$

where R_{oa} is the resistivity of shaly sand when 100% saturated with water of resistivity. R_c is the resistivity due to the clay minerals. $F_R R_w$ is the resistivity due to the distributed water, and F_R is the true *formation factor* of the rock (the constant value when the rock contains low-resistivity water). Eq.3-13 can be rearranged to express the apparent *formation factor*, F_{Ra} in terms of R_c , F_R , and R_w :

$$R_{oa} = \frac{R_c R_w}{R_w + \frac{R_c}{F_R}} \quad \text{and} \quad F_{Ra} = \frac{R_c}{R_w + \frac{R_c}{F_R}} \quad \text{Eq.3-14}$$

As observed, when water resistivity is too low, the apparent *formation factor* F_{Ra} , and true *formation factor* become almost the same.

Archie (1942) realized that as sand becomes more cemented, porosity decreases and therefore, F_R increases. He derived a correlation from laboratory measurements of the formation resistivity factor F_R and with variable porosities. The correlation is expressed as:

$$F_R = \frac{1}{\phi^m} \quad \text{Eq.3-15}$$

The exponent m , which is referred to as “*cementation factor*” is a function of the shape and distribution of pores. It is determined from a plot of *formation factor* versus porosity on a log-log graph. In chalky rocks and compacted formations, m is approximately equal to 2. For compact limestones, which are highly cemented rocks, the value of m may be as high as 3. When the value of m cannot be determined, the following equations commonly referred to as the Humble formula, can be used to estimate the *formation factor*:

$$F_R = \frac{0.62}{\phi^{2.15}} \quad \text{or} \quad F_R = \frac{0.81}{\phi^2} \quad \text{Eq.3-16}$$

Where as the Humble formula is satisfactory for many types of rocks, better results can be obtained using the following generalized form of the Humble formula:

$$F_R = \frac{a}{\phi^m} \quad \text{Eq.3-17}$$

a is called the Humble factor and varies for different rock types.

Effect of Confining Pressure on Formation Resistivity and Cementation Factor

Many investigations have studied the effect of confining pressure on the *cementation factor*, mostly with sandstone rocks, but also with carbonate rock materials, glass beads and sand bonded with epoxy resins (Fatt, 1957; Wyble, 1958; Glandville, 1959; Brace *et al.*, 1965, 1968; Helander and Campbell, 1966; Timur *et al.*, 1972; Focke and Munn, 1987; and Longeron *et al.*, 1989). All investigators concluded that the increase in *formation factor* and *cementation factor* is increased as confining pressure increased and that is greater than the corresponding decrease in porosity. This means that m is a function of pressure even after correction for porosity because the *formation factor* is change due to deformation of pore structure as a result of applying stress. Brace *et al.* (1965) and Wyble (1958) attributed the change of *formation factor* and *cementation factor* by pressure to the closure of the crack-like pore space known to be present in both carbonate and sandstone rocks. Helander and

Campbell (1966) believed change in these two parameters by pressure is due to increase in pore constriction factor. Glandville (1959) showed that increase in *formation factor* and *cementation factor* by pressure is pronounced in medium to low-porosity sandstone samples. Fatt (1957) showed that the increase in electrical resistivity (increase in m) by compression is smaller for rocks that contain conductive solids, assumed to be clays. He also showed that after correction for clay effect, m is only a function of the net confining pressure. In carbonate rocks, m seems to vary less with pressure, as shown by Longeron *et al.* (1989).

Effect of Temperature on Formation Resistivity and Cementation Factor

Another important factor that should be accounted to have effect on measurement of the *formation factor* and *cementation factor* is the temperature. The *cementation factor* has been found, in general, to increase with an increase in temperature in shaly sandstones (Barnnan and Gonten, 1973) and Berea sandstones (Sanyal, 1972). Dolka (1981), however, found that cementation of some sandstones from Saudi Arabian reservoirs decreased when temperature increases. He also found that limestones did not show any significant change in resistivity with change in temperature. Sanyal (1972) found that the rate of change of F_R and m with temperature was a function of both the ion-exchangeable clay content and the internal surface area. However, they concluded that the change in the pore-constriction factor was the primary reason for this. This observation was contradicted by Waxman and Smith (1968), Clavier *et al.* (1984) and Waxman and Thomas (1974) by concluding that changes in temperature did not affect the *cementation factor* when they corrected for clay amounts.

Cementation Factor and Separate-Vug Porosity

Laboratory (Lucia, 1983) and borehole (Lucia and Conti, 1987) data have demonstrated that *cementation factor* value is a function of the ratio of separate-vug porosity to total porosity, a ratio referred to as the vug porosity ratio (VPR) (Figure 3.6). Brie *et al.* (1985) developed the similar relationship using a model composed of spherical pores. The *cementation factor* shows a positive trend with the ratio between separated-vuggy porosity to the total porosity.

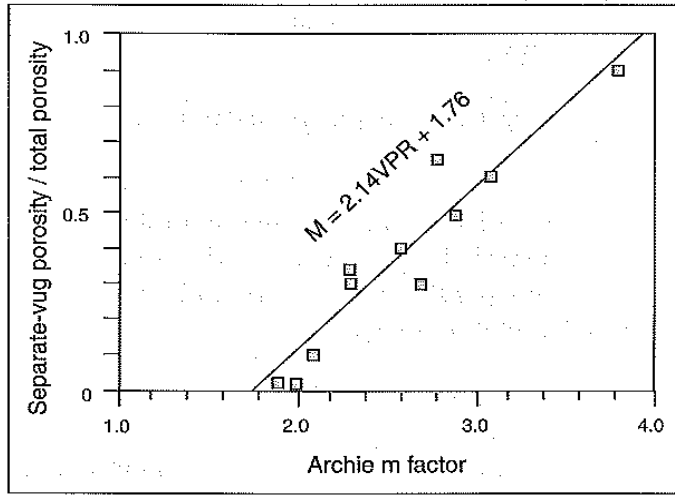


Figure 3.6: Relationship between Archie cementation factor and the ratio of separate-vug porosity and total porosity (Vug-porosity, VPR). (Adapted from Lucia (1983).)

Tortuosity Factor

The departure of the porous system from being equivalent to a system made up of straight capillary tubes is measured by the *tortuosity factor*, τ . By definition, the *tortuosity factor* is defined as:

$$\tau = \left(\frac{L_a}{L} \right)^2 \quad \text{Eq.3-18}$$

L_a is the actual length of the flow and L is the length of the rock sample. For the inclined capillary tube model of porous media, Cornell and Katz (1953) derived the following relationship between *formation factor*, F_R , porosity, Φ and *tortuosity factor*, τ :

$$F_R = \left(\frac{L_a}{L} \right) \frac{1}{\phi} = \frac{\sqrt{\tau}}{\phi} \quad \text{Eq.3-19}$$

The same expression was introduced by Wyllie and Rose (1950) and for a more complex capillary tube model; Wyllie and Gardner (1958) proposed the following equation:

$$F_R = \frac{\sqrt{\tau}}{\phi^2} \quad \text{Eq.3-20}$$

Studies by Winsauer *et al.* (1952) on natural cores yielded the following equation:

$$\tau = (F.\phi)^{1.2} \quad \text{Eq.3-21}$$

Effect of Dead-End Pores on Electrical Properties

If an electric current is passed through a block of non-conducting porous rock saturated with a conducting fluid, only a portion of the pore space participates in the flow of electric current. Therefore, the total porosity, Φ_T can be divided into two parts as described by Rosales (1982):

$$\phi_T = \phi_f + \phi_s \quad \text{Eq.3-22}$$

where, Φ_f and Φ_s are flowing porosity associated with the channels and the porosity associated with the regions of stagnation (traps) in a porous rock, respectively. Figure 3.7 shows that the electrical current can flow only through the channel indicated by C, whereas no current can flow through the traps indicated by T.

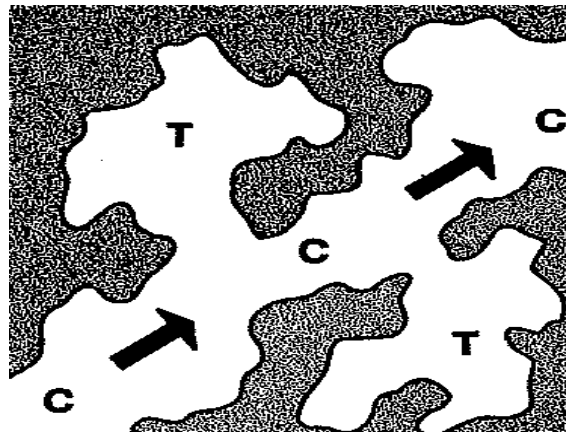


Figure 3. 7: Portions of porous rock showing an open or symmetry trap. (Adapted from Rosales, 1982.)

In Figure 3.7, the traps are of the dead-end pore types. Rosales (1982) derived a general relationship between formation resistivity factor and flowing porosity, Φ_f as:

$$F_R = 1 + G \left(\frac{1}{\phi_f} - 1 \right) \quad \text{Eq.3-23}$$

$$\phi_f = \phi^m \quad \text{Eq.3-24}$$

Where G is defined as the internal geometry parameter of the porous rock and ϕ^m is considered as the flowing porosity. If $G=1$, Eq.3-23 gives the Archie formula. Rosales (1982) also developed a relationship between *tortuosity factor*, τ and flowing porosity, Φ_f :

$$\tau = \phi \cdot \left[1 + G \left(\frac{1}{\phi_f} - 1 \right) \right] \quad \text{Eq.3-25}$$

Inasmuch as the value of G is approximately equal to unity for most porous rocks, Eq.3-25 can be written as:

$$\tau = 1 + \frac{\phi_T}{\phi_f} \quad \text{Eq.3-26}$$

Resistivity Index

In a formation containing oil or gas or both, with a certain amount of water, the resistivity is only a function of water saturation, S_w , since oil and gas are not conductors of electricity. For a partially brine saturated rock, the true resistivity of the rock, R_t is larger than the resistivity of the same rock 100% brine saturated, R_o . Archie (1950) defined the ratio of true formation resistivity, R_t to the resistivity of the same rock 100% brine saturated, R_o as:

$$I_R = \frac{R_t}{R_o} \quad \text{Eq.3-27}$$

For a partially brine saturated rock, Archie (1950) determined experimentally a relationship between the water saturation, S_w and resistivity index, I_R as:

$$S_w = \left(\frac{1}{I_R}\right)^{\frac{1}{n}} = \left(\frac{R_o}{R_t}\right)^{\frac{1}{n}} = \left(\frac{aR_o}{\phi^m R_t}\right)^{\frac{1}{n}} \quad \text{Eq.3-28}$$

n is referred to as saturation exponent. The resistivity index is then a function of the salinity, amount of formation water and how it is been distributed. It is also a function of the amount, distribution, and types of clays present in the formation under evaluation. For instance, the presence of cation exchangeable clays, such as *smeectites*, typically causes a low resistivity index.

Anderson (1986c) examined the effects of wettability (tendency of a fluid to wet its surface) on the saturation exponent and found that:

- 1) n is essentially independent of wettability when the brine saturation is sufficiently high to form a continuous film on the grain surfaces of the porous medium and consequently to provide a continuous path for a current flow. This continuity is common in clean and uniformly water-wet systems and n remains constant around 2 as the water saturation is lowered to its irreducible value, S_{wi} .
- 2) In uniformly oil wet systems, with low brine saturation, large values of the saturation is expected (10 or higher).

The exponent n must be measured at reservoir conditions, i.e., on native or restored-state wettability cores. Sweeney and Jennings (1960) investigated the effect of wettability on electrical properties for carbonate cores. They found that the saturation exponent ranged from 1.6 to 1.9 for water-wet cores, where as oil-wet cores shows two different values. In some cores, n was about 8 even when water saturation was very high. In other cores, the value of n was similar to the water-wet and naturally wet, i.e., $1.5 < n < 2.5$, until a brine saturation of nearly 35% was reached, at which n increased rapidly to 12.

Longeron *et al.* (1989) and Lewis *et al.* (1988) showed that saturation history of the formation has a considerable effect on the saturation exponent, particularly in a water-wet porous system. Both studies found that there is a significant resistivity and saturation

hysteresis between drainage (non-wetting phase displaces wetting-phase) and imbibition (opposite to drainage) saturation cycles. This is because of difference in water and oil distribution for imbibition and drainage processes.

3.4. Miscible Displacement in Porous Media

Local displacement efficiency in miscible floods is significantly affected by mixing taking place in the medium. Mixing in porous medium originates from a complex interplay of *molecular diffusion* and *convective spreading* (mechanical mixing).

Fick's Laws for Diffusion

Diffusion is the result of random motion of molecules when two miscible fluids are in contact with an initially sharp boundary. The concentration gradient between fluids causes the solute molecules to move, on an average, from high concentration regions to low concentration regions. The diffusive flux, J is described by Fick's first law:

$$J = -D_o \frac{dC}{dx} \quad \text{Eq.3-29}$$

where D_o is diffusion coefficient and the derivative is concentration gradient. Fick's first law describes instantaneous diffusive flux across a cross-section. It does not describe how solute concentration changes with time and space due to diffusion. From mass conservation we know that:

$$\frac{\partial c}{\partial t} = -\frac{\partial J}{\partial x} \quad \text{Eq.3-30}$$

Differentiating Fick's equation with respect to x and using the mass balance equation, we get:

$$\frac{\partial C}{\partial t} = D_o \frac{\partial^2 C}{\partial x^2} \quad \text{Eq.3-31}$$

This is the Fick's second law of diffusion. In the case of diffusion through porous media, the cross section area for diffusion is reduced. Moreover, the path length for diffusion is

increased because of the tortuous path through the medium. Noting that laws governing electrical conductivity and diffusion in porous media are analogous, it is shown that diffusion coefficient in porous media is related to *formation resistivity factor* (Perkins and Johnson, 1963; Lake, 1989):

$$D = \frac{D_o}{F_R \phi} = \frac{D_o}{\tau} \quad \text{Eq.3-32}$$

When a solute slug moves through a porous medium, there is additional mixing due to convection. The complex network of interconnected pores causes solute particles to take tortuous paths. Variation in local velocity, both magnitude and direction, along the tortuous flow paths cause solute particles to spread. This is called convective spreading and it is governed by the pore structure. To describe the combined effects of diffusion and convective spreading, a term “dispersion coefficient” is used.

The Convection-Diffusion Equation

For an isothermal miscible-displacement, incompressible fluid and rock, homogenous permeable medium, and one dimensional system, the convection-diffusion equation (CDE) is written as (Lake, 1989):

$$\phi \frac{\partial C}{\partial t} + u \frac{\partial C}{\partial x} - \phi K_l \frac{\partial^2 C}{\partial x^2} = 0 \quad \text{Eq.3-33}$$

CDE describes the conservation of the displacing component with mass concentration C . In the Eq.3-33, u is the Darcy velocity, ϕ is the porosity and K_l is *longitudinal dispersion coefficient*. In dimensionless terms, Eq.3-33 becomes:

$$\frac{\partial C_D}{\partial t_D} + \frac{\partial C_D}{\partial x_D} - \frac{1}{N_{pe}} \frac{\partial^2 C_D}{\partial x_D^2} = 0 \quad \text{Eq.3-34}$$

where dimensionless terms are defined as: Dimensionless concentration,

$$C_D = \frac{C - C_I}{C_J - C_I} \quad \text{Eq.3-35}$$

where C_I is the initial concentration, C_J is the injection concentration.

Dimensionless time (pore volume injected), t_D

$$t_D = \frac{qt}{AL\phi} = \frac{vt}{L} \quad \text{Eq.3-36}$$

where v is the interstitial velocity, L is the length of the permeable medium, t is the injected time, A is the cross-section of the permeable medium, and q is the injection rate.

The dimensionless distance is, x_D

$$x_D = \frac{x}{L} \quad \text{Eq.3-37}$$

The *Peclet number*, N_{Pe} is defined as:

$$N_{Pe} = \frac{vL}{K_L} \quad \text{Eq.3-38}$$

In order to solve Eq.3-34, the following boundary conditions can be applied:

$$C_D(x_D, 0) = 0 \quad x_D \geq 0 \quad \text{Eq.3-39}$$

$$C_D(x_D \rightarrow \infty, t_D) = 0 \quad t_D \geq 0 \quad \text{Eq.3-40}$$

$$C_D(x_D \rightarrow -\infty, t_D) = 1 \quad t_D \geq 0 \quad \text{Eq.3-41}$$

The analytical solution to Eq.3-34 for injection of a tracer slug of size t_{DS} pore volume is (Lake, 1989):

$$C_D = \frac{1}{2} \left[1 - \operatorname{erf} \left\{ \frac{x_D - (t_D - t_{DS})}{2 \sqrt{\frac{t_D - t_{DS}}{N_{Pe}}}} \right\} \right] + \frac{e^{x_D N_{Pe}}}{2} \left[1 - \operatorname{erf} \left\{ \frac{x_D - t_D}{2 \sqrt{\frac{t_D}{N_{Pe}}}} \right\} \right] \quad \text{Eq.3-42}$$

Here erf is the error function and Figure 3.8 shows the concentration profiles predicted by Eq.3-44 with different *Peclet numbers* at a dimensionless time of 0.5 (half of pore volume injected). A large *Peclet number* (>100) yields a sharp displacement front (almost no mixing) and a small number (<100), a more spread out one (significant mixing).

Dispersion Coefficient

In an ideal porous medium and conventional Fickian representation, dispersion is treated in the same manner as diffusion. Along the flow, *longitudinal dispersion coefficient*, K_l is estimated by approximating the distance x over which the fluid travels before mixing, is on the average equal to particle diameter, D_p , and the corresponding time t . The corresponding time t is equal to D_p/v , where v is the interstitial velocity and by adding diffusion term, K_l is expressed as:

$$K_l = \frac{D_o}{F\phi} + \frac{D_p \cdot v}{2} \tag{Eq.3-43}$$

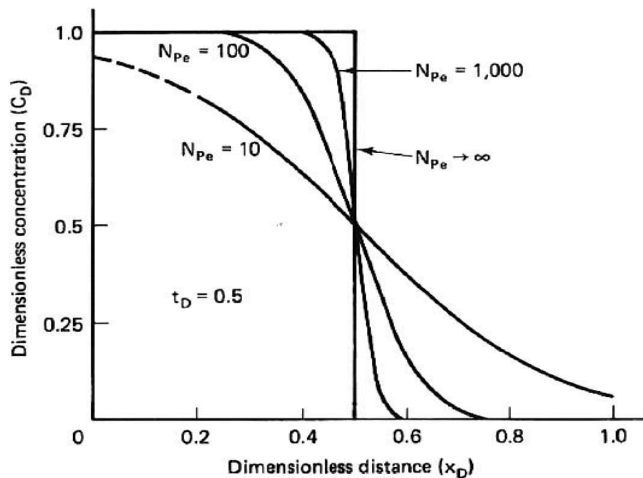


Figure 3.8: Tracer concentration profiles in one-dimensional flow for varying Peclet numbers. (Adapted from Lake, 1989.)

The above model assumes that the porous medium is of uniform pore size and packing. Taylor (1953) derived an expression for dispersion in flow with the average velocity \bar{v} through a capillary tube with radius R as:

$$K_L = D_o + \frac{\bar{v}^2 R^2}{48 D_o} \quad \text{Eq.3-44}$$

Real porous media are more complex than a bed of uniform spheres and a series of capillary tubes. Besides a non-uniform distribution of pore or particle sizes, some other mechanisms also affect dispersion. These include the presence of other, unequal viscosities and densities, and turbulent flow (Perkins and Johnson, 1963). These mechanisms will cause the longitudinal dispersion to be larger than the model given above.

Taking these factors into consideration, for one dimensional flow, the general term for *longitudinal dispersion coefficient*, K_L can be written as (Lake, 1989):

$$\frac{K_L}{D_o} = C_1 + C_2 \left(\frac{v D_p}{D_o} \right)^\beta \quad \text{Eq.3-45}$$

where $C_1 = I / (F_R \Phi)$, C_2 , and β are properties of the permeable medium and flow regime. Experimentally, β has been found in the range of 1-1.25 (Perkins and Johnson, 1963).

Dispersion coefficient has a tensorial form. This observation was verified experimentally by Bear (1972) by observing the dispersion of a tracer from a point source. Biggar and Nielsen (1960) studied the effects of the rock types and particle size and Skibitzke and Robinson (1963) obtained qualitative laboratory results to demonstrate the importance of heterogeneity in dispersion phenomena. Deans (1963) has shown that well-stirred tanks in series give mixing zones that can be described by dispersion coefficients proportional to velocity.

Figure 3.9 shows three flow regimes from Perkins and Johnson (1963), which experimentally confirms Eq.3-45 and shows the relative importance of convection to diffusion.

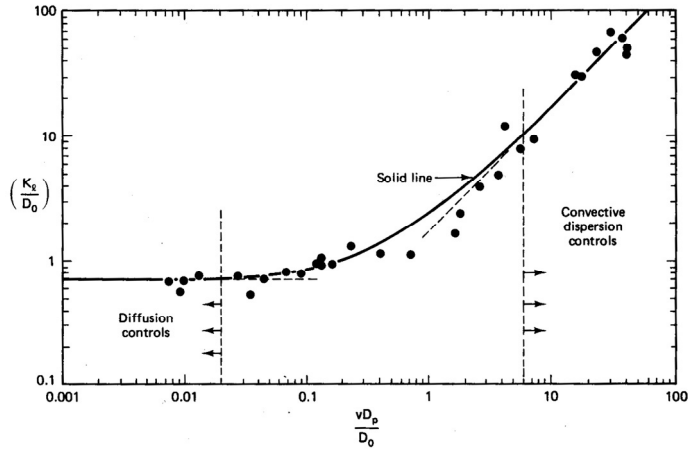


Figure 3.9: Longitudinal dispersion coefficients in permeable media flow. D_o is the effective diffusion coefficient, D_p is an average particle diameter, K_l is longitudinal dispersion coefficient, and v is interstitial velocity. (After Perkins and Johnston, 1963.)

If the interstitial velocity is greater than about 3 cm/day, the local mixing term in Eq.3-45 dominates the first term, and it is written as:

$$K_l = \frac{D_o}{\phi.F_R} + C_2 \left(\frac{v.D_p}{D_o} \right)^\beta . D_o \cong \alpha_L v \quad \text{Eq.3-46}$$

where α_L is the *longitudinal dispersivity* of the permeable medium and also a measure of the local heterogeneity scale. For the local mixing flow regime, α_L is a more fundamental measure of dispersion than *longitudinal dispersion coefficient* K_l .

The dispersivity of a given porous medium is usually measured by performing a one-dimensional miscible displacement experiment. A solute (typically a tracer or diluted brine solution) is introduced with a step change in concentration at the inlet, then Eq.3-42 is fitted to the effluent concentration history and *dispersivity* is estimated (Figure 3.10).

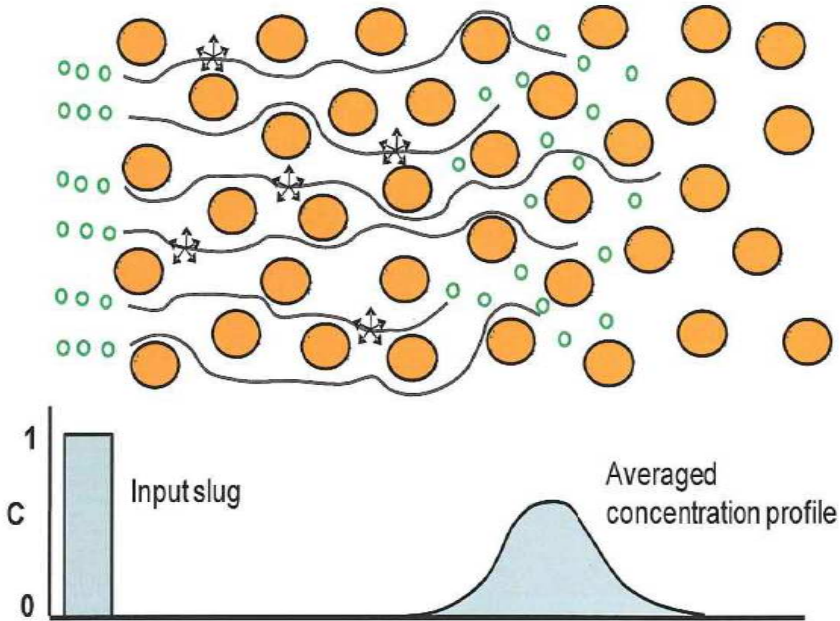


Figure 3.10: Schema of a slug injection of a solute into a given porous medium (a plus injection) and response of the material due to dispersion.

Figure 3.11 shows the *longitudinal dispersion coefficient* versus the mean flowing velocity of the measurement reported by various authors. (Baker, 1977; Batycky *et al.*, 1982; Salter and Mohanty, 1982; Kasraie and Farouq Ali, 1984; Delshad *et al.*, 1985; Bretz *et al.*, 1988).

As seen from Figure 3.11, there is a general trend for dispersion coefficient versus the mean flowing velocity which is adequate with Eq.3-46.

It should be noticed that for fast displacement, the diffusion is not negligible especially for several phenomena involving flow around stagnant regions of porous medium such as dead-end pores, water blocked pores, and adjacent nonflowing zones (Lake, 1989).

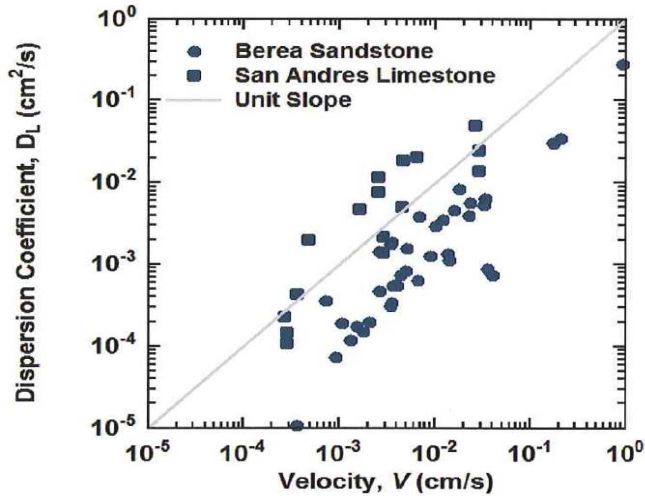


Figure 3.11: Dispersion coefficient estimated for the consolidated porous media. The slope shows the longitudinal dispersivity. (Adapted from Jha, 2005.)

Dimensionless Mixing Zone

When analyzing the efficiency of recovery process, a measure of interest is the dimensionless mixing zone. This is defined as (Lake, 1989):

$$\Delta x_D = \frac{(x_{CD=0.9} - x_{CD=0.1})}{L} \quad \text{Eq.3-47}$$

In Eq.3-44, the second term is usually neglected because its contribution becomes small at *Peclet numbers* larger than 50. With this simplification, Eq.3-42 can be rearranged to solve for mixing zone size defined by Eq.3-47, giving:

$$\Delta x_D = 3.625 \sqrt{\frac{t_D}{N_{pe}}} \quad \text{Eq.3-48}$$

By combining Eq.3-46 and Eq.3-48, the mixing zone length equation can be written as:

$$\Delta x_D = 3.625 \sqrt{\left(\frac{\alpha_L}{L}\right) t_D} \quad \text{Eq.3-49}$$

Eq.3-49 relates the mixing zone to the *dispersivity* which is the more direct measurement of the mixing length and the mixing zone growth is proportional to the square root of the dimensionless travelling time.

Effect of Dead-End Pores on Dispersion

In order to include the effect of dead-end pores and stagnant volume on mixing, Deans (1963) proposed a capacitance model to analyze asymmetrical effluent profiles observed by tracer injection into porous media. In his model, three parameters mainly describe dispersion in the porous media; number of stages, stagnant volume and mass transfer constant representing mass transfer between stagnant volume and flowing stream.

Coats and Smith (1963) by involving diffusion to Deans's model (1963), simulated experimental data of tracer profiles showing the tailing due to the mass-exchange between flowing volume and dead-end pores. Coats and Smith's (1963) model is in fact the corrected form of the (CDE) and is introduced by two equations:

$$K_1 \frac{\partial^2 c}{\partial x^2} - v \frac{\partial c}{\partial x} = f \frac{\partial c}{\partial t} + (1-f) \frac{\partial c^*}{\partial t} \quad \text{Eq.3-50}$$

$$(1-f) \frac{\partial c^*}{\partial t} = M(c - c^*) \quad \text{Eq.3-51}$$

where f is the fraction of the non-stagnant volume, M is the mass-exchange constant between the stagnant volume and flowing volume, C^* is the concentration at the stagnant volume, and C is the concentration of flowing part in the medium. The first equation is derived from material balance and the second equation describes the mass transfer between stagnant volume and flowing part. By representing the stagnant pores as “dimples” (Figure 3.12) with the volume V_s , cross-section area A , the length L , and the molecular diffusion with the coefficient D_o , as the main mechanism for mass exchange; M can be expressed as (Coats and Smith, 1963):

$$M = \frac{D_o A}{L} \quad \text{Eq.3-52}$$

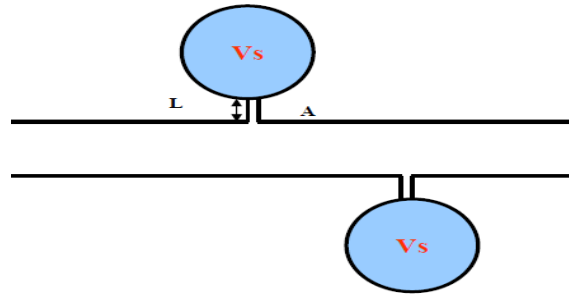


Figure 3.12: Schema of the stagnant volume and connected pores. The stagnant volume is modeled as dimples.

However, M is also velocity dependent as shown by different authors (Coats and Smith, 1963; Goddard, 1966; Baker, 1977).

The solution of Eq.3-50 and Eq.3-51 was given by Coats and Smith (1963). Brigham (1974) showed that for both standard diffusion and differential-capacitance models, different boundary conditions almost give the same solution.

By using Eq.3-50 and Eq.3-51, fraction of dead-end pores ($I-f$), dispersion coefficient K_t , and mass transfer constant M , can be determined from tracer analysis in the porous media.

Scale Dependency for Dispersivity

Numerous studies have shown that the *dispersivity* measured in the laboratory scale fails to give adequate description of the transport behavior on the field scale. Coats and Smith (1963) used the convective-diffusion equation in addition to their capacitance model to fit their experimental data. It was also shown that a significant mixing that occurs in the laboratory cores is impacted by the capacitance effect (tailing observed in the tracer profile due to the stagnant volume). This may lead to overestimation of the dispersion coefficient if CDE is used. Coats and Smith (1963) also showed that on the field scale, the contribution of the stagnant volume to mixing is not significant. Overestimation of the dispersion coefficient in laboratory measurements artificially determines a mixing zone as is revealed from Eq.3-46 and Eq.3-49.

Figure 3.13 shows the *dispersivity* measured in the laboratory core scale and field scale reported by different authors (Pickens and Grisak, 1981; Gelhar *et al.*, 1985; and Arya, 1988). As seen, dispersivity on the field scale is found to be larger than that in laboratory scale by several orders of magnitude. The trend in Figure 3.13 can be qualitatively explained by the fact that the scale of heterogeneity from a given measurement increases as the sample volume increases.

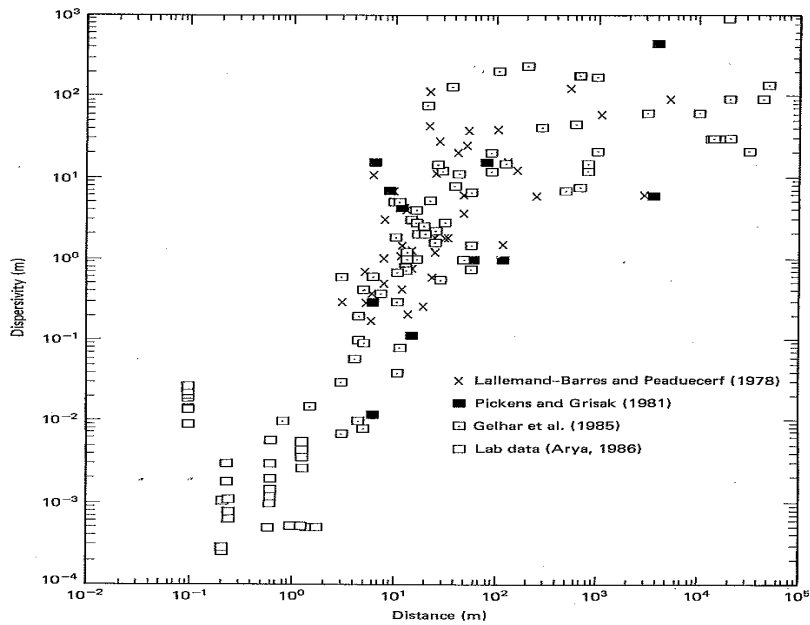


Figure 3.13: Field and laboratory measured dispersivities. (Adapted from Lake, 1989.)

However, it is difficult to judge if the field measured *dispersivities* continue to increase indefinitely or reach an asymptotic value as suggested by standard theories.

Another limitation to applying dispersion measurements from laboratory scale to the field scale is the limitation of laboratory data to only one dimension. In the field scale, dispersion can take place perpendicular to the flow direction which is referred to as the *transverse dispersion* characterized by *transverse dispersivity*. Bear (1972) used the concept of the *dispersivity tensor* to further parameterize the dispersion tensor on the basis of geometrical arguments. *Transverse dispersivity* is about ten to thirty times smaller than *longitudinal*

dispersivity (Perkins and Johnson, 1963; Grane and Gardner, 1961). Gelhar *et al.* (1992) concluded that *transverse dispersivity* is not significantly increased with increase in measurement volume.

Remarkable review by Makuch (2005) also shows the scale-dependency of the *longitudinal dispersivity*. Figure 3.14 shows the *longitudinal dispersivity* for different rocks including sandstones and carbonates. As it is seen, carbonate rock materials have higher *longitudinal dispersivity* with the same range of the scale than sandstone rock materials. This can be explained due to more heterogeneity in carbonates because of various pore types and structural complexities.

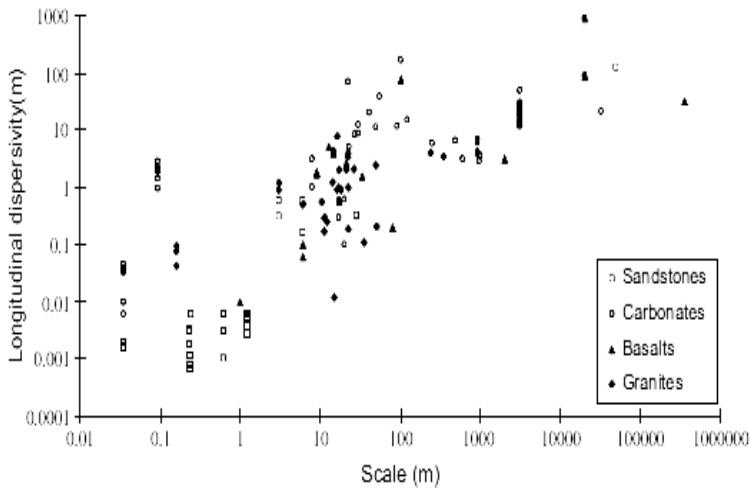


Figure 3.14: Relationship of longitudinal dispersivity to scale of measurement for various rock types. (Adapted from Makuch, 2005.)

3.5. Summary

In this chapter, theoretical backgrounds of single-phase flow properties were presented with their application to characterize porous media. These flow properties characterize various aspects of heterogeneities of porous media.

The applied methodologies to obtain these single-phase flow properties were also reviewed. Particular implementations of these flow properties on carbonates were briefly explained.

CHAPTER 4

Two-Phase Fluid Flow Properties in Porous Media

In the previous chapter, single-phase fluid properties of porous media were reviewed and some of its applications toward carbonate reservoir characterization were summarized.

In this chapter, two-phase flow properties such as capillary pressure, relative permeability, and wettability and its effect on these properties are reviewed. These properties describe the fundamental of the immiscible two-phase flow displacement in porous media. In this thesis, water flooding was applied and therefore, only fluid flow properties for two-phases of water and oil are discussed.

4.1. Capillary Pressure

Definition of Capillary Pressure

The difference in pressure across a curved boundary between two immiscible fluids is called capillary pressure. Concerning wettability, the capillary pressure is defined as the pressure difference between non-wetting and wetting phases. For a system consisting of water as the wetting and oil as the non-wetting phase, the capillary pressure is defined as:

$$P_C = P_o - P_w \quad \text{Eq.4-1}$$

where P_o is the pressure in the oil phase and P_w is the pressure in the water phase. At the pore scale within a given porous medium containing water and oil, the interface between oil and water is curved and as a result, the pressure abruptly increases across the interface to balance the interfacial tension. This pressure jump, which is the capillary pressure, is expressed by the Young-Laplace equation (Leverett, 1941; Adamson, 1982) as:

$$P_C = \sigma_{ow} \left(\frac{1}{R_1} \pm \frac{1}{R_2} \right) \quad \text{Eq.4-2}$$

where σ_{ow} is the interfacial tension between oil and water, R_1 and R_2 are the radii of the interface curvatures measured perpendicular to each other. Depending on the curvature of the interface, capillary pressure can be negative or positive.

For a capillary tube with the radius R at the equilibrium, the capillary pressure can be expressed by the Young-Laplace equation as (Amyx *et al.*, 1960):

$$P_c = \frac{2\sigma_{ow} \cos\theta_{ow}}{R} \quad \text{Eq.4-3}$$

θ_{ow} is the contact angle between the oil and water interface measured through water as the dense phase. The capillary pressure in the porous media depends on wettability, interfacial tension between fluids, pore geometry, pore size and pore size distribution, and the history of the displacement (Anderson, 1987a; Craig, 1971; Dullien, 1992).

Imbibition and Drainage Processes and Hysteresis

Two basic types of immiscible displacement of two phases can occur in the porous media: wetting phase displaces non-wetting phase (this is called the imbibition process) or vice versa (referred to as the drainage process). The capillary path shows hysteresis for these two different processes. For a water/oil system and water-wet condition, imbibition refers to water displacing oil. Figure 4.1 shows the measured capillary pressure for both imbibition and drainage processes for a Berea sandstone core sample (Killins *et al.*, 1953). As shown, imbibition capillary pressure in this case does not overlap the drainage capillary pressure as the water saturation is reversed. The difference between these two is referred to as capillary pressure *hysteresis*.

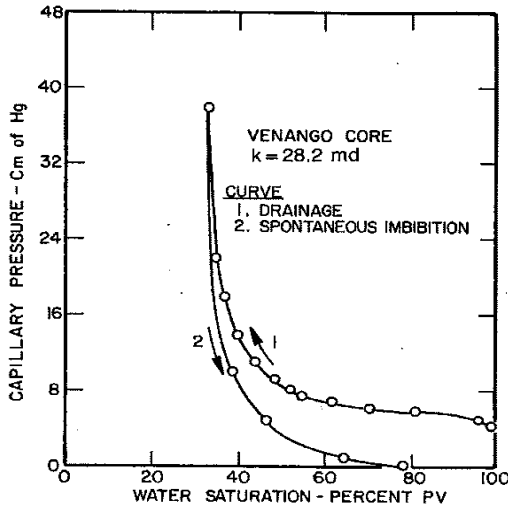


Figure 4.1: Oil/water capillary pressure curve measured on a sandstone core. (Adapted from Killins et al., 1953.)

Macroscopically, there are two reasons for the capillary pressure *hysteresis*: *drag hysteresis* and *trapping hysteresis* (Craig, 1971; Lake, 1989). The *drag hysteresis* or *contact angle hysteresis* is due to the difference in the contact angle during the drainage and imbibition processes. During the drainage process, the wetting phase is pushed back from surfaces it previously covered, so the contact angle between fluids will be receding angle $\theta_{rec.}$, but during the imbibition process, wetting phase saturation increases and the non-wetting phase is pushed from the pore walls and the contact angle advances. The *trapping hysteresis* is trapping of the non-wetting phase due to the capillary retention. Lake (1989) and Stegemeier (1974) explained the physics of *trapping hysteresis*, and the numerical simulation of *hysteresis* is discussed by Aziz and Settari (1979) and Killough (1976).

Capillary Pressure Functions

Leverett (1941) demonstrated that a single, dimensionless capillary pressure function could represent a geological formation, independent of variations in pore size distribution. The Leverett (1941) function, J as a function of the non-wetting phase saturation is expressed as:

$$J(S_{nw}) = \frac{P_c \sqrt{\frac{K}{\phi}}}{\sigma \cos \theta}$$

Eq.4-4

Rose and Bruce (1949) proposed the Leverett J function (1941) for correlating capillary pressure. Brown (1951) found that the use of this J -function is successful in correlating capillary pressure data on a number of limestone core samples.

Other capillary functions have also been proposed by authors in the past (Burdine, 1953; Brooks and Corey, 1964; Bensten and Anlie 1977; Schumaker, 1981; Skjæveland *et al.*; 2000; Lomeland and Ebeltoft, 2008). All these capillary functions are mathematical or empirically derived formulas that relate the capillary pressure to wetting (or non-wetting) phase saturation. Correlations by Burdine (1953) and Skjæveland *et al.* (2000) are focused here because they will be used in the next chapter to simulate experimental data of water flooding.

Burdine (1953) proposed a power-law capillary pressure function to the normalized water saturation derived from drainage process:

$$P_C = P_{cd} \cdot (S_w^*)^{-\frac{1}{\lambda}} \quad \text{for } P_{cd} > 0 \quad \text{Eq.4-5}$$

$$P_C = P_{cd} \cdot (S_w^*)^{-\frac{1}{\lambda}} - 1 \quad \text{for } P_{cd} = 0 \quad \text{Eq.4-6}$$

where λ is related to the pore size distribution, P_{cd} is the entry pressure or threshold pressure, and S_w^* is the normalized water saturation defined as:

$$S_w^* = \frac{S_w - S_{wi}}{1 - S_{wi} - S_{or}} \quad \text{Eq.4-7}$$

where S_w is the water saturation, S_{wi} is the irreducible water saturation, and S_{or} is the residual oil saturation. Recently, Skjæveland *et al.* (2000) introduced a new capillary correlation which can be used mostly for both mixed-wet and strongly wet systems. It is expressed as:

$$P_C = \frac{c_w}{\left(\frac{S_w - S_{wi}}{1 - S_{wi}} \right)^{a_w}} - \frac{c_o}{\left(\frac{S_o - S_{or}}{1 - S_{or}} \right)^{a_o}} \quad \text{Eq.4-8}$$

where a_w and a_o are defined as shape factors, c_o and c_w are respective threshold pressures. These parameters have constraints:

$$c_w \geq 0$$

$$c_o \geq 0$$

$$a_w, a_o \in [0.25, 2.0]$$

Measurement of Capillary Pressure and Applications

Methods of capillary pressure measurements are described in the Table 4.1. With the exception of the mercury injection method, which is only designed for the drainage process, other methods can be performed for both drainage and imbibition processes.

Table 4.1: Comparison of methods for capillary pressure measurement. (Adapted from Torsæter and Abtahi, 2000)

Method	Fluid type	P_c curve type	Max. ΔP in lab.	Test time
Porous plate	Oil-water Gas-water Gas-oil	Imbibition Drainage	2-5 atm.	Weeks
Mercury injection	Hg-air	Drainage	100 atm.	Minutes
Centrifuge	Gas-water Oil-water Gas-oil	(Imbibition) Drainage	10 atm.	Days
Dynamic	Gas-water Gas-oil Oil-water	(Imbibition) Drainage	1-10 atm.	Days

The centrifuge method that is in general use now was first introduced by Hassler and Brunner (1945) and further developed by Slobod *et al.* (1951). The core is placed in a cup containing an extended calibrated small-diameter tube where fluids displaced from the core by centrifugal force are collected. Figure 4.2 shows a core sample with the length L in a centrifuge with rotational speed ω .

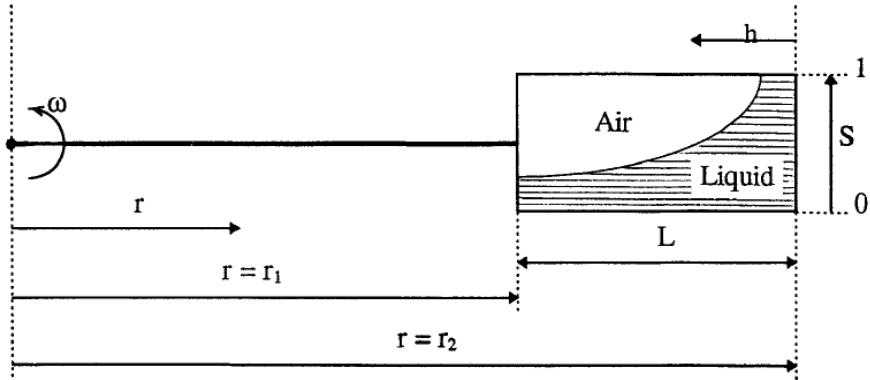


Figure 4.2: Schematic diagram of a core in a centrifuge and its boundary conditions.

The capillary pressure can be calculated by the following equation:

$$P_{cL} = P_c(L) = \frac{1}{2} \Delta \rho \omega^2 (r_2^2 - r_1^2) \quad \text{Eq.4-9}$$

where P_{cL} is capillary pressure measured in the inlet face of the core, r_1 and r_2 are distances from the end faces of the core sample to the center of the axes of the rotation, and $\Delta \rho$ is the density difference between displacing and displaced fluids. The derived capillary pressure can be expressed as a function of the average water saturation \bar{S} or the inlet face saturation S_L .

Most centrifuge data reported in the literature adopt the boundary condition assumed by Hassler and Brunner (1945), i.e., the end face of the core sample remains 100% saturated with the wetting phase ($P_c=0$) at all centrifugal speeds of the test. Melrose (1982, 1988) examined the Hassler and Brunner (1945) boundary condition and concluded that zero capillary pressure assumption is valid for the maximum centrifuge speed used in practice.

It should be noticed that there is capillary pressure gradient along the core sample due to the gradient in gravitational forces perpendicular to the axial rotation. The length of the core can be considered negligible with respect to the radius of the centrifuge. Hassler and Brunner

(1945) stated that if the ratio r_1/r_2 is greater than 0.7, the error introduced by this assumption is negligible and Donaldson (1980) showed for the ultracentrifuge application, it is 0.88. It can be shown that there is a relationship between the average saturation \bar{S} and inlet capillary pressure P_{cL} as:

$$\bar{S} P_{cL} = \cos^2 \left(\frac{\alpha}{2} \right) \int_0^{P_{cL}} \frac{S(P_c) d(P_c)}{\sqrt{1 - \frac{P_c}{P_{cL}} \sin^2 \alpha}} \quad \text{Eq.4-10}$$

where

$$\cos \alpha = \frac{r_1}{r_2}, \quad \cos^2 \left(\frac{\alpha}{2} \right) = \frac{r_1 + r_2}{2r_2}, \quad \text{and} \quad \sin^2 \alpha = 1 - \left(\frac{r_1}{r_2} \right)^2$$

If the length of the core sample is neglected, i.e., $r_1 \approx r_2$, then Eq.4-10 can be written as:

$$\bar{S} P_{cL} = \int_0^{P_{cL}} S(P_c) d(P_c) \quad \text{Eq.4-11}$$

In the differential form, the Eq.4-11 can be expressed as:

$$S_L = \frac{d \left(\bar{S} P_{cL} \right)}{dP_{cL}} \quad \text{Eq.4-12}$$

By plotting the $\bar{S} P_{cL}$ results versus the P_{cL} data, and using the numerical derivative, inlet saturation, S_L can be found (Figure 4.3).

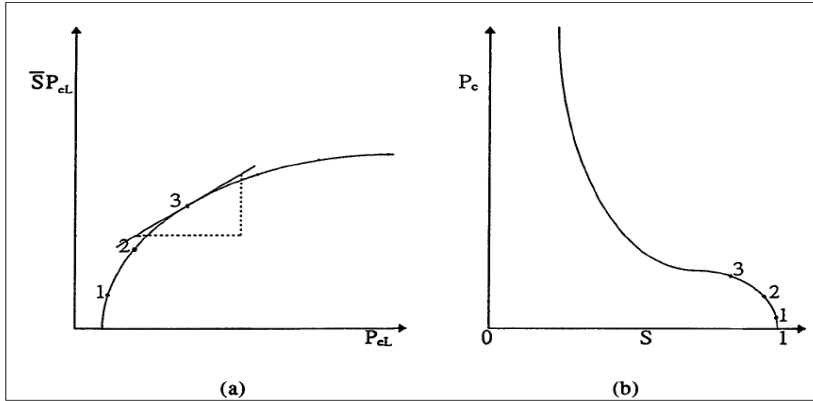


Figure 4.3: A typical SP_{cl} as a function of P_{cl} . Data points indicated on the curves are first, second, and third rotational speeds.

capillary pressure measurement has three main applications: 1) pore size distribution (drainage process), 2) wettability measurement, and 3) simulation of flowing processes.

4.2. Relative Permeability

Definition of Relative Permeability

The basic dynamic property of a porous medium, absolute permeability K , is defined as the ability of the medium to transport fluids. If the medium is completely saturated by a fluid with the viscosity μ , for a laminar flow, incompressible fluids, isothermal condition, and steady-state condition, Darcy's law can be written as:

$$q = \frac{KA}{\mu} \frac{dP}{dx} \tag{Eq.4-13}$$

where A is the cross-section area of the porous medium, dp is the differential pressure along the flow, and dx is the differential length (the ratio of these two denotes the rate of the pressure drop). Eq.4-13 is written for one-dimensional flow and the effect of gravity is neglected. In the reservoir condition, this equation should be written for three dimensions and permeability is treated in the tensorial form.

The concept of the multi-phase flow through the porous media evolved in the 1930s with the extension of Darcy's law for two-phase flow by Muscat (1937). If more than one fluid is present in the porous medium, the ability of the medium to transport one fluid depends on the amount of the other fluid. This is quantified by the effective permeability for a typical fluid which is often less than the absolute permeability. The relative permeability of porous medium to a fluid is defined as the ratio between effective and absolute permeabilities:

$$K_{ri} = \frac{K_i}{k}, \quad i = o, g, w \quad \text{Eq.4-14}$$

where k_{ri} is the relative permeability and K_i is the effective permeability for oil, water, and gas fluids. Relative permeability data are used to quantitatively describe the simultaneous flow of two or more immiscible fluids through porous media. An inherent assumption is that each fluid remains continuous (in perfect pressure communication) and all flow only occurs in one direction. Darcy's law for multi-phase flow is based on a heuristic approach using analogy with single-phase flow.

Factors Effect Relative Permeability

Relative permeability is assumed to be dependent on the saturations of different phases and not the other variables such as pressure, velocity and velocity ratio of fluids. This indeed has been shown to be approximately true for all practical purposes and flow experiments of immiscible fluids carried out by many investigators.

Various factors can affect relative permeability: porosity and permeability, pore size, pore and pore-throat size distributions, wettability, saturation, saturation history, relative dispersion of one phase in other, time of contact of fluids with pore walls, content of polar substances in the oil phase, interfacial tension and density, viscosity, and initial water saturation (Langnes *et al.*, 1972; Standing, 1974, Honarpour *et al.*, 1994). In this chapter only the effect of the saturation history and wettability on the relative permeability is discussed.

Relative Permeability Hysteresis

Similar to the capillary pressure, relative permeability is not only a function of the saturation for a given porous medium; it is also subject to the *hysteresis*. In other words, relative permeability is different for the imbibition process and the drainage process. The *hysteresis*

phenomenon has been described and verified for both gas-oil and water-oil relative permeabilities of sandstone and carbonate rock materials (Geffen *et al.*, 1951; Osoba *et al.*, 1951; Levine, 1954; Josendal *et al.*, 1952; Terwilliger *et al.*, 1951 and Coley *et al.*, 1956).

Figure 4.4 shows the gas-oil and water-oil relative permeabilities for imbibition and drainage processes reported by Osoba *et al.* (1951) and Geffen *et al.* (1951)

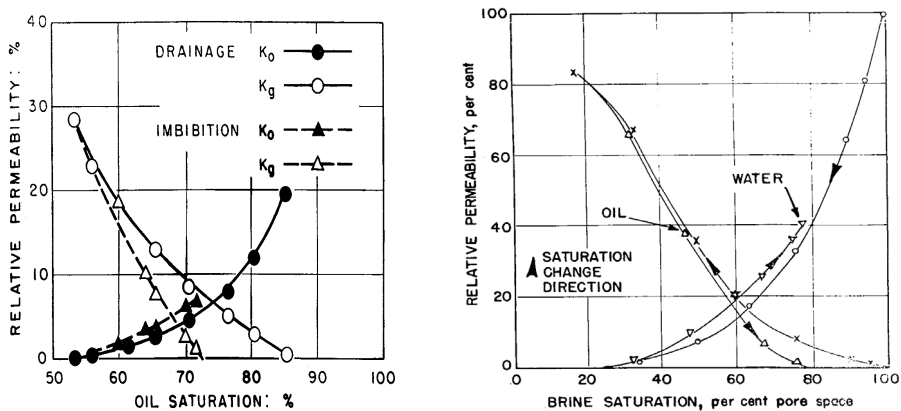


Figure 4.4: Gas-oil relative permeability hysteresis (left). (Adapted from Osoba, 1951.) and water-oil relative permeability hysteresis (right). (Adapted from Geffen, 1951.)

Measurements Methods for Relative Permeability

The relative permeability of a rock to each fluid can be measured in a core sample by either a steady-state or unsteady-state methods (Honarpour *et al.*, 1994). In the steady-state method, a fixed ratio of fluids is injected through the test sample until saturation and pressure equilibrium are established. Different techniques have been reported in the literature for steady-state methods (Morse *et al.*, 1947; Osoba *et al.*, 1951; Richardson *et al.*, 1952; Leas *et al.*, 1950). The primary concern in designing experiments is to eliminate or reduce saturation gradient that can be caused by capillary end-effect. The steady-state method is time-consuming and may take some months.

Unsteady-state relative permeability measurement can be made more rapidly than steady-state measurement, but the mathematical analysis of the unsteady-state is more difficult. The theory developed by Buckley and Leverett (1942) and extended by Welge (1952) is generally used for the measurement of relative permeability under unsteady-state conditions. Details of

measurement of relative permeability and techniques involved are out of the scope of this thesis.

Relative Permeability Functions

Similar to capillary pressure, relative permeability correlations and functions relate the relative permeability only to wetting (or non-wetting) saturations. Different correlations and functions have been proposed by investigators based on theoretical or empirical approaches.

Honarpour *et al.* (1994) classified relative permeability functions into four categories: Capillary models, statistical models, empirical models, and network models. The widely used ones are those suggested by Corey (1954), Sigmund and McCaffery (1979), Chierici (1984) and Lomeland *et al.* (2005). One of the most well known relative permeability correlations is the Corey model (1954). Brooks and Corey (1964, 1966) combined approaches of relative permeability interpretation by Purcell (1949) and Burdine (1953) and introduced relative permeability functions for the drainage process which are simple and expressed in the power law formulas as:

$$k_{r_{wt}} = (S_w^*)^{\frac{2+\lambda}{\lambda}} \quad \text{Eq.4-15}$$

$$K_{r_{nw}} = (1 - S_w^*)^2 \left[1 - (S_w^*)^{\frac{2+\lambda}{\lambda}} \right] \quad \text{Eq.4-16}$$

where $K_{r_{wt}}$ and $K_{r_{nw}}$ denote the wetting phase and non-wetting phase relative permeabilities respectively, while S_w^* is calculated based on the capillary pressure P_c as:

$$S_w^* = \left(\frac{S_w - S_{wi}}{1 - S_{wi}} \right) = \left(\frac{P_b}{P_c} \right)^\lambda \quad \text{Eq.4-17}$$

where P_b is a measure of the minimum capillary pressure and λ is a measure of the pore size distribution and both parameters are constant derived by log-log plot of S_w^* versus P_c .

In general, Corey's (1964, 1966) type of relative permeability for water and oil is expressed as:

$$K_{ri} = K_{ri}^o (S_w^*)^{n_i} \quad i = o, w \quad \text{Eq.4-18}$$

where k_{ri}^o are the end-point relative permeabilities to oil and water, n_i is the saturation exponent for oil and water. The exponent has value for rocks with perfectly uniform pore size distribution. Corey and Rathjens (1956) concluded that the equations are not valid when stratification, solution channels, fractures or extensive consolidation is present and it seems that they are valid mostly for consolidated rocks with mostly intergranular porosity.

For heterogeneous carbonates, the correlation by Sigmund and McCaffery (1979) is believed to be adequate since it is empirically derived by fitting to the relative permeability data of carbonate core materials. Honarpour *et al.* (1994) reported empirical correlations for both gas-oil and water-oil relative permeabilities in both carbonate and sandstone core materials. The correlations are based on the regression toward the fitting to measured data and wettability and lithology have also been taken into account. Results of these correlations were only compared to other correlations and it was concluded that they are in good agreement. However, they have not been tested by another data set for further evaluation.

4.3. Wettability, its Measurements and Effect on Fluid Transport Properties

Definition of Wettability

Wettability is defined as the tendency of one fluid to spread on or adhere to a solid surface in the presence other immiscible fluids (Craig, 1971). In a rock/oil/brine system, it is a measure of the preference that the rock has for either water or oil. Figure 4.5 shows a schematic diagram of water and oil distribution in porous media in different wettability status.

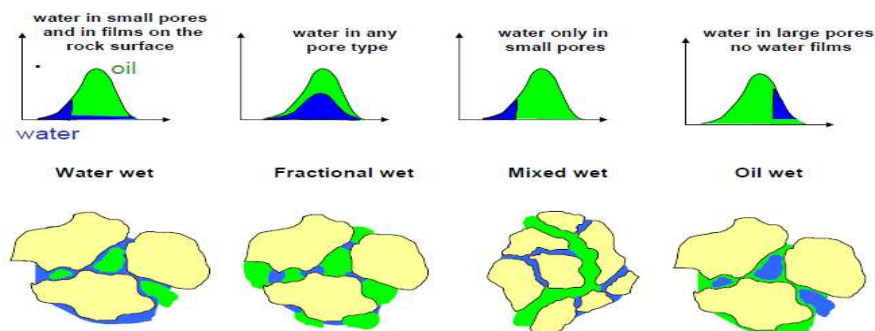


Figure 4.5: Different wettability status for a water/oil/rock system.

When the rock is water wet, there is a tendency for water to occupy the small pores and to contact the majority of the rock surface. Similarly, in an oil-wet system, the rock is preferentially in contact with oil, the locations of the fluids are reversed from the water-wet case, and oil will occupy the smaller pores and contact the majority of the rock surface (no water film is present).

Depending on the specific interactions of rock, oil, and brine, the wettability of the rock can range from strongly water-wet to strongly oil-wet. When the rock has no strong preference for either oil or water, the system is said to be neutral or intermediate wettability (Anderson, 1986a).

Fractional wettability, also called heterogeneous, spotted, Dalmatian wettability, was first proposed by Brown and Fatt (1956). In fractional wettability, crude oil components are strongly adsorbed in certain areas of the rock, as a portion of the rock is strongly oil-wet, while the rest is strongly water-wet.

Mixed Wettability

Salathiel (1973) introduced the mixed wettability for a special type of wettability in which the oil-wet surfaces form continuously through the larger pores and the smaller pores remain water-wet and contain no oil. With respect to rock-surface and to water film stability, the generation of the mixed wettability is closely related to the initial fluid distribution after primary migration of oil into the reservoir. Kovscek *et al.* (1993) followed the observations by Salathiel (1973) to define a pore-level scenario for development of mixed wettability in oil reservoirs. They found that the combined physics of interactions of pore shapes and thin films can explain the development of mixed wettability in the porous media.

Hall *et al.* (1983) and Melrose (1982) developed a theoretical model for stability of the thin water film inside the larger pores. It shows the water film becomes thinner and thinner as more oil enters and after reduction of the thickness to a certain critical value, it becomes unstable and ruptures, allowing the oil to contact the surface.

Wettability of Sandstones and Carbonate Reservoirs

Historically, all petroleum reservoirs were believed to be strongly water-wet (Anderson, 1986a). However, Treiber *et al.* (1972) used the water advancing contact angle measurement

to examine wettability in 55 oil reservoirs. Table 4.2 shows the distribution of reservoir wettability based on the contact angle. As shown, both sandstone and carbonate reservoirs are mostly oil-wet with a contact angle between 105° to 180°.

Table 4.2: distribution of reservoir wettability based on the contact angle. (Adapted from Treiber et al., 1972.)

	<u>Contact Angle (degrees)</u>	<u>Silicate Reservoirs</u>	<u>Carbonate Reservoirs</u>	<u>Total Reservoirs</u>
Water-wet	0 to 75	13	2	15
Intermediate wet	75 to 105	2	1	3
Oil-wet	105 to 180	15	22	37
Total		30	25	55

Water-wet reservoirs were considered by contact angle in the range of 0 to 75° and carbonate reservoirs are more oil-wet than sandstone reservoirs. Studies by Chilingar and Yen (1983) on 161 carbonate cores suggested that most of carbonate reservoirs range from neutral to oil-wet.

Measurements Wettability

Numerous wettability measurements have been reported in the literature. Anderson (1986b) summarizes and describes the majority of wettability measurement methods. In the oil industry, three main methods are generally used: 1) contact-angle measurement, 2) the Amott (1959) method (imbibition and forced displacement), and 3) the USBM method (Donaldson *et al.*, 1969, 1980). Only two last methods are discussed in detail since they were used to measure the wettability in this thesis.

Amott-Harvey Method

Amott (1959) introduced two indices that can be measured through a sequence of displacements of water and oil from a porous rock sample as shown in Figure 4.6. These indices are indicators of the relative displacement of water or oil phase by the other one. Before starting the test, the core is first saturated 100% by oil, then initial water saturation is established in the core, after that the core is put inside the specially made cells which have been graded at the top. The core is surrounded by the same brine used to establish initial

water saturation. Oil produced due to spontaneous imbibition of water is collected at the top of the graduated cell and after spontaneous imbibition; oil is displaced by water by force imbibition to the residual oil saturation. By applying material balance, increase in water saturation due to spontaneous imbibition ΔS_{ws} and force imbibition ΔS_{wf} , the water index I_w is defined as:

$$I_w = \frac{\Delta S_{ws}}{\Delta S_{ws} + \Delta S_{wf}} \tag{Eq.4-19}$$

While the core material is in the residual oil saturation, it is put inside the graduated cell, which is set downward, but this time it is filled by the same oil inside the core. The water produced due to free imbibition of oil is collected at the bottom due to gravity segregation and its volume is recorded. After the oil imbibition, water is displaced by oil injection and its volume is recorded.

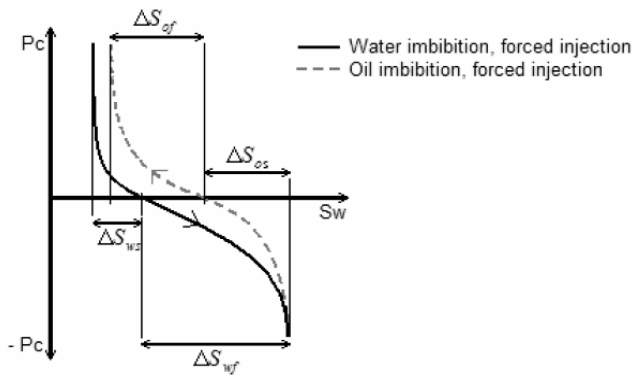


Figure 4.6: Sequence displacements of water and oil which are the basis for the Amott (1959) wettability method. Displacements include free water imbibition, force displacement of oil by water, free oil imbibition, and force displacement of water by oil.

Similarly, by material balance calculations, the increase in oil saturations by imbibition inside the core, ΔS_{os} , and oil injection, ΔS_{of} , are calculated. The oil index I_o is defined as:

$$I_o = \frac{\Delta S_{os}}{\Delta S_{os} + \Delta S_{of}} \tag{Eq.4-20}$$

The Amott (1959) method was modified by Boneau and Clampitt (1977) and Trantham Clampitt (1977) and defined the Amott-Harvey wettability index as:

$$I_{AH} = I_w - I_o \quad \text{Eq.4-21}$$

The wettability index is 1 for a strongly water-wet system and -1 for a strongly oil-wet system. Cuiec (1984) stated that the system is water-wet when $0.3 \leq I_{AH} \leq 1$, oil-wet when $-1 \leq I_{AH} \leq -0.3$ and intermediate wet when $-0.3 \leq I_{AH} \leq 0.3$.

The main problem with the Amott wettability test and its modifications is that they are insensitive near neutral wettability (Anderson, 1986b).

USBM Method

The USBM wettability measurement developed by Donaldson *et al.* (1969, 1980) gives the average wettability of a typical core material. The USBM method compares work necessary for one fluid to displace the other one. As stated before, work necessary to displace a non-wetting fluid by a wetting fluid is less than the opposite case. It has been shown that the work necessary for displacement is proportional to the area under the capillary pressure curve. The area under the secondary (oil) drainage curve is the work needed to displace water (A_1) and the area under the forced (water) imbibition curve is the work needed to displace oil (A_2). See Figure 4.7.

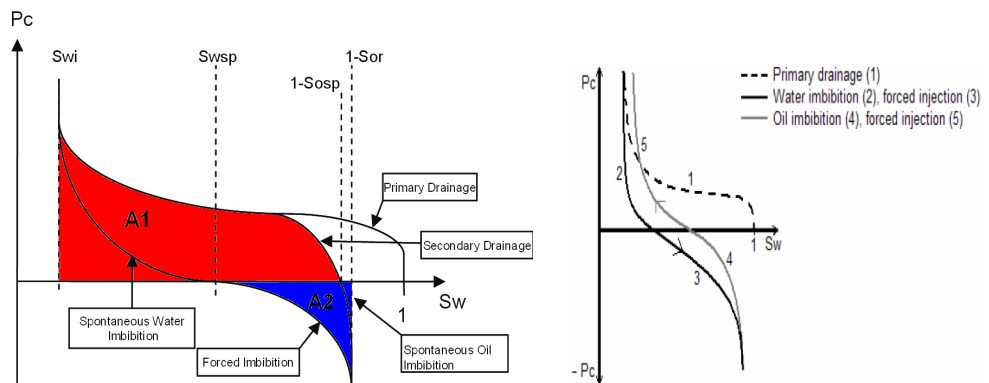


Figure 4.7: Graphical description of the method of USBM wettability measurement. Areas under capillary pressure curves are the work necessary for one fluid to displace the other (left). Combined USBM and Amott-Harvey methods by Sharma and Wunderlich (1985) (right).

The USBM index I_{USBM} is given by:

$$I_{USBM} = \log \left[\frac{A_1}{A_2} \right] = \log \left[\frac{\int_{S_{wi}}^{1-S_{osp}} P_c(S_w) dS_w}{\int_{S_{wsp}}^{1-S_{or}} P_c(S_w) dS_w} \right] \quad \text{Eq.4-22}$$

where, S_{osp} and S_{or} are oil saturation after secondary oil imbibition respectively. S_{wsp} and S_{wi} are water saturation after spontaneous imbibition of water and initial water saturation respectively. Normally the I_{USBM} lies within the interval -1 to 1 and is therefore often compared with the Amott-Havey index. Theoretically however, it can span from $-\infty$ to $+\infty$ for strongly oil-wet and water-wet respectively. The centrifuge method described in the previous section is usually used for measurement of capillary pressure.

The Method by Sharma and Wunderlich

Sharma and Wunderlich (1985) developed a modification of the USBM test that measures both Amott-Harvey and USBM indices in one experiment. The procedure has been illustrated by Figure 4.7. The combined test starts from the primary drainage; it is followed by water imbibition and thereafter by forced water injection using centrifuge. The process is reversed by oil imbibition and oil injection, again using centrifuge.

Table 4.3 compares three different methods for wettability measurement including the contact angle method (Anderson, 1986b). Both USBM and Amott methods show a positive value for water-wet and negative value for an oil-wet system.

Table 4.3: Comparison of wettability measurement parameters by Amott-Harvey, USBM, and contact angle methods. (Adapted from Anderson, 1986b.)

	Water-Wet	Neutrally Wet	Oil-Wet
Contact angle			
Minimum	0°	60 to 75°	105 to 120°
Maximum	60 to 75°	105 to 120°	180°
USBM wettability index	W near 1	W near 0	W near -1
Amott wettability index			
Displacement-by-water ratio	Positive	Zero	Zero
Displacement-by-oil ratio	Zero	Zero	Positive
Amott-Harvey wettability index	$0.3 \leq I \leq 1.0$	$-0.3 < I < 0.3$	$-1.0 \leq I \leq -0.3$

Mixed-Wettability Classification by Amott-Harvey and USBM Indices

The advantage of the USBM method is that it includes the capillary pressure data to evaluate wettability; in contrast to the Amott method, it does not only rely on the saturation points. USBM is also insensitive for cores with neutral wettability state compared to the Amott method although it is limited for short core samples because of the centrifuge test. On the one hand, the USBM index is only based on forced displacements, whereas the Amott index, on the other hand, is dominated by spontaneous imbibed volumes into the core. As argued by Dixit *et al.* (1998a), the two wettability indices are not based on the same process.

Network models studied by Dixit *et al.* (1998b, 2000) indicate that one may distinguish between these intermediate-wet sub-classes based on the relationship between the Amott-Harvey (I_{AH}) and USBM (I_{USBM}) wettability indices. Their approach can improve the understanding of the intermediate-wet state by dividing this group into three sub-classes; Fractional Wet (**FW**), where oil-wet and water-wet sites are random with respect to pore size, and two mixed-wet classes defined by water-wet and oil-wet sites that are sorted by pore size. The Mixed-Wet Large (**MWL**) was described earlier (introduced by Salathiel, 1973), and Mixed-Wet Small (**MWS**) refers to a situation where small pores are oil-wet (see Figure 4.8).

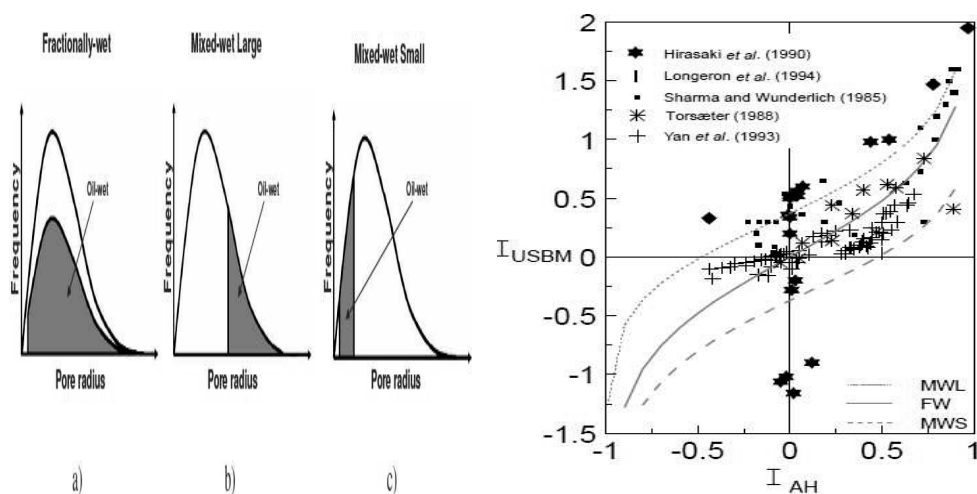


Figure 4.8: Distribution of oil-wet pores for a) fractionally-wet, b) mixed-wet large, and c) mixed-wet small systems (left). I_{USBM} versus I_{AH} which shows the relationship between FW, MWS, and MWL wettability classes (right). (Adapted from Dixit *et al.* 1998a, 2000.)

While I_{AH} and I_{USBM} are almost equal for **FW** class, I_{USBM} is larger than I_{AH} for **MWL** class and smaller for **MWS** class.

By employing the work by Dixit *et al.* (1998a, 2000), Skauge *et al.* (2004) have demonstrated that three different intermediate wetting states can be identified in core materials of sandstone reservoirs from the North Sea. Thirteen North Sea reservoirs were classified as **MWL**, **MWS**, or **FW**, and the different groups showed several important differences with respect to special core analysis properties.

Effect of Wettability on Flow Properties

Wettability has been shown to affect electrical properties, capillary pressure, relative permeability, irreducible water saturation, residual oil saturation, dispersion, and simulated tertiary recovery (Anderson, 1986a, 1986b, 1986c, 1987a, 1987b, 1987c). In chapter three, the effect of wettability on electrical properties was discussed. The effect of wettability on capillary pressure, relative permeability, and water flood behaviour is now given more attention and reviewed.

Effect of Wettability on Capillary Pressure

Wettability affects capillary pressure of both imbibition and drainage processes for a typical porous medium (Anderson, 1987a). Figure 4.2 shows the capillary pressure curves for water-wet Berea sandstone where a spontaneous imbibition process displaces oil and water saturation increases to 80 % while Figure 4.9 shows the capillary pressure curves for cores with intermediate-and oil-wet (Killins *et al.*, 1953).

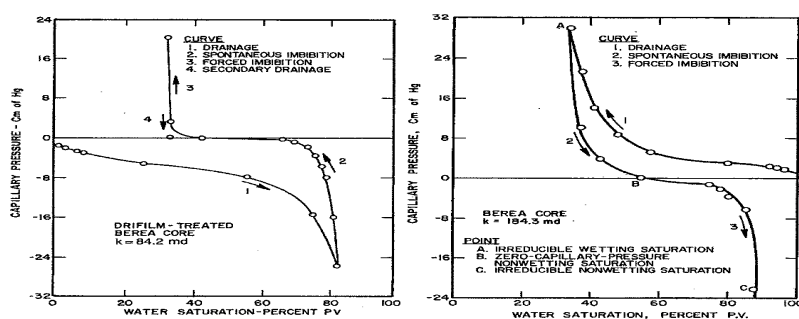


Figure 4.9: Impact of wettability on primary-drainage and imbibition capillary pressure. Strongly oil-wet system (left), and intermediate-wet system (right). (Adapted from Killins *et al.*, 1953.)

No water spontaneous imbibition of water occurs for the oil-wet Berea core while for intermediate-wet; there is still some degree spontaneous imbibition of water. For the

intermediate-wet core sample, both positive and negative capillary pressure can be expected. The contact angle also can significantly affect both imbibition and drainage capillary pressure as shown by Morrow (1976).

Effect of Wettability on Relative Permeability

Wettability affects relative permeability during drainage and imbibition processes (Anderson, 1987b). Figure 4.10 shows typical relative permeability curves for a strongly water-wet and oil-wet system (Craig, 1971).

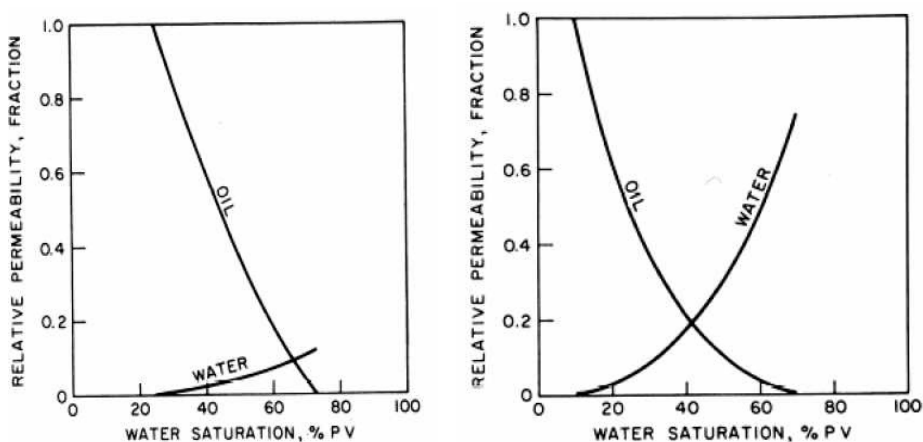


Figure 4.10: Typical relative permeability trends for water-wet (left) and oil-wet (right) systems. (Adapted from Craig, 1971.)

For a strongly water-wet system, saturation of the crossover point in oil and water relative permeabilities is more than 50% while for an oil-wet system the crossover point is less than that (Figure 4.10). The differences in relative permeabilities measured in water and oil-wet systems are caused by differences in fluid distribution due to wettability effect. For a water-wet system, water is located in the small pores and usually does not block oil flow at initial water saturation; therefore the oil relative permeability at initial water saturation approaches the absolute permeability. At residual oil saturation, for a water-wet system, water relative permeability is low because oil in larger pores as a discontinuous phase blocks the flow of the water through the medium. In a strongly oil-wet system, the positions of the two fluids are reversed and oil relative permeability is relatively low because the residual water (inside

large pores) blocks the oil flow. The water permeability at residual oil is higher for an oil-wet system because water is located inside the larger pores and oil as film on the surface.

McDougall and Sorbie (1995) studied the effect of wettability on relative permeability to oil and water in fractional and mixed-wettability conditions by network modeling. Their studies show a different trend for the effect of oil-wet fraction (α) on fractional and mixed-wet systems. They found that for a fractionally-wet system, the crossover point in relative permeabilities experience a general shift toward lower water saturations as α increases. Such a trend was not apparent for a network system with a mixed-wet wettability condition. The crossover point no longer moved toward lower water saturation as α increases. For α between 0 and 0.5, it actually shifted to higher saturations; it only began to move back toward lower saturation once α was above 0.5

Effect of Wettability on Water Flooding

Wettability can also affect water-flood behavior as well as recovery efficiency and residual oil saturation (Anderson, 1987c). During the waterflood of a strongly water-wet system at a moderate oil/water viscosity ratio, a large fraction of the oil in place is recovered before breakthrough (Figure 4.11).

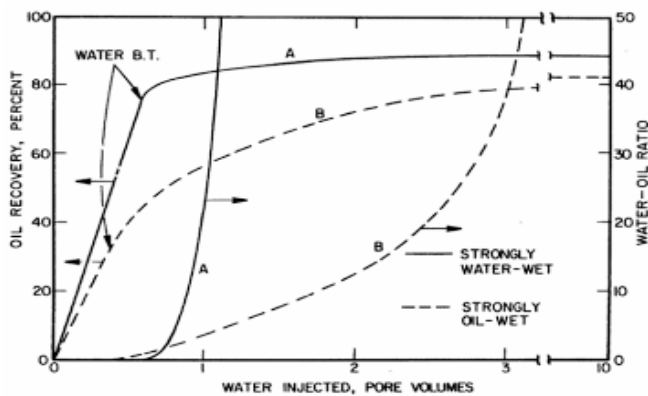


Figure 4.11: Typical waterflood performance in water-wet and oil-wet sandstone cores at moderate oil/water viscosity ratios. (Adapted from Raza et al., 1968.)

For a strongly oil-wet system, water breakthrough occurs early and most of the oil is produced after water breakthrough. A similar result for the effect of wettability on waterflood

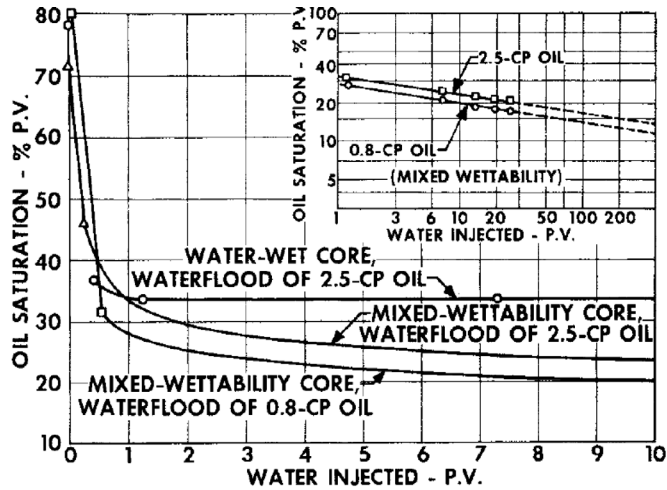


Figure 4.12: Comparison of waterflood behavior for mixed-wet and water-wet sandstone cores. (Adapted from Salathiel, 1973.)

behavior was reported by Salathiel (1973) for mixed-wet and water-wet sandstone cores.

For a water-wet core sample, even after 10 pore water injections, no additional oil is recovered while for a mixed-wet core sample; low residual oil saturation can be expected after significant water injection. The reason for this behavior was the film-flow drainage process which allows the oil to leave the core through the continuous oil film on the surface.

CHAPTER 5

Experimental Procedures and Workflow

In previous chapters, theoretical topics of this thesis were presented which form the background for this chapter and chapter 6. In this part, workflow of the experiments and analysis of experimental results are summarized.

The experimental program consists of following measurements: porosity and permeability measurements, dispersion experiments, measurement of electrical properties, assessment of wettability at cleaned state by Amott-Harvey method, unsteady-state water flooding, dispersion test at waterflood remaining oil saturation, wettability restoration by aging process, assessment of wettability by Amott-Harvey method after aging, and water flooding after aging.

5.1. Procedures and Workflow

A special core analysis program was planned to study waterflood efficiency of carbonate rocks with different carbonate pore types and their relationship to single-phase flow properties. Figure 5.1 shows a flow chart that describes the sequence of different experiments in the program.

Carbonate materials included in this study are about 50 reservoir core samples selected from different formations of carbonate reservoirs located in both the Middle-East and the North Sea. Careful examination was made by CT-scan of core samples to exclude fractured samples to avoid any effect of fractures on fluid flow properties. In addition to the CT-scan, tracer injection into samples was also analyzed to compare with CT-scan images to determine any possible fracture inside cores, and also determine miscible properties of porous media.

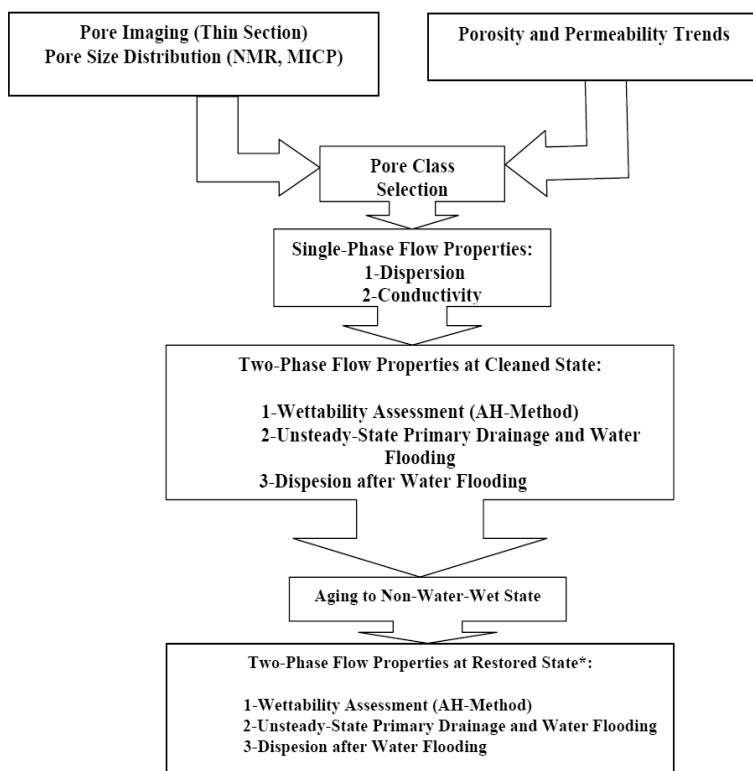


Figure 5.1: Diagram of the SCAL program for the study of carbonate materials with different carbonate pore classes. (*:two-phase flow program for aging part performed only for one class and dispersion results after water flooding are not presented at this thesis.)

Material Selection

After core material selection, experiments according to the flow chart presented in Figure 5.1 are explained in the following sections.

5.2. Pore Class Determination

Core materials were selected that followed the porosity/permeability relationship for each pore class from Lønøy's (2006) definition. This decision was made because of the main objective which to test the pore class concept.

Thin-section images were from core materials and pore types of carbonate samples were known before the start of experiments. In addition, mercury injection capillary pressure and

NMR data were available to provide additional information (pore size distribution) about the pore structure.

Thin-section data coupled with semi-log cross-plot of permeability versus porosity was used to classify carbonate core samples based on Lønøy's (2006) approach (see chapter 2). The thin-section image analysis and permeability-porosity cross-plots identified nine carbonate pore classes and two mixed pore classes.

Figure 5.2 shows the semi-log cross-plot of permeability versus porosity for the selected carbonate core samples. These identified pore classes were considered for the next studies in the program. In some pore classes, only three samples were included in such a way that they formed a positive trend in cross-plot of permeability versus porosity (Figure 5.2).

As seen, carbonates with *IP-UMa* pore class have highest permeability and those with *Tertiary Chalk (TC)* pore class have highest porosity compared to others.

Preparation of Core Samples

Core materials were received in a fresh state and they were cleaned by injection of sufficient pore volumes of toluene, mixed mixture of toluene and methanol, and finally pure methanol at an elevated temperature (50°C).

After drying the samples, the porosity of the samples was measured by the saturation weight method. Permeability of the samples was measured by brine injection of 5 constant rates and recording the differential pressure. Injection rates were kept constant until the differential pressure became constant and steady-state condition was established. When the Darcy conditions were satisfied, Eq.4-13 in section 4.2 was applied to calculate absolute permeability of carbonate samples to synthetic sea water (SSW).

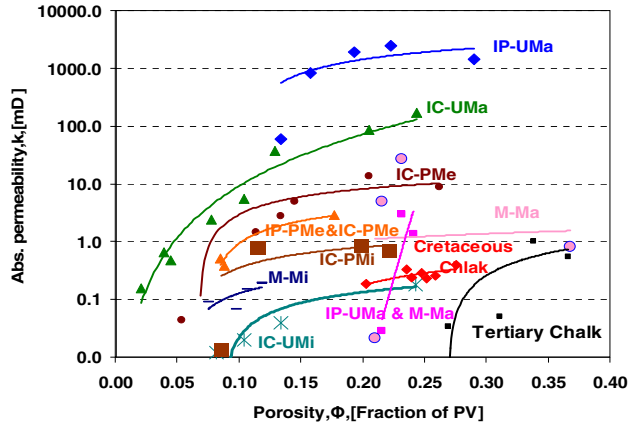


Figure 5.2: Semi-log cross-plot of absolute permeability versus porosity for 11 different carbonate pore classes based on Lønøy's approach (2006): IP-UMa, IC-UMa, IC-UMi, IC-PMe, IC-PMi, M-Ma, M-Mi, TC, CC, IP-UMa & M-Ma, and IP-PMe&IC-PM. (Pourmohammadi et al. , 2007).

5.3. Pore size Distribution from Mercury Injection Capillary Pressure and NMR

NMR derived pore size distribution (PSD) and mercury injection capillary pressure were two sources of information used to characterize pore size distribution of samples. Figure 5.3 shows NMR pore size distribution from the NMR method compared to mercury injection.

As seen, PSD from mercury is shifted toward the smaller pore size for two types of carbonate pore types. This has been observed for all of the carbonate pore samples with other pore types. The reason for this, as described in chapter three, is associated with the weakness of the mercury intrusion method to determine the pore size distribution. Another observation is that both types of data show a bio-modal distribution where the left response is the contribution from the micro-porosity and it is minor compared to the macro-porosity. Figure 5.3 indicates that derived pore size distributions for samples of M-Ma and IP-PMe&IC-PMe pore class from NMR and mercury method are not similar.

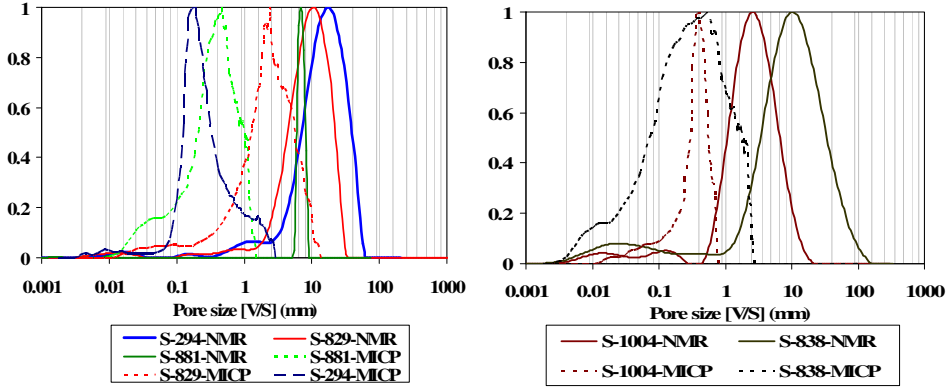


Figure 5.3: Pore size distribution derived from NMR and Mercury Injection Capillary Pressure (MICP) for Marco-Moldic (M-Ma) (left) and mixed-pore classes of Intercrystalline Patchy-Meso and Interparticle Patchy-Meso (IP-PMe&IC-PMe) (right).

Because NMR pore size distribution reflects the response of all pore and throat-sizes compared to the mercury method, it is more informative and therefore is used to define a uniform pore size distribution index (*UPSDI*) or simply a pore size distribution (*PSDI*) index as (Pourmohammadi *et al.*, 2007):

$$PSDI = \frac{r_{\min}}{r_{\max}} \cong \frac{\left(\frac{V}{S}\right)_{\min}}{\left(\frac{V}{S}\right)_{\max}} \tag{Eq.5-1}$$

The index is simply the ratio between the minimum pore radius characteristics (r_{\min}) observed in the second part of bio-modal pore size distribution spectrum (ignoring the response from micro-porosity) to the maximum pore radius characteristics (r_{\max}). For a homogenous porous medium, the index approaches unity (like a bundle of capillary tubes with the same radius) whiles for a heterogeneous medium representing a broad pore size distribution the value of the index is lower.

5.4. Single-Phase Dispersion Experiments and Simulation Analysis

By analysing the effluent profiles from miscible displacement of the pore fluid, mixing properties of the plug samples are obtained.

Dispersion Experiment and Tracer Selection

In the early part of the project, *perfluoro benzoic acid* was used as the tracer in the injected water. The effluents were sampled in glasses, and tracer concentration was measured for each of them by calibration of amount of tracer to *UV-spectroscopy*.

A more time-saving and precise method was later developed and used in the rest of the program. The SSW was miscible displaced by the same SSW but with slightly higher salinity (one percent extra NaCl), and thereby with higher electrical conductivity. The effluent concentration was estimated from resistance measurement over an insulated portion of outlet tubing where the effluent was the only conductor. Thereby, the profile could be estimated directly from the resistance data from the test log file.

Compared to the previous method, this is time saving as all necessary measurements are performed true time and more precise because measured concentration is averaged through smaller volumes. Results of the two methods showed good agreement when compared for identical core samples. The initial method procured 15-20 effluent samples (equals number of measure points) per pore volume, while approximately 200 points per pore volume are used to plot the dispersion profile in the conductivity method.

Synthetic sea water (SSW) with added tracer was injected into samples at constant rate into the 100% SSW saturated plugs. After some time interval (typically 2-4 pore volumes), only undiluted tracer is produced, and the procedure is reversed by injecting the same amount of SSW with no added tracer. In this way the dispersion profile is inversely repeated, and the system is reset to the initial situation with only SSW in the pores.

According to Lake (1989), the mechanical dispersion term dominates the molecular diffusion for interstitial velocities above 3 cm/day, or approximately 3.5×10^{-5} cm/s. For a core sample with diameter 3.8 cm, this corresponds to a volumetric rate in the region of 0.02 ml/min.

In order to undermine the impact of injection rate on dispersion profiles, a common interstitial velocity (v) for all plugs was chosen for all tests and majority of samples. This value was selected equal to 0.067 cm/min and then by employing the following equation, the rate was determined:

$$v = \frac{q}{A \cdot \phi} \quad \text{Eq.5-2}$$

where q is the tracer injection rate in ml/min, A is the cross section area of the sample in cm^2 , and ϕ is the porosity. The injection rate was selected in the range that the effect of diffusion mechanism on mixing be minor. The sensitivity of dispersion experiments to the injection rate performed for only three samples and indicated that it the effect depends on the amount of flowing fraction of the medium. Samples with higher dead-end pore fractions showed more sensitivity to the injection rate.

However, a few plug samples had low permeability and calculated rate which would impose a confinement pressure beyond the matrix' yield point (assumed to be higher than 40-50 bar). In these cases, lower rates were used to keep the injection pressure well below a reasonable confinement pressure.

The effluent tracer will ideally be produced after nearly one pore volume injection. Further, the front and the tail of the tracer pulse are distorted due to diffusion and hydraulic mixing. Figure 5.4 illustrates the principle of the method. Effluent tracer concentration is monitored over the time of the experiment.

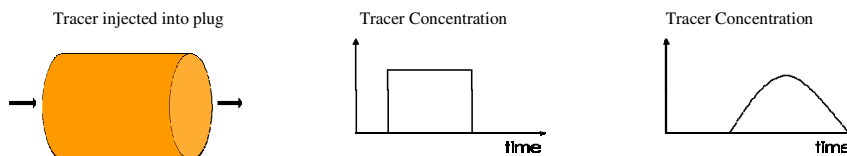


Figure 5.4: Principle of tracer injection into a core plug, with the pulse tracer injection scheme (middle) and the corresponding dispersed effluent profile (right).

The tracer concentration in the effluents provides information about how well the individual pores in the core sample are connected, the amount of dead-end pores, and *dispersion coefficient* measured from the slope of the tracer curve. *Inaccessible pore volume* shifts the dispersion curve towards the left (lower “flowing” pore volume).

Effect of Dead-End Pores and Inaccessible Pores on Effluent

Presence of dead-end pores creates asymmetry due to concentration exchange by diffusion from the flowing volume into the dead-end pores (see Figure 5.5).

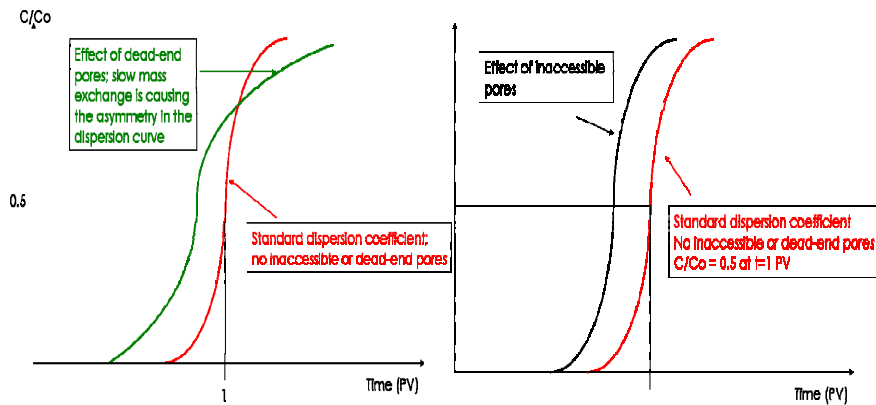


Figure 5.5: Effect of dead-end pores on tracer profile (left). Inaccessible porosity decreases the effective pore volume, and shifts the effluent profile left-wards (right).

Fluid in dead-end porosity is displaced by diffusional exchange rather than viscous flooding, and hence relatively more injection time and fluid is needed to completely displace the initial fluid in-place. The concept of the dead-end pores does not only refer to single pores, but could also be clusters of pores that are not a part of the flowing fraction.

Experimental Results

Figure 5.6 shows examples of tracer profiles obtained by tracer type one (*perfluoro benzoic acid* added to the brine) and tracer type two (one percent extra NaCl in SSW).

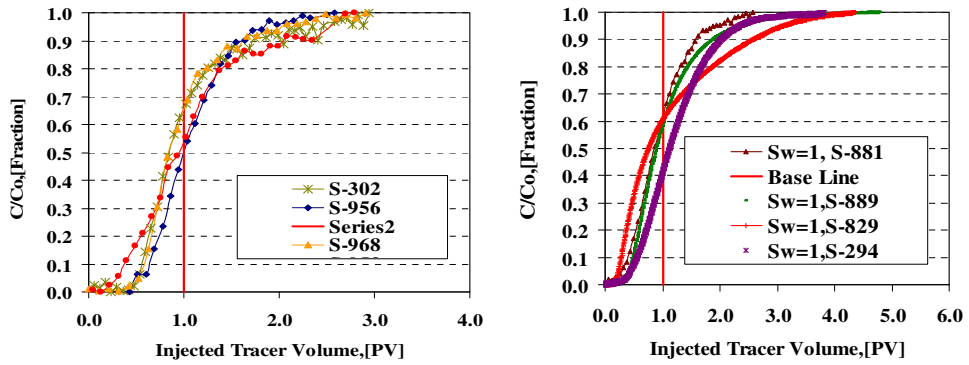


Figure 5.6: Normalized effluent concentration of injected tracer into carbonate core materials saturated with 100 % saturated SSW versus volume of tracer injected normalized against the pore volume. Carbonates with IP-Uma pore class and perfluoro benzoic acid as the tracer (left). Carbonates with M-Ma pore types and 1% extra NaCl added to the SSW as the tracer (right).

Simulation of Experiments

Coats and Smith’s (1963) model was used to reconcile and match trace effluent. For this purpose, The *UTCHEM* (2000) simulator was setup to simulate tracer injection into one dimension of *Cartesian* system with 100 grid cells (Figure 5.7).

One injection and one production well were assigned for injection and monitoring produced effluents respectively and also satisfying boundary conditions for the model. Three main assumptions were made during simulation steps; transversal dispersion is negligible, mass transfer coefficient between stagnant volumes and flowing stream (*M*) is constant and value of 0.0005 [S^{-1}] was used (see Eq.3-52 and Eq.3-53 in chapter three).

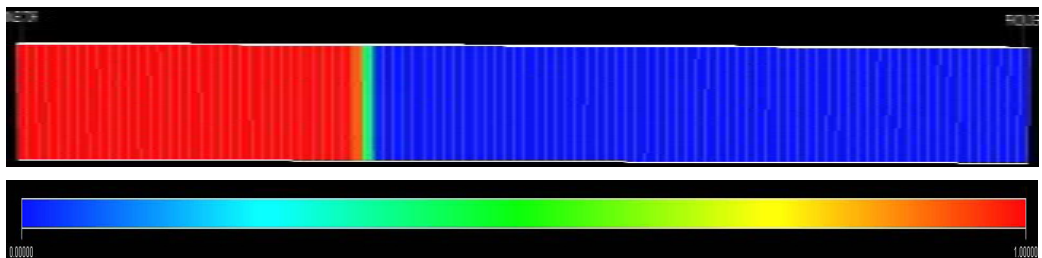


Figure 5.7: Visualization of miscible displacement in a one-dimensional *Cartesian* system designed for simulation of tracer injection into carbonate core samples. In-situ normalized concentration varies from zero (blue color) to unity (red color) at the front.

Two main parameters were changed to match the effluent history: fraction of non-stagnant volume (f) and dispersivity (α), which is a measure of mixing length as described in chapter three. Figure 5.8 shows examples of tracer profiles obtained by dispersion experiments performed by two types of tracer associated with plotted simulated results.

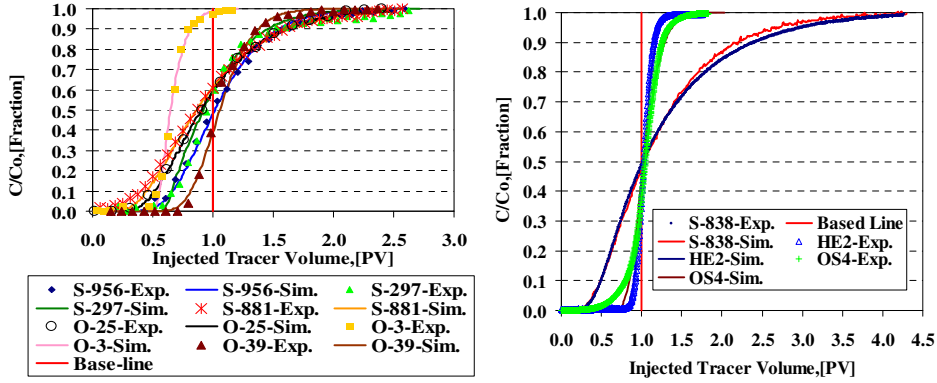


Figure 5.8: Effluent profiles of injected perfluoro benzoic acid as the tracer (left) and one-percent extra NaCl as the tracer (right) (both added to Synthetic Sea Water (SSW)) associated with simulated results for different carbonate pore types.

As seen, the Coats and Smith's (1963) model can successfully model the miscible displacement in carbonates with variable pore classes. Dispersion measurements in different carbonate pore classes were reported by Skauge *et al.* (2006a) and employed to characterize carbonates. Simulations of dispersion measurements provide information about dispersivity (α) and flowing fraction defined (f) as:

$$f = \frac{\text{Total pore volume} - \text{Stagnant volume}}{\text{Total pore volume}} = \frac{\text{Flowing volume } (V_f)}{\text{Total pore volume } (V_p)} = \frac{\phi_f}{\phi_T} \quad \text{Eq.5-3}$$

where ϕ_f is the flowing porosity and ϕ_T is the total porosity. Eq.5-3 assumes that all pores are accessible. In the presence of initially inaccessible porosity (ϕ_I), it can be shown that:

$$\phi_T = \phi_f + \phi_D + \phi_I = f \cdot \phi_T + (1 - f - I) \cdot \phi_T + I \cdot \phi_T \quad \text{Eq.5-4}$$

where I is the fraction of initially inaccessible porosity and can be derived from pore volume adjustment by comparison of simulation results and experimental data. No adsorption was observed during tracer injection as confirmed by material balance and therefore it was not included in simulation approaches.

5.5. Conductivity Experiments

The conductivity tests were performed with temperature and pore pressure held at ambient conditions. In order to pre-stress each plug equally, and to control that the resistivity had reached a fairly stable value, the confinement pressure were increased in steps of 5 bara between 5 and 40 bara, and decreased in steps of 10 bara back to atmospheric pressure. The formation resistivity factor and cementation exponent integrated with other parameters are based on resistance readings at 30 bara overburden pressure. Water resistivity (R_w) was measured to 0.1933 Ωm at ambient conditions. Eq.3-17 in chapter three was used to measure the *formation factor* by using the following equation to determine resistivity from measured resistance(r):

$$R = r \frac{A}{L} \tag{Eq.5-5}$$

where A is the cross-section area of core samples and L is the core length. The *cementation factor* was also derived in each applied pressure. Figure 5.9 shows the *formation factor* and *cementation factor* measured for carbonate samples with different pore classes. As seen, both electrical properties are increase as more stress is applied and above 30 bara, insignificant variation is expected. The dependency of electrical properties on stress was described and discussed in more detail in chapter three. *M-Ma* pore class has high *cementation factors* while *IC-UMi* and *IC-PMi* pore types have low *cementation factors*. Among the pore types, mixed pore class of *IC-PMe* and *IP-PMe* has a high *formation factor* while *Tertiary* chalk, *Cretaceous* chalk, and *IP-PMi* pore types have low *formation factors*.

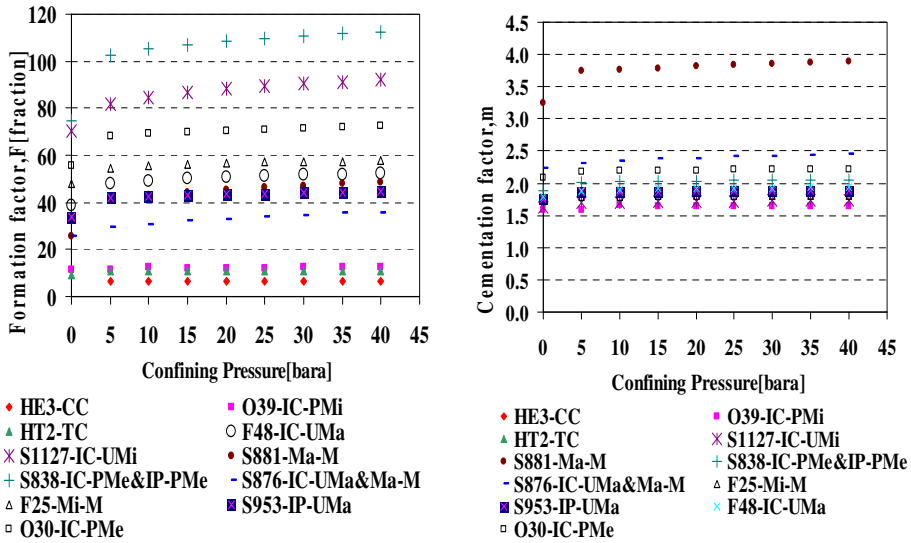


Figure 5.9: Formation factor of carbonate rock samples with variable pore types versus applied stress (left) and corresponding cementation exponent (right).

The *tortuosity factor* (τ) of carbonate samples was determined according to Eq.3-19 in chapter three. The *formation factor* at 30 bara was used to obtain the *tortuosity factor* and results were integrated with single-phase and two-phase flow properties.

5.6. Wettability Assessment of Core Samples in Cleaned State

Wettability behavior of cleaned core samples was determined by following the Amott-Harvey test procedure prior to any water flooding. All core samples showed some degree of spontaneous imbibition while no oil imbibition was observed during the full cycle of the Amott-Harvey test. Normal decane and SSW were used as fluid phases for wettability studies of carbonate samples in the ambient condition. The spontaneous imbibition was performed with the plugs in Amott cells for a minimum of 14 days. Forced imbibition was performed with water flooding (SSW) or decane injection with constant differential pressure and water or produced oil collected and measured in a graduated glass.

Figure 5.10 shows increase in average water saturation due to spontaneous imbibition versus measured time for carbonate with different pore types (left) and also measured Amott-Harvey index. As seen, chalk samples show a strong degree of spontaneous imbibition while a low-degree of spontaneous imbibition was observed for *M-Ma* pore type and it is mixed with *IP-UMa* pore type (see Figure 5.10 (left)).

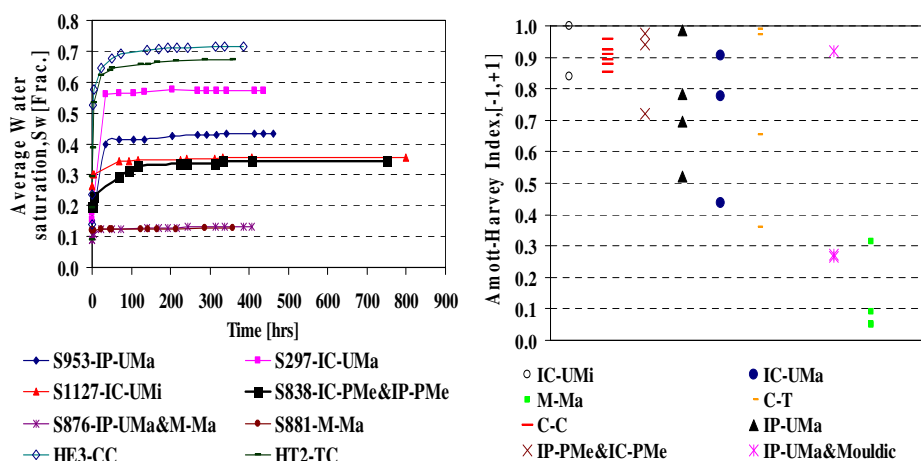


Figure 5.10: Increase in average water saturation due to spontaneous imbibition into carbonates with variable pore types (left) and Amott-Harvey wettability indices derived from wettability tests.

Variation in Amott-Harvey index of carbonate samples with different pore types characterize the wettability behavior of studied carbonate materials composed of different pore classes from intermediate to strongly water-wet. As seen, majority of carbonate samples with different pore types are by definition weakly to strongly water-wet. *IC-UMa* and *Cretaceous Chalk (TC)* pore types show a strongly water-wet behavior while all samples with *M-Ma* pore type shows intermediate behavior.

5.7. Unsteady-State Water Flooding Experiments, Simulation Analysis, and End-effect Investigations

After study of wettability behavior of carbonate samples with different pore classes, water flooding experiments were followed and before that, initial water saturation (S_{wi}) was established.

Initial Water Saturation

All experiments were conducted at the ambient condition by using again normal decane as the laboratory oil and SSW as the brine. Initial water saturation was established by applying the primary drainage flooding in the vertical mode to have gravity-stable displacement and core samples were flooded on both sides to secure a uniform-initial water distribution. Primary drainage to establish S_{wi} was performed by oil flooding. Decane was injected at constant rate, while differential pressure across the core, and water production were measured continuously.

Through a lightweight and low-friction tubing connection, the effluent was conducted to an oil and water-filled glass separator placed on a scale. As water and oil entered the separator at the bottom, oil was displaced from the top. This way water produced from the core was measured by the increasing water-oil level in the separator. The scale was connected to a computer for data acquisition. As SSW and decane have different, and well known, densities, the increasing water amount in the separator was detected continuously by the scale readings.

When no more water was produced, the plug was moved to another set-up for further drainage with oil of higher viscosity (Marcol 152) to achieve a lower S_{wi} . The additional water produced was collected and measured in a graduated glass. At the end point, Marcol 152 was removed from core samples by injection of decane as a miscible displacement and finally it was replaced by decane. After replacement of Marcol 152 by decane, base permeability, $K_o(S_{wi})$ or effective permeability to decane at initial water saturation was measured with the same procedure applied for measurement of absolute permeability. During the all experiments, the net confining pressure was not allowed to excess more than 20 bara.

Water Flooding Experiments and Recovery

Unsteady-State water flooding experiments performed by injection of pore volumes of SSW at the constant rate and differential pressure across the core and oil production were measured simultaneously. In addition to manual visual readings, oil production was also automatically measured by scale readings. Increasing oil amount in the separator was detected as decreasing weight by the scale and recorded during the experiment.

In order to evaluate sensitivity of oil production to injection rate, the flooding rate was increased in two steps (rate bumps) when with the initial rate no additional recovery is

achieved. At the end, water permeability at remaining oil saturation (S_{or}), $K_w(S_{or})$, was measured in the same way as absolute permeability.

Oil recovery efficiency (recovery factor- RF) which is the amount of oil produced as a fraction of the initial oil in place can be determined by following equation:

$$RF = \frac{1 - S_{or} - S_{wi}}{1 - S_{wi}} \quad \text{Eq.5-6}$$

Figure 5.11 shows profiles of recovery factors of carbonate samples with different pore classes versus volume of injected SSW.

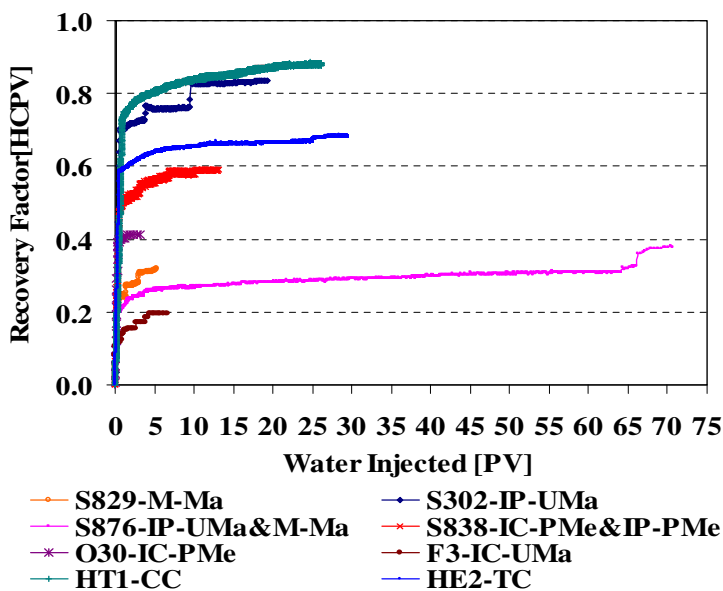


Figure 5.11: Profiles of water-flood efficiency of different carbonate pore classes versus number of pore volumes injected by SSW into core samples.

As the water-flood efficiency profiles in Figure 5.11 show, carbonate with different pore classes may require different amounts of water to be injected to achieve the final recovery. In

the next chapter, reasons for this and factors that may control recovery factors are discussed in more detail.

5.7.1. Simulations of Water Flooding Experiments

Unsteady-state water flooding experiments provide information about the relative permeability, recovery, and possibly capillary pressure (if it influences relative permeability of oil and water during the experiment life). In order to verify the waterflood experiments, ensure the quality assurance of experimental data; improve the results, and estimation of relative permeability and capillary effect, experimental results were reconciled by simulation.

Simulation Approach

The *SENDRA* (2008) simulator was employed to reconcile the experimental data consisting of measured differential pressure and produced oil for each sample and to estimate the relative permeability, capillary pressure, and water saturation profiles.

Although *SENDRA* (2008) is capable of utilizing different correlations for both relative permeability and capillary pressure, Corey correlation (1954, 1956) for relative permeability and the correlation by Skjæveland *et al.* (2000) for capillary pressure were employed (see Eq.4-8 and 4-18 in chapter four).

Figure 5.12 shows examples of measured differential pressure and produced oil from two water flooding experiments of two different carbonates reconciled by the described simulation approach. *SENDRA* (2008) simultaneously estimates capillary pressure and relative permeability by auto-history matching procedures and gives the best match to experimental data. Since in unsteady-state flooding, two-phase flow occurs in a short period and at high water saturation, the majority of available data before break-through were eliminated to increase the accuracy of relative permeability estimation (Figure 5.12). Measured remaining oil saturation (S_{or}) was allowed to be changed by simulator to achieve a better match since there might be some uncertainty involved in the measurement of this parameter.

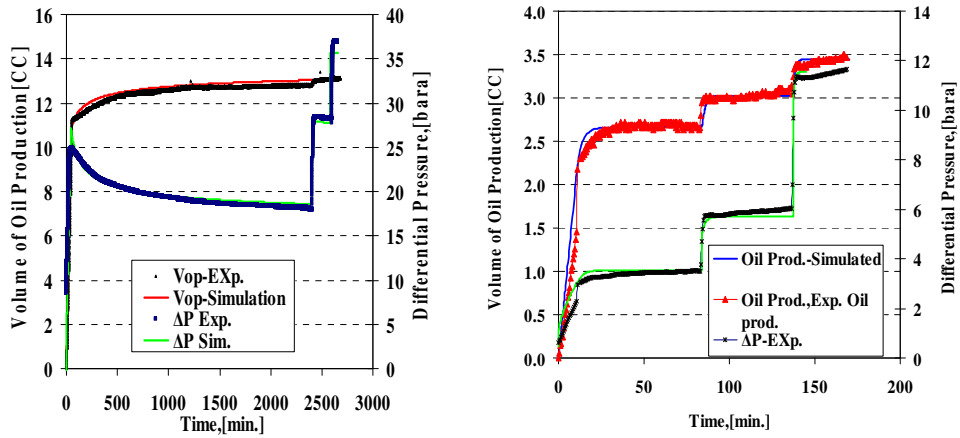


Figure 5.12: Experimental results of unsteady-state water flooding of a Tertiary chalk sample (left) and a sample of mixed pore classes of M-Ma and IP-UMa reconciled by simulation (right).

In order to reconcile waterflood experimental data with differential pressure and oil production, one of two solutions are possible. One presumed solution is to ignore capillary pressure ($P_c=0$) which gives the relative permeability using the analytical approach of Johnson *et al.* (1959) known as the *JBN* technique. The other solution is to include the capillary pressure in simulation to match the experiments. Our simulation results for the majority of experiments showed that the capillary pressure should be included in the analysis to reconcile experimental data more accurately and provide a better match. This means that capillary pressure is important and influential on experimental waterflood data.

Figure 5.13 shows estimated relative permeability and capillary pressure by history matching of differential pressure and oil production from a mixed-pore class carbonate sample shown in Figure 5.12.

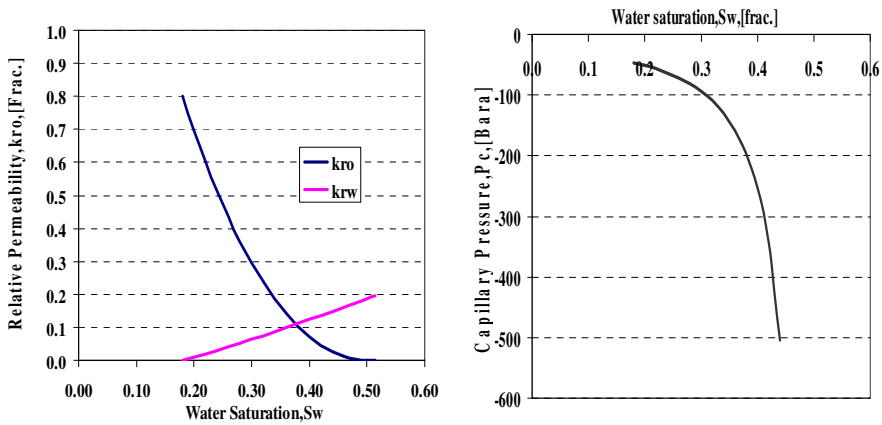


Figure 5.13: Relative permeability and capillary pressure estimated for a carbonate sample with mixed-pore class. Relative permeability is based on Corey (1954) correlation and capillary pressure is based on the correlation developed by Skjaveland et al. (2000).

Water saturation profiles versus normalized core length due to water flooding by simulation approach for the mixed-pore class carbonate sample are presented in Figure 5.14. The water saturation profiles show variation in the average water saturation in different times along the core sample. As seen, average water saturation is not constant and is reduced toward the outlet face and all profiles converge to a unique value. This phenomenon is referred to “end-effect” which is discussed in more detail in the next section.

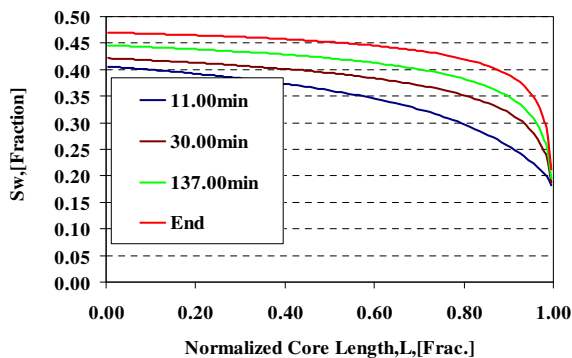


Figure 5.14: Water saturation profiles estimated by SENDRA simulator by history matching of experimental data of mixed-pore class sample (Figure 5.12 (right)).

5.7.2. Evaluation of Factors Controlling Water Flooding

Water injection rate is one the most important parameters that influences the quality of the experiment. In order to design a proper water flooding experiment, a proper injection rate should be selected; otherwise measured relative permeability and remained oil saturation are sensitive to the applied rate.

In one dimensional-immiscible displacement, if gravity forces are ignored, water displacement is controlled by both viscous and capillary forces. Injection rate should be selected high enough to dominate viscous forces on the one hand compared to capillary forces, and on the other hand, low enough to prevent sensitivity of remaining oil to water injection rate.

Criteria for Selection the Injection Rate

Table 5.1 shows different criteria suggested by different investigators to design a proper water flooding experiment. Rapoport and Leas (1953) defined a scaling criterion (second row in Table 5.1) as the product of interstitial velocity, length of the system, and water viscosity. It was concluded that in linear waterfloods, this factor should be above a value between 0.1 and 1 to make flooding behavior independent of rate and the length of the system. It was shown that in this condition, capillary forces do not affect the flooding process and can be ignored. The flooding behavior was called “stabilized” and the Buckley-Leverett theory (1942) is applicable to model the process since capillary forces are ignored.

Lake (1989) modified the Rapoport and Leas (1953) scale parameter and defined a dimensionless number called the Rapoport and Leas number (N_{RL}). According to Lake (1989), to undermine the effect of capillary pressure on flooding behavior, the dimensionless number should be above 3 for a water-wet porous media.

Sigmund and McCaffery (1979) reported a different expression for taking into account the effect of capillary pressure on water flooding results as presented in Table 5.1. As seen, the critical dimensionless factor (R_D), above which capillary pressure is ignorable is higher for drainage process compared to imbibition process.

In order to account for the upper limit of water injection rate, the capillary number which is the ratio of viscous to capillary forces should be considered. Although various expressions have been reported in the literature and many of them shown to be equivalent (Taber, 1981), the following expression was used to calculate the capillary number:

$$N_c = \frac{K \Delta P}{L \sigma} \quad \text{Eq.5-7}$$

where K is the absolute permeability, ΔP is the pressure gradient across the medium with the length L , and σ is the interfacial tension between two phases of water and oil.

Table 5.1: Scaling criteria for water flooding experiments.

Scaling criteria	Expression	Acceptable values to avoid capillary pressure effect
Rapoport and Leas	$L\mu_w v$	< 0.1-1
lake	$N_{RL} = \sqrt{\frac{\phi}{K} \frac{\mu_w UL}{K_{rw} \phi \sigma \cos \theta}}$	>3
Sigmund and McCaffery	$N_{RL} = \frac{\sqrt{\frac{K}{\phi}} L \mu_w v \big _{x=0}}{AK \sigma}$	Imbibition: > 0.1-1 Drainage: > 0.1-1
Capillary Number	$N_c = \frac{\mu_w v}{\sigma \cos \theta}$	< 10^{-6}

L = length, μ = viscosity, Φ = Porosity, k = abs. perm., u = superficial velocity, σ = IFT, v = interstitial velocity, θ = contact angle, A = area

Results of laboratory experiments show that remained oil saturation after water flooding becomes a function of the injection rate for a capillary number above 10^{-6} for mostly sandstones (Lake, 1989; Chatzis and Morrow, 1984). Decrease in remained oil saturation with increase in capillary number is a result of mobilization of trapped blobs of oil due to effective forces. However the value of critical capillary number and its relationship to remained oil saturation depends on wettability, pore size distribution, and saturation history (Lake, 1989).

Figure 5.15 shows results of estimated Rapoport and Leas number (N_{RL}) and critical capillary number (N_c) of waterflood experiments. N_{RL} was calculated based on a more direct way according to following equation (Lake, 1989):

$$N_{RL} = \left(\frac{k}{\phi}\right) \frac{\Delta P}{\sigma_{ow} \cdot \cos\theta_{ow}} \quad \text{Eq.5-8}$$

where ΔP is the pressure drop across the core materials measured for the water phase and because it is variable, an average value between differential pressure at the breakthrough and stabilized differential pressure at the steady-state were used. The interfacial between n-decane and SSW (σ_{ow}) was measured at the room condition around 35 dyne/cm. The $\cos\theta_{ow}$ was assumed to be unity since it was difficult to give accurate of this parameter during the flooding.

N_{RL} (from Eq.5-8) is below the value 3 for the majority of our experiments. This may lead to the conclusion that capillary pressure has influenced flooding behavior and should be accounted for by analyzing obtained results. This was confirmed later by a simulation approach in such a way that including capillary pressure in simulation contributed to a better match in experimental data.

The estimated capillary numbers for all employed injected rates of water flooding were below the critical value. This was confirmed by two steps (double and five times higher) increase in the injection rates and observation of not significant increase in oil recovery.

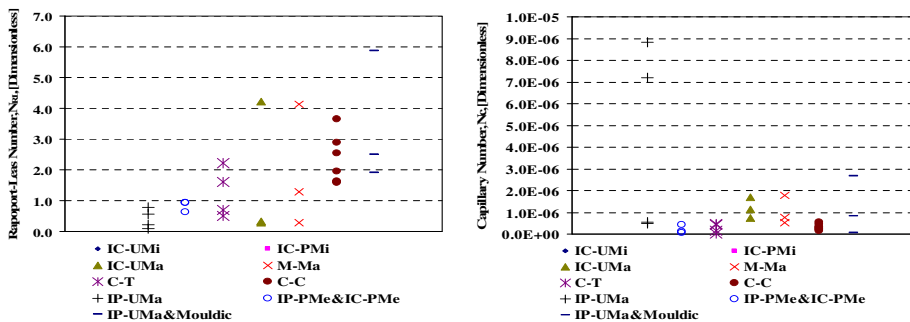


Figure 5.15: Estimated Rapoport and Leas number (N_{RL}) for performed water flooding experiments (left) and capillary number (N_c) (right).

Sensitivity of Remaining Oil saturation to the Injection Rate

Kamath *et al.* (2001) reported lower critical capillary number (N_c) (around 10^{-8}) by studying the residual oil saturation of four carbonate samples. They employed CT images and pore network modeling to understand the effect of increase in injection rate on residual oil saturation. It was concluded that for cleaned-carbonate samples, increase in injection rate will contribute to more water invasion and therefore will lead to reduce the regional remaining oil saturation.

Tie and Morrow (2005) studied both effect of heterogeneity and wettability on sensitivity of residual oil saturation to the flow rate. They concluded that for all studied limestones, the remaining oil saturation is sensitive to the rate and critical capillary number is lower than for what is reported for sandstones.

Capillary End-effect

One of the most important aspects of capillary effect on waterflood experiments is the “end-effect” which is an artifact made in the laboratory. The capillary “end-effect” occurs at the both faces of the core samples in one dimensional displacement because the permeable medium is ended and flow enters into a non-permeable medium. At this condition, capillary pressure everywhere in the outlet region is zero and to satisfy that, the wetting phase saturation has to reach to a certain value (see Figure 5.16). In other words, due to capillary effect, water saturation is different to what is predicted by the Buckley-Leverett theory (1942).

Two-phase flow occurs mostly at the outlet-face of the core (depending on the type of the displacing wave) and relative permeability is estimated after breakthrough. As a result, derived relative permeability and measured remaining oil saturation may not be reliable due to the “end-effect”. This phenomenon can be expected in both imbibition and drainage processes and also depends on the wettability of the system.

“End-effect” can be experimentally determined by measurement of the average water saturation along the core during the flooding experiments by gamma-ray absorption techniques or visualization by CT scan images. The diagnosis to eliminate or reduce “end-effect” is to decrease capillary forces by making viscous forces dominant during water flooding. This can be done by selection of long-core materials and injection with a high rate

or placing a second permeable material (like porous plate) at the outflow end to ensure good capillary contact.

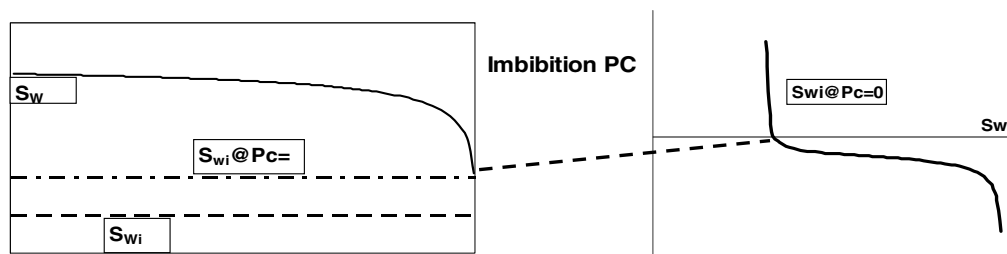


Figure 5.16: Illustration of capillary end-effect by water flooding process. Water saturation at the outlet is adjusted to zero-capillary pressure.

Another simple way of evaluating the capillary “end-effect” is to reconcile the experimental data and predict the saturation profiles. If capillary “end-effect” is remarkable, the relative permeability and remaining oil saturation should be corrected. This is performed automatically by the *SENDRA* (2008) simulator and the estimated relative permeability is corrected. What is observed in the saturation profiles is the “end-effect” assumed by *SENDRA* (2008) and relative permeability is corrected accordingly.

Simulation Approach for Evaluation the Capillary End-effect

The simulation approach was selected to evaluate the impact of capillary “end-effect” on waterflood experiments in this thesis. As described earlier, derived dimensionless parameters based on selected water injection rates (Rapoport and Leas number (N_{RL})) suggested that capillary forces have to some extent influenced experimental data. This was consistent with the fact that ignoring capillary pressure in simulation analysis does not reconcile experimental results accurately.

The approach to evaluating the significance of capillary “end-effect” is only described for one selected sample since it was repeated for all other samples and similar conclusions were made.

Our simulation results showed that for capillary pressure, there is a confidential interval that can reconcile the experimental data. In other words, various capillary pressure curves can be used to reconcile data which for most of the time may give similar relative permeability for one experiment. Results showed that variation in water saturation profiles were dependent on the shape of the capillary pressure curve. Figure 5.17 shows a simulation case where three different capillary pressure curves reconcile experimental data for waterflood experiment of a core sample with *IP-UMa* pore type. The corresponding saturation profiles at the end of experiments for these three cases are also presented. As seen, for the case 3, capillary pressure is zero at the interval between the initial water saturation to the water saturation around 0.8. It is negative for the rest of the interval and therefore this capillary pressure type impacts a significant end-effect.

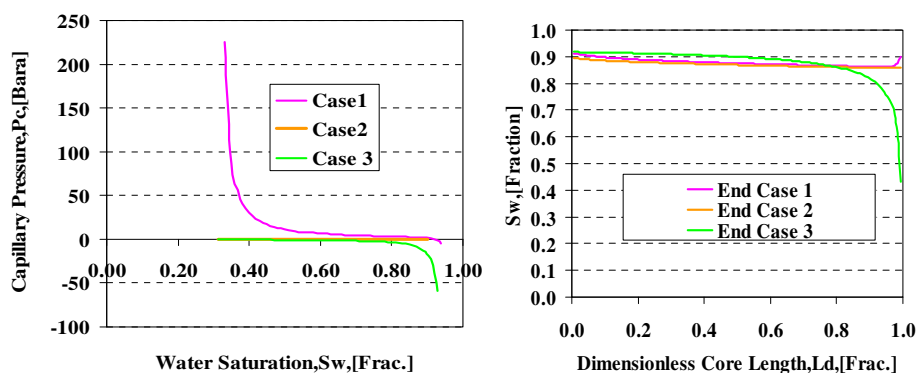


Figure 5.17-Three different scenarios to reconcile experimental data for waterflood experiment of a carbonate sample with *IP-UMa* pore type. Cases 1 and 2 show insignificant capillary end-effect, while case 3 impacts considerable end-effect.

This observation was similar for the majority of waterflood experiments and revealed that the evaluation of capillary “end-effect” depends on employment of a correct capillary pressure.

The majority of all simulation results for the first run suggested a negative capillary pressure during the water flooding and a corresponding “end-effect”. This negative capillary pressure estimated by the simulator was not trusted because from wettability behavior tests as discussed in section 5.6, we knew that there is some degree of spontaneous imbibition as a

part of the process. In other words, the water saturation at which the capillary pressure was zero was known from wettability measurements by the Amott-Harvey test for each sample.

However, a problem arose when the endpoints of wettability tests and water flooding were not the same for each sample. Therefore, it was decided to rescale the endpoints of the imbibition process in the Amott-Harvey test to the endpoints of the water flooding test by the following relationship:

$$S_w \Big|_{WF}^{Pc=0} = S_{wi,WF} + \left(\frac{S_{w,WF} - S_{wi,WF}}{S_{w,AH} - S_{wi,AH}} \right) \left(S_w \Big|_{AH}^{Pc=0} - S_{wi,AH} \right) \quad \text{Eq.5-9}$$

Eq.5-9 gives the estimation of the water saturation in which capillary pressure could be zero if both imbibition processes (by Amott-Harvey test and water flooding) started from the same initial water saturation, i.e. $S_{wi,WF}=S_{wi,AH}$. The main argument for rescaling the water saturation endpoints of capillary pressure to water flooding saturation endpoints is similarity in both processes (both processes are imbibition). In order to check this, endpoint water saturation data were plotted against each other in Figure 5.18.

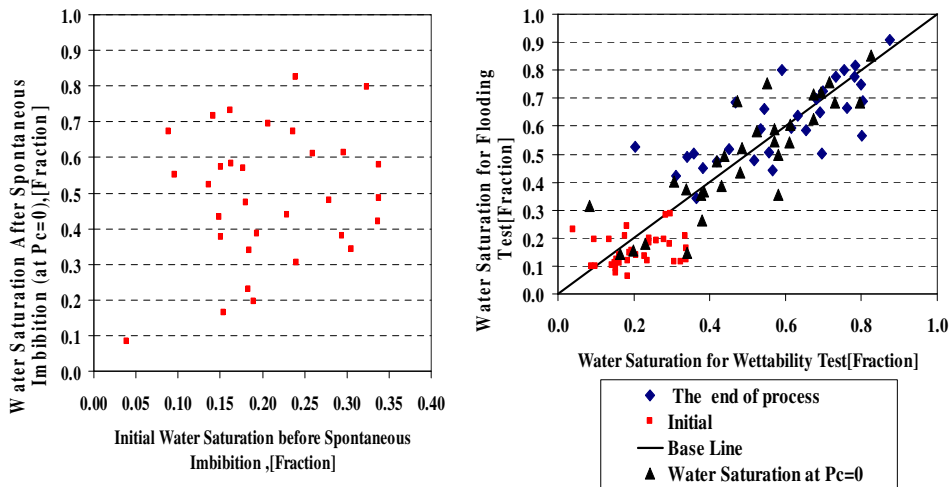


Figure 5.18: Water saturation at the end of spontaneous imbibition versus initial water saturation (left). Initial water saturation, endpoint water saturation, estimated water saturation at zero capillary pressure of water flooding experiments versus Amott-Harvey tests (right).

The water saturation at zero capillary pressure versus initial water saturation in the Amott-Harvey test shows no strong correlation (left plot). This means that the amount of water spontaneous imbibition in cleaned state for the studied samples is independent of the amount of initial water in the system.

Water saturation at the end of both processes shows a good correlation. This strong correlation can justify the rescaling approach for estimating the water saturation at zero capillary pressure for water flooding experiments. As seen, though Eq.5-9 predicts a linear relationship between rescaled water saturation of zero capillary pressure for water flooding versus water saturation of zero capillary pressure at the Amott-Harvey test, results only show a strong correlation. This is because there is no strong correlation between initial water saturation established by primary drainage for both water flooding experiments and wettability tests (see Figure 5.18).

Including Capillary Pressure to Evaluate End-effect in Simulation

After the rescaling the water saturation at zero capillary pressure for water flooding experiments, the initial water saturation, zero capillary pressure water saturation, and end point water saturation were put into the correlation by Skjæveland *et al.* (2000). The parameters of correlation were changed in such a way that it can pass through the saturation points. Derived parameters were imported to the simulation files and locked to be constant and simulation was run to reconcile waterflood experimental data.

In order to account for sensitivity of “end-effect” to capillary pressure path, another capillary pressure curve was again subjected to pass through rescaled saturation points. Simulation was rerun with a new capillary pressure curve to reconcile the experimental data.

Simulation results of two corrected capillary pressure data were compared to the reference case which let the simulator estimate a capillary pressure to reconcile data. Figure 5.19 shows simulation results of water flooding experiments of one of the carbonate core samples selected as an example to be presented.

Simulation results give estimated saturation profiles and relative permeability curves based on reconciled experimental data. Three different capillary pressure data are shown (left) and corresponding saturation profiles estimated by simulator at the end of the experiment. For

case 1, *SENDRA* (2008) was allowed to reconcile the data with free estimation of capillary pressure and relative permeability. The saturation profile in this case shows a significant “end-effect”. In cases 2 and 3, *SENDRA* (2008) used the modified capillary pressure as described above to reconcile data and predicated the saturation profiles.

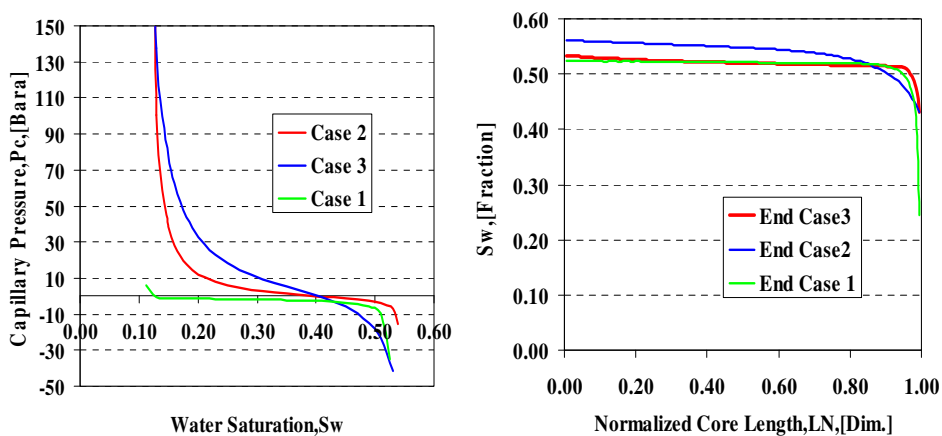


Figure 5.19: Three different capillary pressure scenarios used to reconcile experimental data of water flooding (left) and corresponding final saturation profiles (right) for a selected carbonate sample.

As seen, by employing modified capillary pressure data, significantly less “end-effect” is pronounced for water flooding. This was the case for all other carbonate core samples in this study. Simulation results showed that capillary “end-effect” is not significant in our waterflood experiments and therefore calculated remaining oil saturation and estimated relative permeabilities are reliable.

Inlet Capillary Effect

Another concern was about evaluating whether “inlet-effect” is significant in performed water flood experiments since it was observed from simulation results that for some cases water saturation values are relatively high at the inlet-face. For this purpose, simulation results of saturation profiles with including capillary pressure were compared against the case with zero capillary pressure. If higher saturation water purposed by simulation the inlet-face be due to the “inlet-effect” as a result of capillary pressure equilibrium, water saturation at the inlet-face face should be sensitive to capillary pressure. Simulation results did not confirm

this sensitivity therefore the high saturation at the inlet-face is due to higher viscous forces in this region due to pressure gradient. Figure 5.20 provides an example among others to support this conclusion. As seen, saturation profiles are not different for two cases of non-zero capillary pressure curves as compared with the case of zero capillary pressure (case 3). Only a minor “end-effect” is observed at the outlet for case 2 as compared to case 1 and case 3.

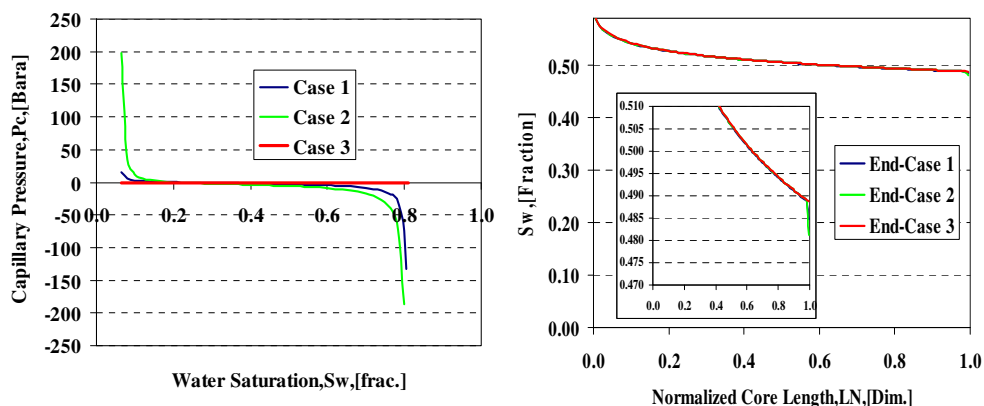


Figure 5.20: Simulation results of waterflood experiments according to three assumed capillary pressures (left). Higher saturation at the inlet-face is not eliminated in the case of zero capillary pressure(right).

5.8. Dispersion Experiments at Remaining Oil Saturation after Water Flooding and Simulation Analysis

After waterflood experiments, dispersion experiments were performed for core samples at remaining oil saturation. Similar procedures to dispersion experiments at 100 % water saturated state were followed. All experiments were performed by using the tracer type two (1% NaCl extra dissolved in SSW) and effluents were analyzed by the conductivity method as described in section 5.4. The tracer injection rate was calculated by modification of Eq.5-2 to volume of water and considering the same interstitial velocity used in 100 % water saturation as:

$$v = \frac{q}{A \cdot \phi \cdot (1 - S_{orw})} \tag{Eq.5-10}$$

where total porosity is corrected based only on the amount of water in the core sample at the end of the water flooding. It should be noticed that all dispersion experiments were performed at the steady-state condition.

Figure 5.21 shows results of two example tracer experiments of carbonate with *IP-UMa* pore type (left) and another with mixed pore class *IP-PMe&IC-PMe* (Intercrystalline Patchy-Meso and Interparticle Patchy-Meso) pore type (right) at both 100 % and remaining oil saturation. In 100 % water saturated samples, tracer dispersion within the porous media is controlled by the structure of the matrix while at the two-phase flow it is affected by relative distribution of phases as a result of their wettability preferences, film layer, and continuity or discontinuity of phases.

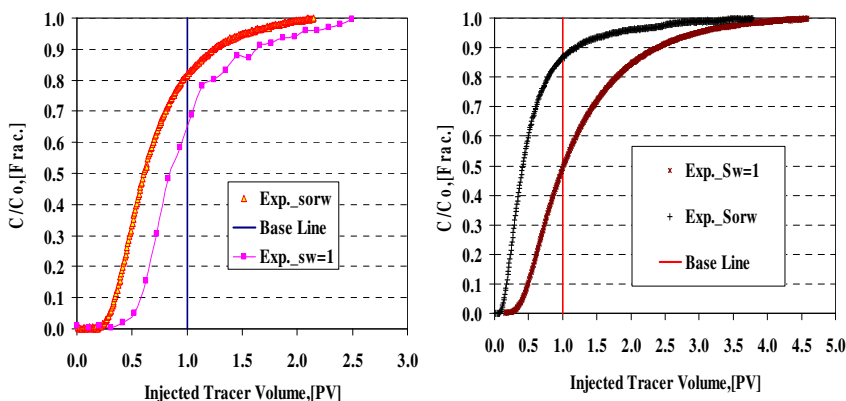


Figure 5.21: Effluent profiles of dispersion experiments at 100 % water saturation and remaining oil saturation after water flooding for two different carbonate samples. A sample with *IP-UMa* pore type (left) and *IP-PMe&IC-PMe* pore type (right).

In order to simulate dispersion experiments at remaining oil saturation, the same procedures for 100 % water saturated were followed and only pore volume was corrected. Samples at remaining oil saturation were assumed to be single-phase considering that oil-phase is immobile. As a result, Eq.5-3 and Eq.5-4 were modified based on new pore volumes of water and flowing fraction at the water phase by definition is:

$$f_{w.Sorw} = \frac{\text{Volume of flowing water } (V_{wf})}{\text{Volume of water } (V_w)} \tag{Eq.5-11}$$

where $f_{w,sorw}$ denotes the fraction of non-stagnant volume of water to the water volume of the medium in the presence of the remaining-immobile oil. This fraction can be expressed as the fraction of total pore volume alternatively as:

$$f_{Sorw} = \frac{\text{Volume of flowing water } (V_{wf})}{\text{Total pore volume } (V_p)} = f_{W,Sorw} \cdot (1 - S_{orw}) \quad \text{Eq.5-12}$$

where the fraction of the non-stagnant volume of water, f_{sorw} now is expressed with respect to the total pore volume.

Figure 5.22 shows dispersion experimental data associated with corresponding simulation results at both 100 % saturated and after water flooding by *UTCHEM* (2000) for two carbonate samples containing two different pore types.

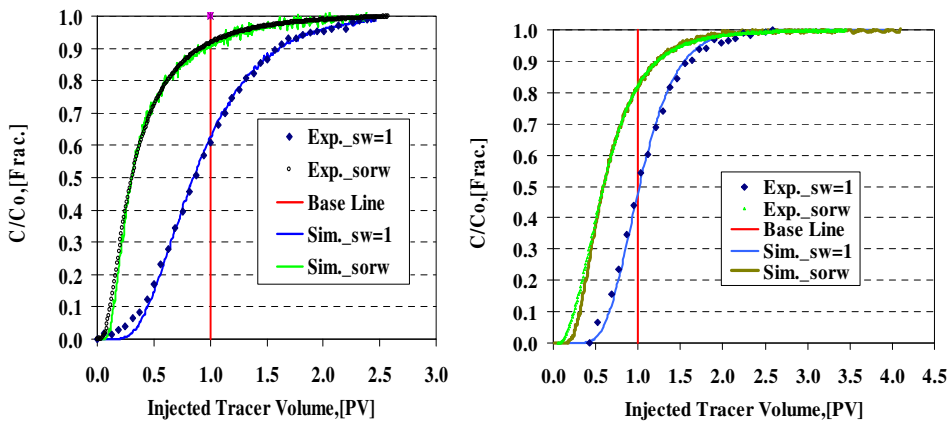


Figure 5.22: Normalized effluent profiles of injected tracer into two different carbonate samples at 100 % brine saturated and at remaining oil saturation associated with simulated results. Carbonate with Macro-Moldic pore type (left) and IP-UMa pore type (right).

Coats and Smith's (1963) model could successfully simulate the majority of dispersion experiments performed in both single-phase and two-phases.

Dispersivity at remaining oil saturation was also estimated by simulation analysis for all carbonate samples which flooded by water by dispersion experiments.

5.9. Restoration of Wettability by Aging Process and Evaluation of Wettability Alteration

Wettability was restored for mainly chalky micro-pore type and a few samples from other pore classes. Initial water saturation was established before start of aging process by primary drainage with the Marcol 152 and replacement of that by decane. The drainage process into both sides of samples was performed in vertical mode to provide gravity-stable displacement to secure a uniform initial water distribution.

The samples were aged in crude oil at 80°C. The crude oil was prepared by degassing at 90°C. To avoid possible precipitation of heavy components at contact between crude and the slug, toluene was used to miscible displace decane from the pores. The solvent slug was followed by degassed crude, and the ageing process occurred at one month. Fresh crude oil was injected at a very low rate at the second and final weeks to make the wettability alteration process more efficient.

Evaluation of wettability alteration after aging process was performed by measuring the wettability index by both the Amott-Harvey and USBM methods described in chapter 4. The procedure of wettability measurement is according to Sharma and Wunderlich (1985) in which both wettability indices are obtained (see chapter 4).

Reduction in water spontaneous imbibition into *Tertiary* and *Cretaceous* chalk samples due to wettability alteration is shown in Figure 5.23. As seen; at restored state, water spontaneous imbibition into chalk samples is reduced due to less water-wetness.

Capillary pressure was also measured by the centrifuge technique explained in the previous chapter. Both force imbibition and secondary drainage capillary pressure were measured and used to calculate the USBM wettability index.

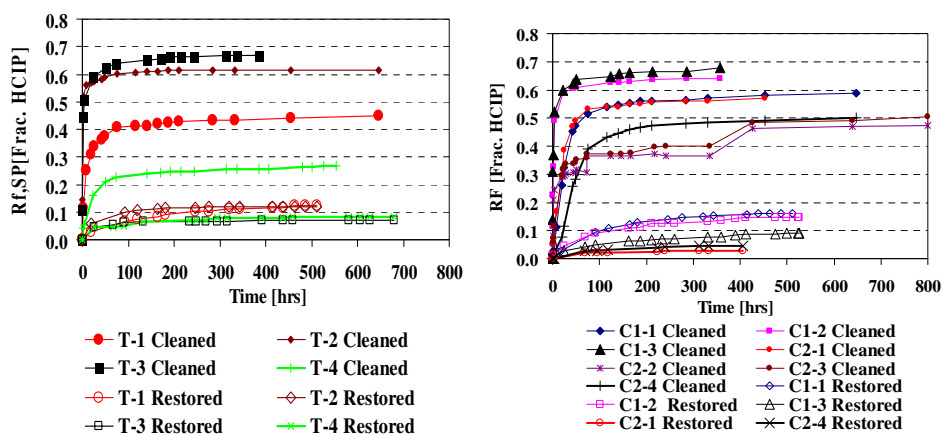


Figure 5.23: Reduction in spontaneous imbibition due to change in wettability into Tertiary chalk (left) and Cretaceous chalk (right).

Examples of measured forced imbibition and secondary drainage capillary pressure of both Tertiary and Cretaceous chalk samples are presented by Figure 5.24. Spontaneous imbibition of oil was a little during wettability tests. As a result, forced secondary drainage started at water saturation close to that ended by forced imbibition processes. Wettability of samples as revealed by wettability indices and shapes of capillary pressure curves behaves mixed-wet where the pores can prefer to be water-wet or oil-wet depending on their own pore sizes (see chapter 4).

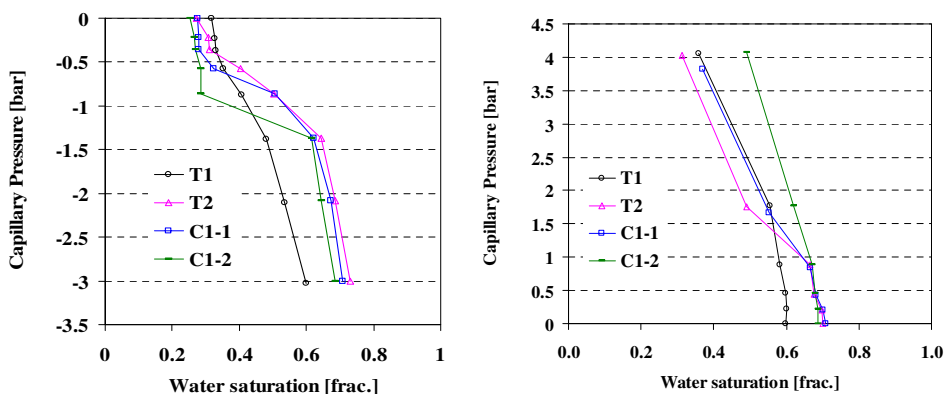


Figure 5.24: Forced imbibition capillary pressure (left) and secondary drainage capillary pressure measured for Cretaceous chalk (C1-1, 2) and Tertiary chalk (T1, 2) samples by centrifuge.

5.10. Water Flooding of Restored Samples and Simulations

Waterflood experiments were performed right after wettability tests were accomplished based on similar procedures in the cleaned state. They were performed at the ambient condition with an unsteady-state constant injection rate and two sequent bump rates. Water injection rate at restored state for each sample was the same as at cleaned state to reduce the rate effect to be able to compare remaining oil saturation and other important parameters.

Similar to waterflood in cleaned-state condition, factors that may have influenced on water flooding of restored samples were evaluated by the simulation approach. Production history and differential pressure along the core during water flooding were reconciled (Figure 5.25).

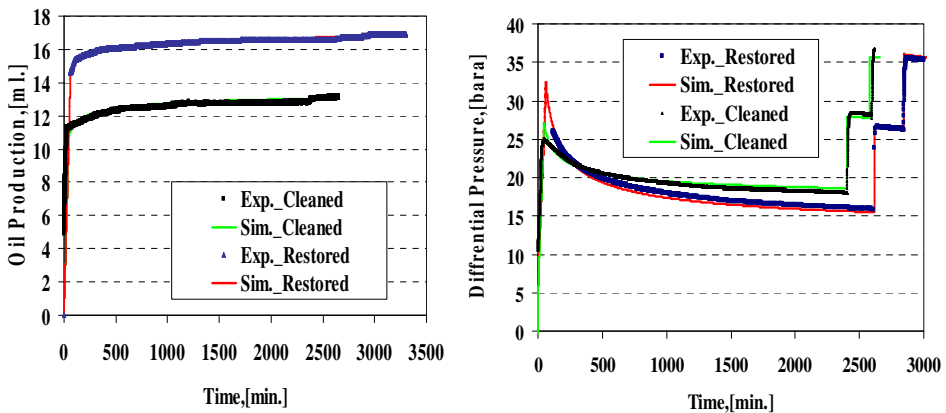


Figure 5.25: Reconciled oil production by water flooding experiments (left) and differential pressure along the core for a Tertiary chalk sample in both cleaned and restored state.

It was again found that including capillary pressure into simulation is needed to reconcile and qualify data. Figure 5.25 shows one selected example of water flooding performed at both cleaned and restored states associated with simulated results. For this purpose, the correlation by Skjæveland *et al.* (2000) was fitted by regression analysis to measured capillary pressure data and end-point saturations. After estimation of the parameters of the capillary model, they were imported to the simulator and were locked while relative permeability parameters in the Corey functions were allowed to be changed to get the best match. Figure 5.26 shows

capillary pressure curves and estimated oil and water relative permeabilities estimated by *SENDRA* (2008).

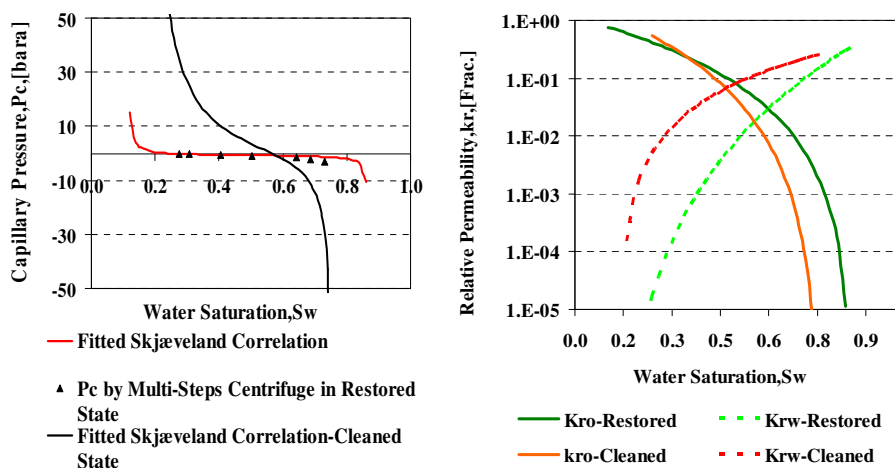


Figure 5.26: Employed capillary pressure data (left) and estimated relative permeabilities (right) of water flooding results for the core sample shown in Figure 5.25 by simulation.

Water saturation profiles during and at the end of experiments were used to evaluate the possibility of capillary “end-effect” and its influence on waterflood experiments at the restored state. Results indicated that the “end-effect” is not significant during the water flooding and obtained remaining oil saturation and relative permeability data are reliable which means the qualification of results is satisfactory.

Simulated saturation profiles during the water flooding suggested by simulator for the selected *Tertiary* chalk sample (among others as the representative sample) are given in Figure 5.27.

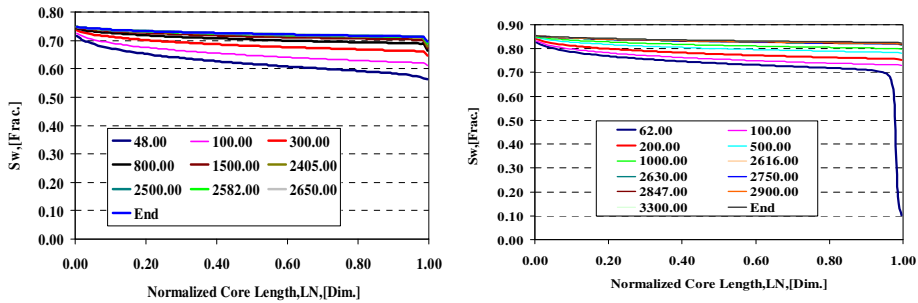


Figure 5.27: Average water saturation profiles along the Tertiary core samples during the water flooding at cleaned state (left) and restored-state (right).

Variation in the average water saturation due to the water flooding of the Tertiary chalk sample in both cleaned state and restored state is slightly different.

As seen, at the cleaned state, more “end-effect” is pronounced compared to restored state, however, it does not significantly affect saturation profiles on a considerable length of the sample.

5.11. Summary

A special core analysis program was planned and followed for almost 50 different carbonate samples. Carbonate core materials were grouped into 11 pore classes by integration of thin section images to semi-log cross plot of permeability versus porosity.

Derived NMR pore size distribution was compared to pore size distribution derived by mercury injection technique. NMR data were considered more reliable to provide information about pore size distribution compared to the mercury technique.

Dispersion experiments were performed before and after water flooding and modeled successfully to provide information about mixing properties and the effect of dead-end pores in different carbonate pore classes on dispersion.

Conductivity measurements were performed at room temperature and variable pressure measurements to determine electrical properties of carbonate pore types at single-phase flow. The electrical properties were not change dramatically above 30 bara.

The wettability behavior of samples at the cleaned state for carbonate samples was evaluated by the Amott-Harvey method and the majority of samples showed weakly water-wet to water-wet behavior.

Unsteady-state water flooding experiments were performed at cleaned state at room conditions and results were reconciled by simulation. Simulated results showed that capillary pressure should be taken into account in waterflood experiments and derived relative permeability. This is consistent with results of analytical approach where Rapoport and Leas number (N_{RL}) is below the critical value which shows capillary pressure has influenced the water flooding during the experimental life. However, as it was revealed the “end-effect” is not significant at the end of waterflood experiments and shows that injection rate has selected properly. The remaining oil saturation by increasing the water flooding rates did not change dramatically which means that capillary number is below the critical value.

Wettability restoration with the aging process and at 80 °C and 35 bara pressure was performed mostly for chalk samples with *Tertiary* and *Cretaceous* chalky pore classes. The study of wettability after restoration of samples showed mixed-wet behavior by both the USBM and Amott-Harvey methods.

Unsteady-state water flooding was performed for restored samples at room conditions to evaluate the impact of wettability on water flooding and recovery efficiency. Experimental data were reconciled and simulated for quality check and derived relative permeability. The measured capillary pressure during the USBM wettability study was used to simulate the experimental data. Results showed that the “end-effect” is not considerable and no significant sensitivity of remaining oil saturation to the injected rate was observed.

For all waterflood experiments, it was shown that the high water saturation purposed by simulation at the inlet-phase is not sensitive to capillary pressure; thereby it is due to higher pressure in this region.

CHAPTER 6

Main Results and Discussions

This chapter reviews the main results according to experiments and the workflow described in chapter 5. Most of the results and discussions in this section were presented in four papers and therefore details are not repeated in this chapter. The emphasis has been on additional analysis beyond what was obtained in the papers.

In this chapter, first, variation in single-phase flow properties in different carbonate pore classes are presented, then, correlations between these properties are examined. After that, two-phase flow properties, mainly recovery efficiency and remaining oil saturation after water flooding, are interrelated to the single-phase flow properties. The objective is to find single-phase flow properties that may control recovery efficiency or alternatively remaining oil saturation. The validity of the pore class concept is also examined during the discussion and finally, the impact of wettability on recovery efficiency of carbonate core materials by water flooding is discussed.

6.1. Pore Structure Variations in Selected Carbonates

Lønøy's (2006) approach towards pore classification according is mainly based on thin-section image analysis or more accurately two-dimensional observation and cross-plots of permeability versus porosity. New information in three-dimensions (thin-section analysis porosity-permeability, and pore size distribution) was added in this work to improve the understanding of pore structure of studied carbonate pore classes. This information consists of derived pore size distribution from NMR and mercury porosimetry and results for comparison between them. The new information is summarized in the Appendix section.

NMR Pore size Distribution and Sub-Pore Classes

Results reveal consistency between derived pore size distribution by NMR and defined sub-pore classes according to the thin-section image. Figure 6.1 shows that NMR derived pore

size distribution of the sample containing pore class of *IP-PMe&IC-PMe* covers smaller pore sizes compared to sample of *IP-UMa&M-Ma*. The same argument is valid for derived pore size distribution from NMR for *M-Mi* as compared to *M-Ma* samples. This was a general observation for all selected carbonate samples, a few examples of which were also published previously (Pourmohammadi *et al.*, 2007).

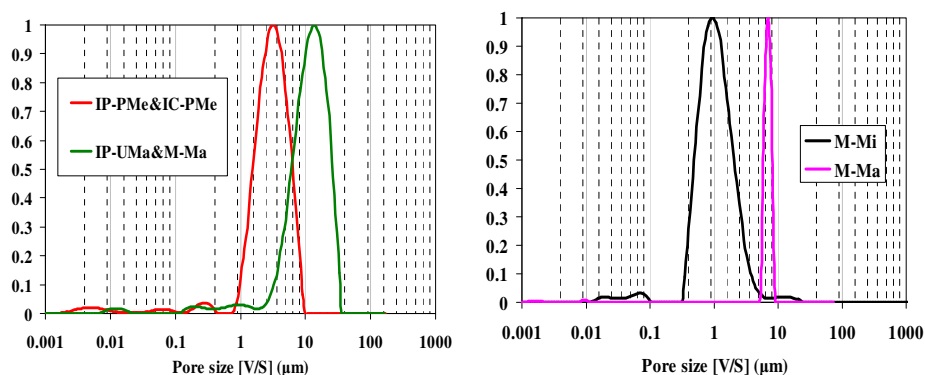


Figure 6.1: Derived pore size distributions of four sub-pore classes according to Lønøy's classification.

Discrepancy between NMR pore size and Mercury pore throat-size distributions comparison between derived pore size distribution of these carbonate pore classes by NMR and the mercury injection method has been recently published by Djurhuus *et al.* (2009).

Results revealed discrepancy between pore size distributions from the mercury intrusion capillary pressure and the NMR approach for all studied pore classes except the *IP-UMa* pore type. *IP-UMa* pore class behavior was similar to sandstones and the minor differences were explained by well connectivity of these materials as confirmed by high measured permeability (Pourmohammadi *et al.*, 2007) and thin-section images (see the example in the Appendix).

Surprisingly, for *IC-UMa* pore class, it was found that there is a significant discrepancy in both derived pore size distribution from NMR and mercury injection. Based on information from geological deposition and uniformly formed pores between crystals, it is presumed that

this pore class would behave as interparticle porosity and like Lucia (1983), group them together. However, it shown by Djurhuus *et al.* (2009), based on the information about the pore structure, this pore class is the most heterogeneous one among others. This observation is in good agreement with our foundation regarding variations in other single-phase and two-phase flow properties of *IC-UMa* samples compared to other pore classes.

The pore size distributions in core plugs of *IC-PMe&IP-PMe* porosities did not show bimodal distribution or dual-porosity behavior.

Samples of moldic pore class showed more variation in derived pore size distributions from mercury than NMR pore size distributions. This was more significant for most core plugs of *M-Ma* pore class compared to those of *M-Mi* pore class.

Because of domination of moldic pores in samples of *IP-UMa&M-Ma*, a similar discrepancy in pore size distributions from NMR and from mercury was observed.

6.2. Single-Phase Flow for Different Carbonate Pore Classes

In this section, at first variations of single-phase flow properties for selected samples with respect to their pore classes are reviewed, then correlations between these properties are discussed. The single-phase flow properties include *PSDI*, *formation and cementation factors*, derived *tortuosity factor*, *flowing fraction*, and *dispersivity*.

6.2.1. Variations in Single-Phase Flow Properties

Earlier studies by Skauge *et al.* (2006a) showed that the majority of miscible displacement in samples of different carbonate pore classes can be interpreted by the capacitance model proposed by Coats and Smith (1963). It was also shown that mixing properties obtained by simulation of dispersion experiments can be interrelated with waterflood efficiency of carbonates.

The study was expanded by Pourmohammadi *et al.* (2007) to include more carbonate pore classes and add more measured single-phase flow properties. It was shown that single-phase flow properties of carbonates are variable and the pore class concept can improve the understating of variations. Single-phase flow properties, which were measured were pore size distributions; electrical properties (*formation factor*; derived *tortuosity*, Archie parameters), and hydrodynamic properties (*flowing fraction* and *dispersivity*). Details of variations were presented in the second paper and are reviewed in this section for each pore class.

Chalky Micro-Porosity

Micropores in chalk materials are primary in origin and occur between grains of planktonic calcareous algae (*coccospheres*) or their component crystal plates (*coccoliths*). Among electrical properties, *tortuosity factors* derived from measured *formation factors* are lowest for chalky micro-porosity.

Less twistedness or crookedness in flow path in both *Cretaceous* and *Tertiary* chalk materials with micro-porosity is believed to be related to very small size of pore-throats and pore bodies (around 1 micron) with narrow pore size distributions. In addition, micro pores are also well connected as revealed by high *flowing fractions* found from simulation of miscible displacement. Above 90% flowing pore volume for all four *Tertiary* chalk samples and five out of six samples of *Cretaceous* chalk was obtained by simulation the effluent data from tracer displacement (Pourmohammadi *et al.*, 2007).

The distinction between *Tertiary* and *Cretaceous* deposited chalky rocks is important because the general decrease in the size of calcareous nannoplankton across the *Cretaceous-Tertiary* boundary (Macleod *et al.*, 1997), corresponds to a decrease in reservoir quality in *Tertiary* chalks (Hardman, 1983). According to Lønøy (2006), *Tertiary* chalk has higher micro-porosity and lower permeability compared to *Cretaceous* chalk.

Results of variations in single-phase flow properties of chalky rock samples also highlighted the necessity to distinguish between *Cretaceous* and *Tertiary* micro porosity rock samples (Pourmohammadi *et al.*, 2007) and found in accordance with Lønøy (2006). Pore size distributions from NMR are less broad for *Cretaceous* chalk compared to *Tertiary* chalk (see Appendix) which characterizes the former as more homogenous than *Tertiary* chalk.

Interparticle Porosity

Pore size distribution for samples of the *IP-UMa* pore class as found by Djurhuus *et al.* (2009) resembles the typical distribution of well characterized sandstones (see Appendix). A minor discrepancy between the mercury porosimetry data and the NMR distributions were observed. Measured permeabilities for samples of this pore class are high and they are in the range of Darcy (Pourmohammadi *et al.*, 2007).

The porosity is preserved between particles during the deposition and it is expected that the samples of the *IP-UMa* pore behave like well-sorted sandstones. Results showed that *tortuosity factors* of rock materials preserving this porosity are less than *tortuosity factors* of those with moldic porosity (with highest *tortuosity factors*) and higher than those with chalky-micro porosity (with lowest range of *tortuosity factors*).

Miscible displacement analysis showed that samples with *IP-UMa* pore class can have *flowing fractions* from 55 to 90 percent. In other words, up to 45 percent of interparticle porosity can be stagnant in carbonates. The NMR pore size distributions for core plugs of *IP-UMa* porosity were not so different to other pore classes except chalk materials of micro-porosity which, as mentioned earlier, had the most uniform pore size distributions (Pourmohammadi *et al.*, 2007).

Macro and Micro-Moldic Porosities

Among samples, those containing *M-Ma* have a high degree of crookedness in flow path. The derived NMR pore size distributions of three out of four *M-Ma* core materials are not too different compared to samples of other pore classes and for the fourth one, it is uniform (Pourmohammadi *et al.*, 2007). However, as stated in section 6.1, there are significant variations in pore throat-size distribution derived by mercury injection capillary pressure. This discrepancy could be due to the fact that the connectivity between molds is varied from well interaction to poor communication. This variable connectivity between molds can justify to some extent low *flowing fraction*, high *tortuosity factors*, and high *cementation factors* obtained for samples of this pore class compared to other carbonates.

Lucia's (1999) classification considers moldic pore type and a vuggy pore system in the same pore class and basically molds are regarded as small vugs. These studies showed that selected rocks containing moldic porosity behave like a single-porosity system with respect to

variations in single-phase flow properties while vuggy carbonates are well known to have dual-porosity behavior (Lucia, 1999).

It was observed that smaller size of the molds changes the single-phase flow properties (Pourmohammadi *et al.*, 2007) single-phase flow properties were different for samples of M-Mi and M-Ma pore classes. Although, larger span and broad NMR pore size distributions were obtained for the micro-moldic pore systems, compared to the *M-Ma* pore class, the pore throat-size distribution showed to correlate well with the pore size distribution. This basic information from the pore structure reveals that rock samples of *M-Mi* pore class is more homogenous than that of *M-Ma* pore class. *Tortuosity* is considerably reduced for carbonates of *M-Mi* pore class and a higher range of *flowing fraction* is measured.

Mixed Porosities of Molds and Interparticle Porosities

Core samples that contain this mixed pore class have lower permeabilities than those containing pure interparticle porosity (Pourmohammadi *et al.*, 2007). This is because samples of this pore class containing dominant moldic porosity which the connectivity between them might not be so strong.

Information from mercury injection and NMR revealed a discrepancy between pore throat-size distributions and pore size distributions respectively. Uniform pore size distributions were interpreted by NMR approach while a broad distribution appeared in pore throat-size distributions. The behavior of samples of this mixed pore class was similar to those of pure macro-pore class in terms of pore size distribution.

Single-phase flow properties of cores containing *IP-UMa&M-Ma* class were in the range between *IP-UMa* core plugs and *M-Ma* samples. *Tortuosity factors* of *IP-UMa&M-Ma* samples are in a higher range compared to those with only *IP-UMa* porosity and lower range compared to those with *M-Ma* porosity. Similar to core plugs of *M-Ma* pore system, higher *cementation factors* were measured for three selected samples representing *IP-UMa&M-Ma* which confirm the dominant influence of molds on electrical properties (Pourmohammadi *et al.*, 2007).

Results from miscible displacement showed that *flowing fraction* of *IP-UMa* porosity carbonates is higher than those containing *IP-UMa&M-Ma* pore class. Therefore, the

presence of the moldic pores compared to the case where only interparticle porosity exists may reduce the total connectivity between all pores as well as increase fraction of dead-end pores (Pourmohammadi *et al.*, 2007).

Intercrystalline Uniform Marco-Porosity

The intercrystalline porosity is by definition the porosity between crystals, which may be of either primary or secondary origin (Choquette and Pray, 1970). A primary origin is generally related to evaporite precipitation (porosity between evaporite crystals) while secondary porosity is created by diagenesis processes such as dolomitization and recrystallization (Lønøy, 2006). The intercrystalline and interparticle porosities have been grouped together by Lucia (1983). Lønøy (2006) realized that the distinction between them improves coefficients of correlation in cross-plots of permeability versus porosity.

One might presume since pores between crystals are uniform with respect to both the shape and the size, the material would behave like those with a well-sorted and homogenous medium like sandstones. However, single-phase and two-phase flow properties of carbonates containing this pore class were unpredictable and could be in the range of a homogenous material (chalk) or a heterogeneous rock sample (moldic pore system). This study advises the classification of interparticle and intercrystalline porosities into two pore classes because their single-phase flow as well as two-phase flow properties were considerably different (Pourmohammadi *et al.*, 2007, 2008a).

Flowing fractions from 0.35 to 1 were obtained by miscible displacement and low *tortuosity factors* (in the range values for chalk) to high *tortuosity factors* (in the range values for moldic porosity) were obtained. These variations in flow properties can be explained by discrepancy between derived pore size distributions from NMR and pore throat-size distributions from mercury injection. (see Appendix). The observed discrepancy can be due to the fact that there are variable pore sizes which are connected by different pore throat-sizes. As a result, pores between crystals can be well connected or have very low communication. All these observations led us to regard the samples of *IC-UMa* porosity as the least homogenous pore class.

Intercrystalline Uniform Micro-Porosity

Only three samples of *IC-UMi* porosity were selected to be studied. The single-phase flow properties were not too far from the *IC-UMa* porosity although pore size distributions from NMR and mercury injection showed that it is more homogenous.

Intercrystalline Patchy Micro-Porosity

Less discrepancy between pore size distributions from NMR and mercury injection for *IC-PMe* distribution reveals that it is more homogenous compared to *IC-UMa* porosity. As shown by Lønøy (2006), patchy distribution of pores creates special connectivity regions inside of the medium in such a way that less area is available to flow and acts like fractures in carbonate samples and thus enhances the permeability. Among the single-phase flow properties, flowing pore volume was in higher range for carbonates containing *IP-PMi* and *IC-PMe* porosities compared to samples of *IC-UMi* and *IC-UMa* pore classes. Although, pores are patchily distributed, no significant change in the range of *tortuosity factors* was observed for samples with intercrystalline patchy porosities compared to samples of *IC-UMi* and *IC-UMa* pore classes.

Generally, it seems that the size of pores between crystals and their distribution within the medium impacts on the single-phase flow properties.

Mixed Porosities of Intercrystalline and Interparticle Patchy Porosities

The preservation of mixed interparticle and intercrystalline porosities is due to partial diagenesis which can happen sometime after formation of primary interparticle porosity. Therefore, diagenesis processes such as crystallization and dolomitization alter some particles and the porosities between particles are overprinted by new porosities between crystals.

Measured permeabilities of three core plugs of *IC-PMe&IP-PMe* were lower than permeabilities of those with *IP-UMa* and *IP-PMe* porosities from the same reservoir formation (Pourmohammadi *et al.*, 2007). Pore size distributions from NMR compared to pore throat-size distributions did not show any significant discrepancy and relatively uniform distributions were observed.

The *flowing fractions* of porosities in samples with this pore class however were in the lower range (60 to 75 percent) and *tortuosity factors* were to some extent in the higher range

compared to the samples containing only interparticle porosity. Since samples of intercrystalline porosities showed generally higher heterogeneity than those with interparticle porosity, samples with a mixed pore class of these two also seem to be more heterogenous than those containing only interparticle porosity.

6.2.2. Miscible Displacement in Carbonates Containing Different Pore Classes

Impact of the pore structure on miscible displacement and particularly CO₂ miscible flood has been investigated in the past (Spence and Watkins, 1980; Baker, 1977; Bretz *et al.*, 1988). Dispersion experiments performed by Bretz *et al.* (1988) showed that the degree of dispersion controls the mixing zone and in addition to a broad pore size distribution, a preferential flow path is necessary to have high dispersion coefficients and low *flowing fractions*. However, the influence of different pore types of carbonates on mixing during the miscible displacement has not been systematically studied. This section addresses this topic for selected carbonates in this study for which pore class concept used to group them and they were used for dispersion experiments

It should be recalled that all fluid properties and the average interstitial velocity used in all miscible displacement experiments are identical (see Brigham *et al.* (1961)) about the impact of these properties on miscible displacement). Therefore, it would be convenient to compare mixing properties which were obtained by simulation of the effluent from miscible displacement.

Normalized Dispersivity from Miscible Displacements of Carbonate Cores

The dispersion coefficient is a measure of the rate of the dispersion but not the amount. The *dispersivity* is a measure of the local heterogeneity scale and for the local mixing flow regime; it is a more fundamental measure of dispersion than the dispersion coefficient. Since the *dispersivity* is scale dependent, the normalized *dispersivity* is more appropriate to be used.

Figure 6.2 shows normalized *dispersivity* from miscible displacement of carbonate cores. As seen, the normalized *dispersivity* is varied for carbonate samples as function of the pore class. The range of normalized *dispersivity* is small for homogenous chalk and moldic samples containing micro porosity and increases for core plugs with *IC-PM_e* and *IC-PM_i*, *IP-UM_a*,

IC-PMe&IP-PMe, *IC-UMi*, *IP-UMa&M-Ma*, *M-Ma* pore types respectively. The most unpredictable normalized *dispersivity* is dedicated to samples with the *IP-UMa* pore types which cover almost the entire range.

Normalized *dispersivity* for samples of a typical pore class is varied as other single-phase flow properties are changed. Local heterogeneities control pore size distribution, pore throat-size distribution, *tortuosity*, *flowing fractions* and the connectivity between pores. Normalized *dispersivity* is a function of all these parameters and as described in the previous section, these properties are varied in selected carbonates containing a particular pore class.

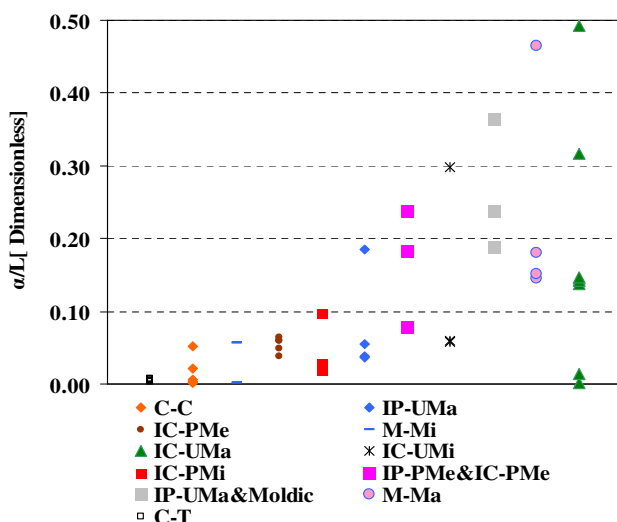


Figure 6.2: Normalized dispersivity of carbonates with different pore types.

However, results in this study indicate that in addition to pore size distribution and the preferential flow path, the miscible displacement in carbonate porous media is influenced by the type of the porosity, *tortuosity*, and amount of *flowing fraction*.

6.2.3. Relationship for Single-Phase Flow Properties

Measurement of different single-phase flow properties in this study enables us to examine interrelations between them and to find possible trends and correlations. Measured *formation factors* of samples were plotted versus their permeabilities and porosities in a log-log cross-plot (Pourmohammadi *et al.*, 2007).

Formation Factor and Porosity

Results of *formation factor* versus porosity were in good agreement with the Archie equation (1942) which predicts that with increase in the porosity, resistance of the medium to electrical flow will be reduced. A linear relationship can be found between the porosity and *formation factor* in log-log plot. Samples with *M-Ma* and *IP-UMa&M-Ma* porosities however grouped together and were out of the general trend.

Results show although the porosity is high for these samples, the *formation factors* are relatively high compared to others. This observation for carbonates with the moldic-porosity is well-known but for the *IP-UMa&M-Ma* pore class it is new. In other words, it was revealed that if some of the interparticle porosity due to incomplete diagenesis is partially overprinted by moldic porosity, the *formation factors* of such samples are increased.

High *formation factors* in cores with *IP-UMa&M-Ma* are indicator of high resistance to the electrical flow. The high resistance to flow can be due to poor connectivity of molds present between the particles as result of variations in pore throat-sizes.

Formation Factor and Permeability

The log-log cross-plot of the *formation factors* versus the permeability did not show a general trend (Pourmohammadi *et al.*, 2007). This means that carbonates with a high contrast in permeabilities (micro-Darcies to Darcies) may have the same range of *formation factor*. However, except for the core samples with *M-Ma* pore type, all measured *formation factors* showed negative trends with absolute permeabilities. This trend is strong if the pore class concept is taken to account. It is obvious that increase in the permeability is an indication of less resistance to the connection between pores and thereby lower resistivity of the medium to the electrical flow.

Formation Factor and PSDI

The question arose why *formation factors* or more precisely the derived *tortuosity* of some samples were in the range of (around 10) those derived for homogenous chalk samples with micro-porosities. Review information from pore size distributions derived from NMR and mercury injection revealed that those particular samples have the most narrow pore size distribution (characterized by higher *PSDI*) among other samples in their group (Figure 6.3).

Figure 6.3 generally suggests a negative trend between the degree of the pore size distribution and *tortuosity factors*. In other words, as pore size distribution in carbonates becomes more uniform, less crookedness path is available for the particles to flow through the medium.

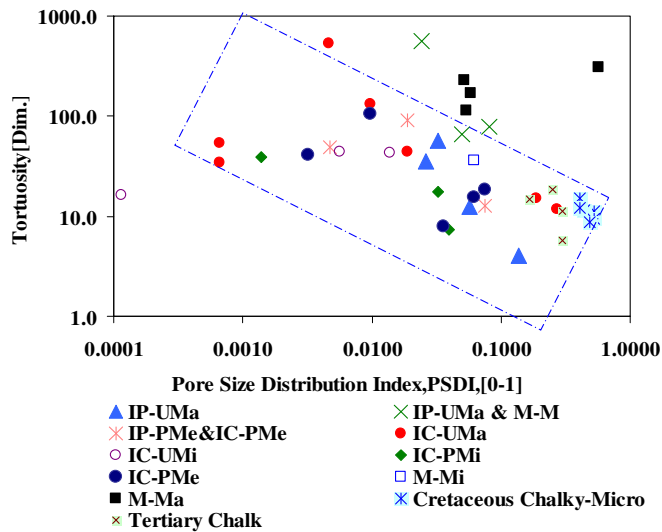


Figure 6.3: Semi-log correlation between tortuosity and pore size distribution index of carbonates with different pore types defined by Lønøy's classification.

As seen, two samples of *IC-UMa* have broad pore size distributions while the *tortuosity factors* are low. These two samples are coded F-108 and F-03 in the Appendix.

The pore throat-size distribution of these two samples derived from mercury capillary pressure showed left shoulder compared to other samples and NMR pore size distribution

showed left shoulder for F-108 and significant contribution of micro- porosity for F-03. These observations and a further look at the thin-section image revealed that these two samples contained smaller pores compared to others. Thus the smaller pore size could be one of the reasons that these two samples show lower *tortuosity factors*.

One sample of *IC-UMi* (coded as O-35) which has a broad pore size distribution and low *tortuosity factor* was given further attention to find out the reason for this by taking other parameters into account. Although the NMR pore size distribution was not available for O-15 and mercury data for S-1127, however, the thin-section analysis showed that this sample (O-35) has higher pore sizes (see NMR and mercury data in the appendix). On the other hand, flow fraction of this sample is high (0.96) as compared to others (one with *flowing fraction* of 0.43 and other with *flowing fraction* of 0.82).

Normalized Dispersivity versus PSDI and Tortuosity

Figure 6.4 shows the semi-log cross-plot of the normalized *dispersivity* versus the derived *PSDI* and *tortuosity factors* of selected samples.

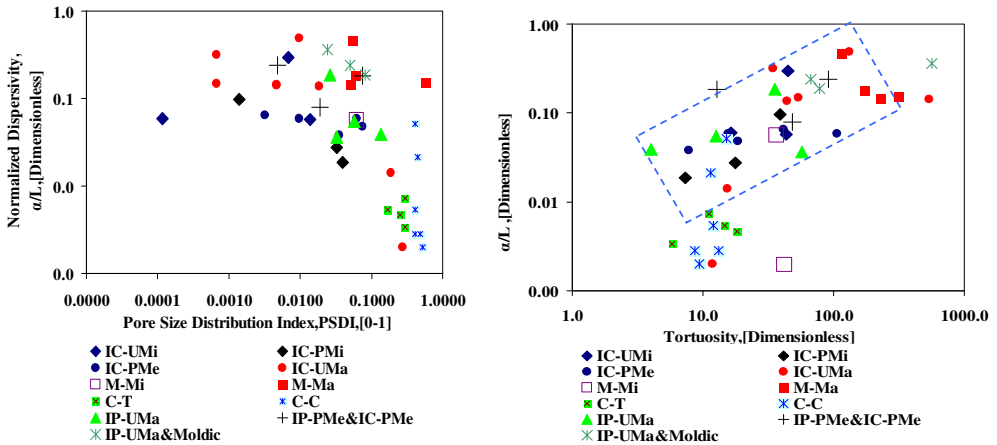


Figure 6.4: Semi-log correlation between normalized dispersivity and PSDI (left) and tortuosity factors (right) for all samples.

As seen, there is not any general correlation between normalized *dispersivity* and the *PSDI* (Figure 6.4(left)). There is not also any correlation among the majority of pore classes and a few like samples of *IP-UMa* & *M-Ma* and *IC-PMi* express a negative trend between normalized *dispersivity* and the *PSDI* (Figure 6.4). This means that for the majority of

selected carbonate samples, pore sizes can be distributed from uniform to a broad range while changes in normalized *dispersivity* can be minor.

Generally, a positive trend can be considered between normalized *dispersivity* and the degree of crookedness in flow (*tortuosity*) path inside selected carbonate core plugs where chalk samples and one sample of *IC-UMa* pore class are outside of the trend.

The stronger correlation between normalized *dispersivity* and *tortuosity factors* of carbonate samples is conceptually more logical because the traveling path of tracer particles (per length) depends on crookedness of the flow path (Figure 6.4 (right)). However, not trends among all pore classes are in good agreement with the general trend. Moldic porosity, *IC-PMe* & *IP-PMe* porosities, and to some extent chalky materials do not follow the general trend.

Low *tortuosity*, uniform pore size distribution, and high flowing fraction in chalk samples provide shorter mixing length during the miscible displacement. However, variations in the normalized *dispersivity* for chalk materials particularly for *Cretaceous* samples were related to different flowing fractions.

The samples of *IC-PMe* porosity do not show a strong trend of increase in the dimensions of mixing zone with respect to the higher *tortuosity factors* compared to those with only *IC-UMa* pore types

Two samples of *IC-UMa* porosity, which were outside of the general trend for the normalized *dispersivity* as a function of the *tortuosity factor*, were paid more attention. One of them has the lowest normalized *dispersivity* compared to other samples. The lowest normalized *dispersivity* for the sample of *IC-UMa* pore class is because this sample has the lowest *tortuosity factor* and the most uniform pore size distribution. The other one shows highest *tortuosity factor* and is located to the far right with respect to the general trend. The information from the pore structure by NMR and mercury (see Appendix) showed a bimodal pore size distribution (core ID F-89) which shows the sample has considerable micro-porosity. The significant crookedness in the flow path of this sample which is characterized by a high *tortuosity factor* is due to the contribution from the micro-porosity which surrounds macro-porosity (revealed by thin-section analysis). On the other hand, derived flowing pore

volume fraction from a miscible tracer dispersion test was around 0.96 which was high compared to other samples of this pore class. The high flowing fraction in this sample impacts low dispersion during the miscible displacement despite the significant crookedness in the flow path.

6.3. Link between Initial Water Saturations and Flow Properties

Before water flooding, the initial water saturation (S_{wi}) was established in selected samples by primary drainage with the same fluid system and identical procedures as described in chapter 5. In addition, single-phase flow properties of the selected samples were known from other measurements. These two reasons provide the possibility to examine the relationship between the S_{wi} and other properties of the medium such as porosity, permeability, *flowing fractions*, *tortuosity factor* and so on.

Influence of Flow Properties on S_{wi}

The S_{wi} at reservoir scale is a function of the capillary pressure or equivalent capillary height, wettability, and the rock-fabric (Lucia, 1999). Empirical equations were proposed by Lucia (1999) to predict the S_{wi} in interparticle porosity by conversion of the air/mercury capillary pressure to oil/water capillary pressure data by the Leverett J function (1941). These empirical equations are functions of the reservoir height (derived from capillary pressure) and porosity based on data sets of two selected fields. The equations predict reduction of the water saturation in a specific height in reservoirs with respect to increase in the porosity for non-vuggy interparticle porosity.

As mentioned, the water saturation is a function of the capillary pressure and wettability in the reservoir scale. Therefore, the capillary pressure and wettability should be undermined to be able to compare the S_{wi} for selected carbonates in this study. In order to undermine capillary pressure, it is shown that for all selected carbonate samples, the applied pressure during the primary drainage process is sufficient to achieve the water saturation equivalent to the asymptotic capillary pressure (see the point A in Figure 4.9 in chapter 4). If it is shown that this condition is valid for selected carbonate cores with variable permeability values (from 1md to 1 Darcy), S_{wi} are comparable. For this comparison, it should also be assumed that core materials are located at the same reservoir height.

Drainage Capillary Pressure for Chalky Core Samples

It is enough to examine the argument about the sufficiency of the applied pressure for primary drainage as discussed above, for chalk samples as the lowest permeable carbonates in this study. This is because the capillary pressure is lower for other carbonates since their permeabilities are higher than the chalk. In order to check that the mercury capillary pressure data for one sample of *Cretaceous* chalk and one of the *Tertiary* chalk samples were rescaled from air/mercury to brine/decane fluid system by employing the Leverett J function (1941). Results are shown by Figure 6.5. The permeabilities of these two chalk samples are 0.394 and 0.498 md.

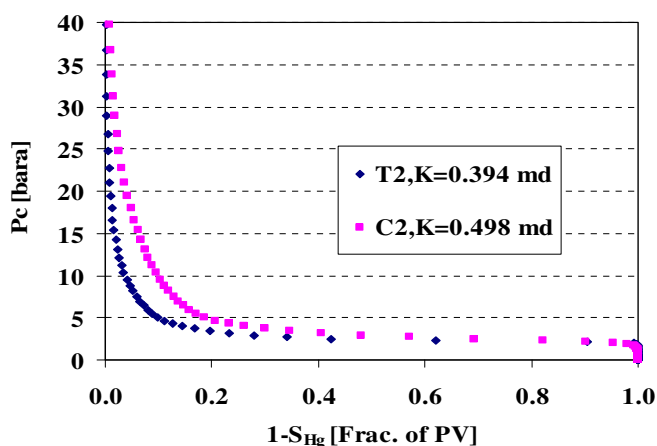


Figure 6.5: Rescaled brine/decane capillary pressure data from mercury/air system as a function of the air saturation for two chalk samples.

As seen, the asymptotic capillary pressure part starts from 20 bar and there is not any significant mercury occupation within the medium as the capillary pressure is increased.

During the primary drainage process, the initial injection rates were increased (doubled and then multiplied by a factor of 5) and significant water production was not observed. The maximum differential pressure which was allowed for injection rates were 30 bara for all experiments. As seen in Figure 6.5, applied differential pressure of 30 bara is in the range of asymptotic part of the capillary pressure curve.

Therefore it is concluded that the S_{wi} obtained by primary drainage process should not changed dramatically by capillary pressure variations. Since other selected carbonate samples are more permeable, it can be concluded that the applied pressure during the primary drainage with viscous oil is more than enough to establish water saturations which are not significantly sensitive to capillary pressure.

On the other hand, the S_{wi} of chalk samples are changed from 9 to 29 percent for *Cretaceous* chalk samples and 10 to 20 percent for *Tertiary* chalk cores. If these water saturations are compared with capillary pressure data for chalk materials reported elsewhere (Torsæter, 1984; Graue *et al.*, 1997), it is revealed that they are in the range of irreducible water saturations (asymptotic part in capillary pressure curve). Therefore, it is inferred that the S_{wi} established by primary drainage process for other carbonate samples are in the range of saturations equivalent to the asymptotic capillary pressure part.

For further discussion, we assume that our samples are from the same height of a reservoir and the interest is to verify the impact of flow properties on S_{wi} .

S_{wi} as a Function of Flow Properties

Figure 6.6 shows the cross-plots of established S_{wi} versus permeability and porosity as two fundamental properties of the medium to define pore classes.

As seen, although carbonate samples are grouped according to their variable permeabilities, there is not any general trend or any specific trend for a selected pore class between the S_{wi} and the absolute permeability of the medium.

The S_{wi} of samples compared to their porosities does not show any general trend or trends with respect to the pore class scheme. This means that the pore class concept initiated with the definition of the porous-permeability cross-plot, cannot be expanded to the relationship between S_{wi} , porosity and permeability.

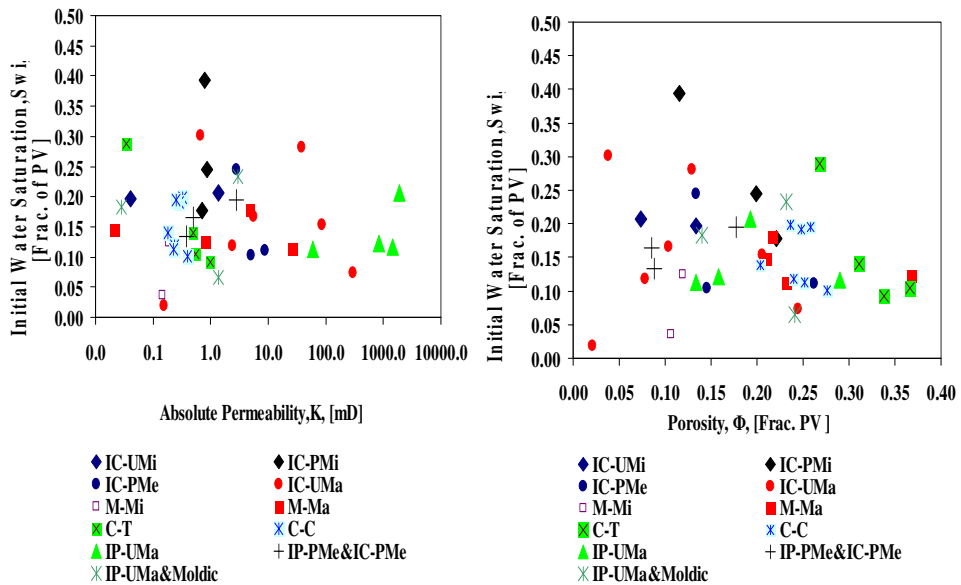


Figure 6.6: Cross-plots of S_{wi} versus permeability (left) and porosity (right).

Among other single-phase flow properties, *flowing fraction* was also considered as a parameter that may control the S_{wi} . As seen in Figure 6.7 (left), the *flowing fraction* does not hold any relationship with S_{wi} .

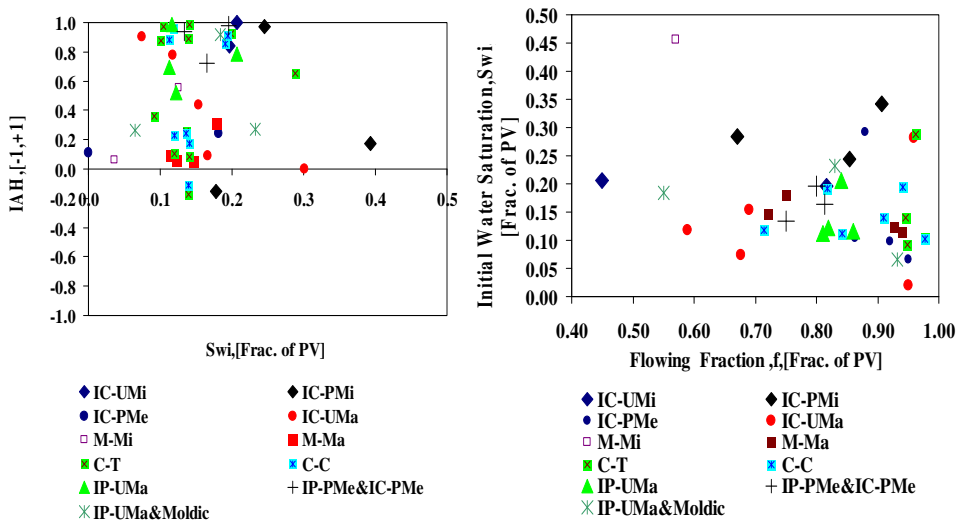


Figure 6.7: Cross-plots of S_{wi} versus flowing fraction (left) and Amott-Harvey index (right).

The study of 350 core samples from 30 different reservoirs from the North Sea by Skauge and Ottesen (2002) showed that S_{wi} decreases toward the neutral state. The Amott-Harvey wettability index was also included to find any wettability control on S_{wi} . As seen, S_{wi} mostly from 10 to 20 percent can be achieved by primary drainage over a range of wettability behavior from neutral to strongly-water.

The lack of relationship between S_{wi} and single-phase flow properties and wettability can be explain by the fact that the complexity in the pore structure of selected carbonate core samples is more influential on S_{wi} than flow properties.

6.4. Main Factors Influencing Remaining Oil Saturation

The remaining oil saturations of carbonate samples studied by Wardlaw (1976) showed increasing S_{orw} with decreasing porosity and the behavior explained by increasing pore to throat-size contrast which accompanies decreasing porosity. Chatzis *et al.* (1983) studied the effect of the pore structure on the remaining oil saturation in random packing and bead packs. The study emphasized snap-off and bypassing as two different mechanisms of oil-trapping. It was also found that the effect of the coordination number for a system by a high aspect ratio (the ratio between the dimensions of pore throats and pore body) is minor. For Berea sandstones it was shown that the mechanism of trapping due to high aspect ratio is mainly snap-off.

Similar to S_{wi} , no distinct or general trends between S_{orw} , the porosity and absolute permeability were revealed. The observation is that carbonates with low permeabilities (less than 1 mD) may also give low S_{orw} after water flooding.

Among the single-phase flow properties, *flowing fractions* of selected samples generally showed a weak negative trend with S_{orw} . Trends by including the pore class concept become stronger (Figure 6.8 (left)). In other words, S_{orw} for carbonate samples with a typical porosity with relatively higher flowing volume fraction (less stagnant volumes) is low. This may confirm that oil is displaced by water mostly from flowing volume of the medium.

There is evidence that for sandstones, there is a relationship between *cementation factor*, pore to pore coordination number, and consequently the amount of oil trapping in water-wet systems (Fatt, 1956; Chatzis and Dullien, 1977).

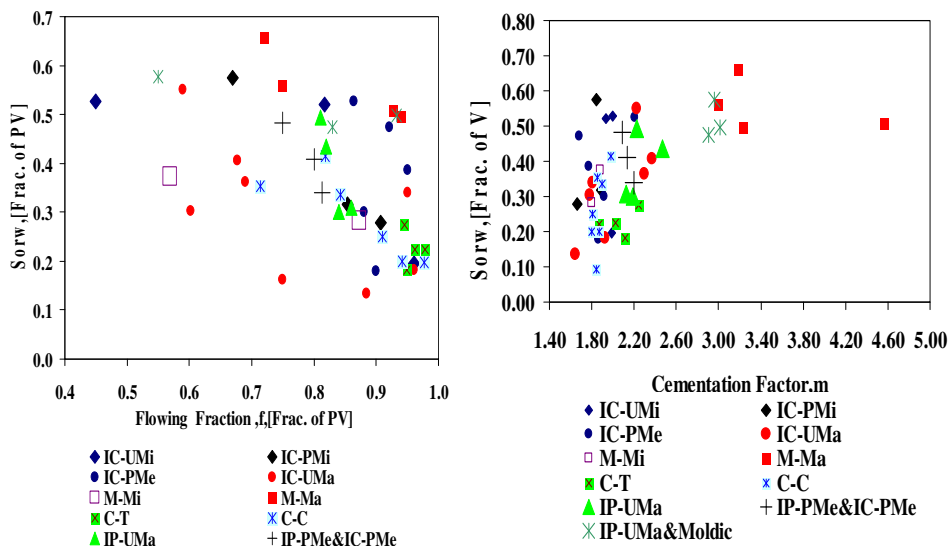


Figure 6.8: Remaining oil saturation after water flooding as a function of flowing fraction (left) and cementation factor (right).

The higher *cementation factor* is correlated with a higher pore coordination number and thereby more oil trapping or more remaining oil saturation. Such a correlation was examined for the data set available in this study and as seen there is not any strong correlation (Figure 6.8). The only notable observation is the grouping of samples of *IP-UMa* & *M-Ma* porosity and *M-Ma* in the cross-plot which reflects the similarity of these two pore classes with respect to the unfavorable pore connectivity which contributes to oil trapping during water flooding.

The pore size distribution index and the wettability index from the Amott-Harvey test were also examined for evidence of any possible influence on remaining oil saturations of samples after water flooding. Results are plotted and presented in Figure 6.9 (left) for remaining oil saturation versus the pore size distribution index. As seen, there is not any considerable relationship or general trend between variations in the pore sizes and remaining oil

saturations. Figure 6.9 (right) shows a negative trend between remaining oil saturations of samples and their *tortuosity factors*. A simple explanation could be that more oil-trapping is expected for carbonates with higher crookedness in the flow path during the water flooding.

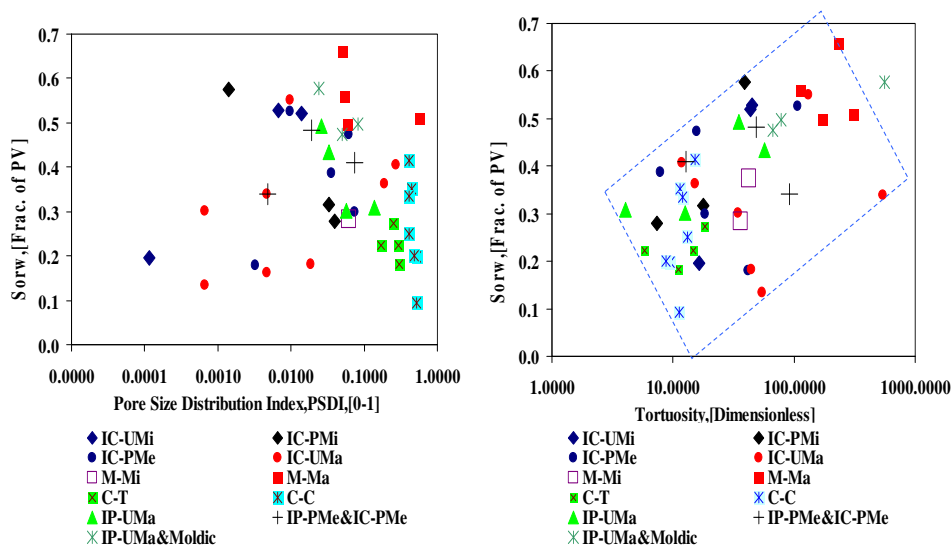


Figure 6.9: Remaining oil saturation after water flooding as a function of PSDI (left) and tortuosity (right).

6.5. Relative Permeability by Water Flooding of Carbonates

Neither interpreted relative permeabilities (Corey exponents) nor end-point relative permeabilities showed any correlation or link to the pore class scheme or single-phase flow properties. Combining information from wettability tests with the pore class concept also did not improve the link between relative permeability curves derived by reconciling the production history and differential pressure data recorded during the experiment.

Results are in accordance with Hamon (2003), who noted that for the rock-typing it is required to consider the process (imbibition or drainage) because the rock-typing is more related to the drainage process. He also showed that the wettability should be included for rock-typing. O’Hanlon *et al.* (1996) also stated the relationship between rock-types (geometry, topology, and pore type) and relative permeability curves vanish when the wetting conditions depart from strong preference.

Our results indicated that the pore classification scheme for selected carbonate samples does not specify any particular set of relative permeability for a typical selected pore type. Relative permeability thus is not discussed and instead water displacement efficiency is given attention.

Single-phase flow properties which can influence recovery were presented mostly in Paper III. It was shown that three main single-phase flow properties of carbonates in addition to porosity and permeability may control the waterflood recovery efficiency. These three main single-phase flow properties are *formation factor* (or derived *tortuosity*), *flowing fraction*, and *dispersivity*.

6.5.1. Correlations between Recovery Efficiency and Single-Phase Flow Properties

This section reviews the correlations between single-phase properties and waterflood efficiency for carbonate samples by unsteady-state flooding. The pore structure in porous media can be characterized by parameters such as pore to throat-size ratio, coordination number, the arrangement of pores and throats. Studies by Wardlaw and Cassan (1978) evaluated the impact of pore structure on recovery efficiency for imbibition processes (air displacing mercury) of carbonate samples. The study showed a positive trend between mercury recovery efficiency and the total porosity. However, low porosity rocks could have as high recovery as high porosity carbonate cores. Wardlaw (1976) explained the reduction in the recovery efficiency of less porous carbonates due to higher pore throat-sizes and lower pore sizes which accompanies decrease in the porosity.

Waterflood Efficiency, Absolute Permeability, and Porosity

Figure 6.10 presents the waterflood efficiency as a function of the porosity and permeability of selected carbonates in this study.

As seen, a general trend between recovery efficiency and porosity of core samples can be assumed. Some samples of *IP-UMa* porosity, moldic porosity, and *IC-PMe&IP-PMe* porosities are outside of the trend. Some pore classes may show an increase in recovery

efficiency as the porosity is increased such as *IP-UMa* & *M-Ma*, *IC-PMe* and *IC-PMi*, and *Cretaceous* chalky porosities. Figure 6.10 (left) shows that the carbonates with low porosity (less than 10 %) may give as high recovery as high porosity samples.

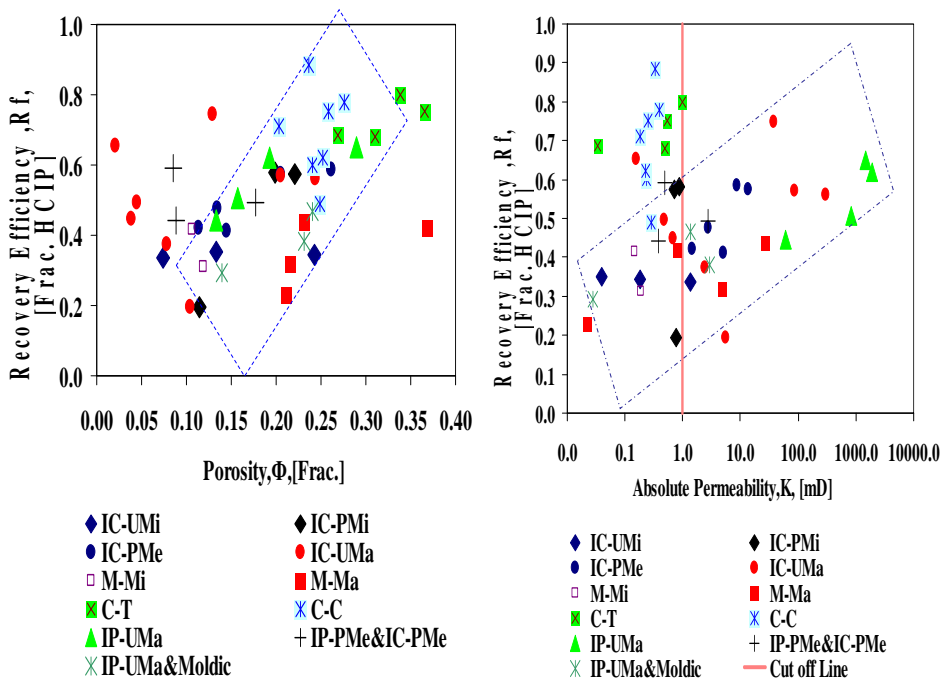


Figure 6.10: Waterflood efficiency as a function of the porosity (left) and the permeability (right).

Particular attention was given to samples of *IC-UMa* porosity and two of *IC-PMe* & *IP-PMe* porosities outside the assumed trend. Miscible displacement results showed that these samples have high *flowing fractions* and as a result, they can give high recovery efficiencies although they have low porosity.

Figure 6.10 (left) shows a negative between recovery efficiency and porosity for samples of *IC-UMa* which have porosities low 10 %. The decrease in recovery efficiency of these samples is related to decrease in *flowing fraction*. In other words, the increase in porosity accompanies increase in fraction of the stagnant volume and decrease in flowing volume which can lead to more trapping of the oil and consequently decrease in recovery efficiency.

There was a general observation among samples of other pore classes (except the rock samples of *IC-PMi* pore class where recovery efficiencies are close together) that if the development in porosity creates more less stagnant volume, it is favorable with respect to the recovery efficiency.

Figure 6.10 (right) shows the recovery efficiency by water flooding as a function of the permeability. The permeability of the medium is in fact a measure of the degree of restriction in pore connectivity and is related strongly to the pore throat-sizes (Pittman, 1992). A weakly positive trend between waterflood efficiency and the absolute permeability for carbonates with non-chalky micro-porosities can be considered. However, this general trend does not propose that carbonate with low permeability (even less than cut-off of 1 md) may give low recovery efficiency.

The permeability of porous media is controlled by the size of the pore-throats which connect pores to each other. The weak trend observed in Figure 6.10 (right) can be explained by the fact that higher permeability can be due to higher pore-throat sizes and consequently the lower pore aspect ratio. For the porous medium with water-wet behavior, low pore aspect ratio is in the favorite of less oil trapping and as a result higher recovery efficiency is expected (Wardlaw, 1976).

Waterflood Efficiency and Miscible Displacement

The impact of dispersion on the solvent miscible displacement particularly for CO₂ injection has been paid attention in the past (Bretz *et al.*, 1988; Dai and Orr, 1987; Baker, 1977; Stalkup, 1970). All studies showed the higher dead-end pores in coreflood scale may lead to less recovery by CO₂ miscible flooding.

The author is not aware of any reported attempt to evidence link between the miscible displacement and immiscible displacement for carbonate samples of different pore types. Comparison between miscible displacement parameters and waterflood efficiency reveals that carbonates with higher *flowing fraction* and lower *dispersivity* give higher recovery efficiency.

Waterflood Efficiency and Electrical Properties

Among electrical properties of the medium, a negative general trend was found between formation factor and recovery efficiency (Pourmohammadi *et al.*, 2008a).

Waterflood Efficiency and a Combined Property

It was found that if two flow properties are related together by multiplying or division to derive a new property, the correlation between the recovery efficiency and the new property becomes stronger. For example, Figure 6.11 shows a general trend between the ratio of tortuosity to *PSDI*, which shows recovery efficiency of carbonate samples decreases as this parameter increases. When carbonates contain porosities with a broad size distribution and with more crookedness in flow path, they become less homogenous (corresponds to higher values of the derived parameter) and thereby the amount of recoverable oil from them by water flooding is decreased. This parameter can be a measurement of heterogeneity in carbonates and a measure of the ability of the medium to trap the oil.

Chalk materials are grouped at the top of this trend with low *tortuosity factors* and uniform pore size distributions. The trends among the majority of samples contain different pore types are in a good agreement with the general trend. As seen, at a certain value of the heterogeneity parameter, recovery efficiency may change 20 to 60 percent which depends on the pore type and amount of *flowing fraction* of that pore type.

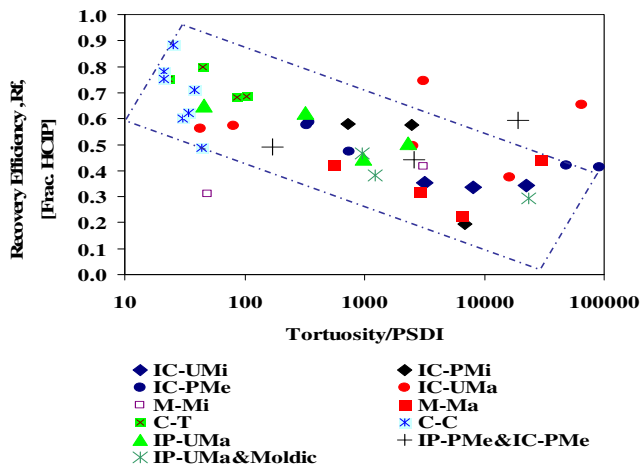


Figure 6.11: Recovery efficiency as a function of tortuosity/PSDI.

Waterflood Efficiency and Normalized Dispersivity

The dependency of recovery efficiency on *dispersivity* was discussed in Paper III; however, as mentioned earlier, the *dispersivity* is scale dependent. Length of core samples in this study varied from 5 to 7 cm and thereby the scale dependency might be concern. Therefore, it was decided to use the normalized *dispersivity*, which is the *dispersivity* of the medium per unit of the length.

Although in two-phase flow immiscible displacement, the wettability determines the flow path at the pore scale, hydrodynamic communication between pores determines the flow path at the larger scale (core scale). Effective hydrodynamic communication between pores perpendicular to and along the flow path makes the mixing zone length smaller and thereby in immiscible displacement, the front is smeared. The thick-front in immiscible displacement will lead to more vertical sweep efficiency and less oil is left behind and as a result, recovery efficiency is increased. Figure 6.12 shows that generally, if the measure of the normalized mixing length (normalized *dispersivity*) in the core flood experiments become smaller, recovery efficiency by water flooding may increase.

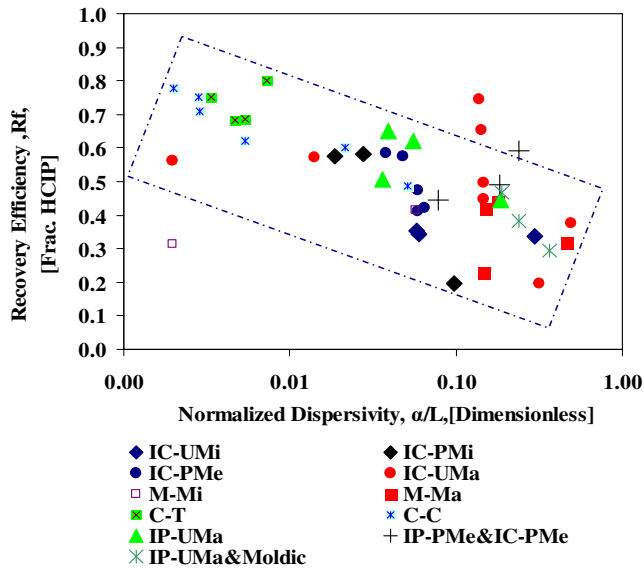


Figure 6.12: Recovery efficiency as a function of normalized dispersivity.

However, as seen in Figure 6.12, this is not entirely true for all pore classes. Samples of *IC-PMe&IP-PMe* show the opposite behavior so that higher normalized dispersivity is not correlated with lower recovery efficiency.

As seen in Figure 6.12, normalized *dispersivity* of four samples of *IC-UMa* porosities are around 0.15 while recovery efficiency varied from nearly 45 percent to 75 percent. These samples showed that they have different *flowing fractions* although the normalized *dispersivities* are not too different. This observation may lead us to conclude that if the medium possesses high fraction of stagnant volume, effective hydrodynamic communication and thick front of immiscible displacement may not enhance the recovery efficiency. This is because oil phase is likely to be trapped in stagnant volumes.

6.5.2. Wettability Effect on Recovery Efficiency

The Effect of restoration of wettability from water-wet on water flooding for only chalk samples and for a few samples of other pore classes were studied. The rest of carbonate samples is the subject for further investigation. In this section, relationship between S_{orw} and AH wettability index, waterflood efficiency as a function of spontaneous imbibition recovery in cleaned state, and effect of wettability alteration on waterflood efficiency for chalk samples are discussed

Remaining Oil Saturation and Wettability

The remaining oil saturation as a function of the wettability index does not show any specific trend for samples with the majority of pore classes. Figure 6.13 shows that S_{orw} has a tendency to be reduced when the wettability behavior of carbonate rock materials shifted from strongly water-wet toward the neutral. This general trend is in good agreement with what has already been observed from other studies for only sandstones (Anderson, 1987c; Skauge and Ottesen, 2002).

Two-phase flow properties (waterflood efficiency, S_{orw} , and S_{wi}) of only cleaned samples were compared to single-phase flow properties elsewhere. The additional data (data from restored samples inside the circle) were added to the main data-set (cleaned samples) to give more information about the impact of the wettability on remaining oil saturation.

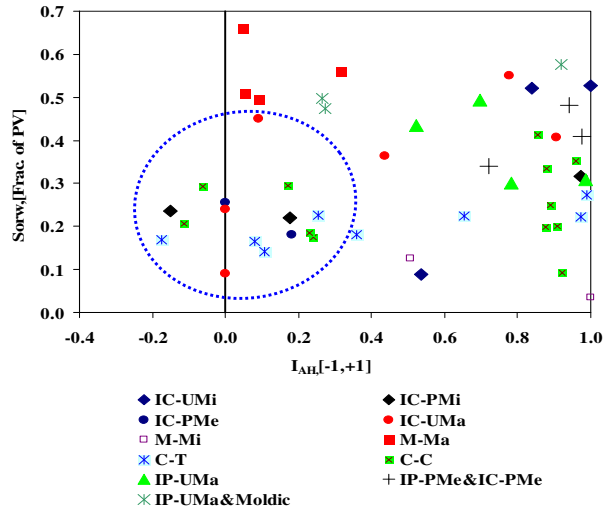


Figure 6.13: Remaining oil saturation as a function of AH wettability index.

Figure 6.13 shows that for the moldic porosity, although the wettability behavior is neutral, high remaining oil saturations are expected after water flooding. The reason for this is of course the impact of the pore structure which was discussed earlier. The same argument may be valid for the *IP-UMa&M-Ma* porosity which shows that despite a significant difference between the wettability of two samples and a third one, only 10 percent difference in S_{orw} is observed.

Waterflood Efficiency and Spontaneous Imbibition

Our results show that spontaneous imbibition is neither an indication of wettability nor an indication of total waterflood recovery for selected carbonate sample in this study. As seen, in Figure 6.14, samples which have a low degree of spontaneous imbibition can give the same range of total waterflood recovery as those with highly amount of spontaneous imbibition. Earlier studies by Skauge *et al.* (2006b) on 6 carbonated samples showed that waterflood efficiency of two samples after wettability restoration was not improved as compared to others. The only difference was that spontaneous imbibition did not happen for these two carbonate samples at restored state and the rest of samples had only a little spontaneous imbibition (less than at cleaned state).The recovery at restored state improved significantly

compared to the water-wet state. Studies by Webb *et al.* (2005) on core materials from the Valhall field, which is Tor formation (lower Cretaceous), showed that high waterflood efficiency is independent of the degree of spontaneous imbibition.

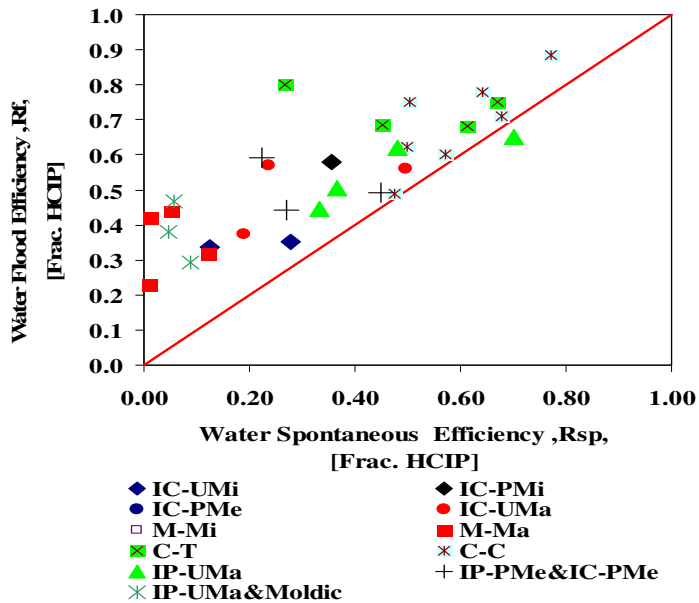


Figure 6.14: Remaining oil saturation as a function of recovery by spontaneous imbibition.

Although one can consider a general trend between total recovery efficiency and the spontaneous imbibition in Figure 6.14, the fact that they are independent should not be undermined. This study confirms that in order to achieve high waterflood efficiency carbonates, significant amount of spontaneous imbibition is not required. This is due to the fact that a little spontaneous imbibition can initiate sufficient pore accessibility for water phase to invade pores and create effective continuity in the water phase inside the medium.

Effect of Wettability on Waterflood Efficiency for Selected Chalk Samples

Studies have shown that wettability behavior of both sandstone and carbonate reservoirs varies with depth. The wettability behavior of core plugs from upstructure is close to oil-wet compared to midstructure, and water wetness is increased toward the water-oil contact (Hamon, 2000, 2004; Okasha *et al.*, 2003, 2004).

In particular, studies by Hamon (2004) on core samples from the *Ekofisk* field showed that there is a strong relationship between the water wetness and the elevation above the free water level. Since it is well known that wettability influences the recovery as discussed in chapter 4, an extended SCAL program was set up to investigate the effect of the wettability on recovery efficiency only for chalk samples.

The wettability of chalk materials from the *Ekofisk*, *Tor*, and *Oseberg* formations, which had already been used as the chalky pore class in earlier studies, were restored at reservoir conditions and flooded at the ambient condition. The restoration process reduced the spontaneous imbibition and the wettability behavior shifted significantly from water-wet toward the intermediate or more precisely mixed-wet; waterflood efficiency did not change significantly (Pourmohammadi *et al.*, 2008b). Therefore, study the effect of wettability behavior for chalk samples on water flooding reveals that petrophysical properties, as reflected in dispersion measurements on fully brine saturated samples, are more important in determining oil recovery than changes in wettability (Pourmohammadi *et al.*, 2008b).

These observations are in good agreement with the recent work of Johannesen *et al.* (2007a, 2007b) on 75 *Rødal* outcrop chalk which shows the maximum total water recovery is at a value of Amott-Harvey index of 0.4. However, in their results the difference between maximum recovery and the rest is not considerable (in the range of 0 to 10 %). It was also found that for restored chalk samples with the neutral wettability, higher capillary numbers (impacted by increasing the differential pressure or viscous forces) enhance waterflood efficiencies more compared to strong-wet condition.

CHAPTER 7

Concluding Remarks and Further Work

7.1. Main Conclusions

The carbonate reservoir rocks selected in this study were based on the pore system classification developed by Lønøy (2006). The concept of rock-typing has been tested against single-phase flow properties. Further correlations between single-phase and two-phase flow were studied, with emphasis on understanding the main factors that control efficiency of water flooding.

Variations in single-phase flow properties of selected carbonate core samples could not be described by only the pore classification. The supplemental information about pore structure from NMR and MICP further improved the understanding of variations in single-phase flow properties and waterflood efficiency. The possible rationale for these results is due to the fact that pore size distributions and also pore throat-size distributions, correlate with the connectivity between the pores which controls the single-phase and two-phase flow properties.

Rock-typing by study of single-phase flow properties was improved by including the pore class concept as the reference for comparison. Two-phase flow rock-typing was not inclusively successful with all employed information since relative permeability to water and oil did not show any relationship with the pore class and single-phase flow properties. The introduction of wettability variations further complicated the relationship between different properties.

Carbonate samples that contain well-sorted porosities with respect to pore geometries, pore shapes, and pore sizes may still behave as heterogeneous rocks when single-phase flow or two phase-flow properties are measured. This was well documented for carbonates containing intercrystalline and moldic pores, because samples of these pore classes behaved as

heterogeneous materials. The intercrystalline pore class showed large scatter in both *dispersivity* and oil recovery. Moldic porosity in carbonates may have good connectivity as indicated by the high *flowing fraction* inferred from the dispersion measurements. The size of the moldic pores seems to be a key element to link single- phase flow characteristics such as *dispersivity*, flowing and non-flowing fraction porosity and other petrophysical properties like *tortuosity*.

Definition of pore classes and selection of carbonate samples was initially based on trends between permeability and porosities in accordance with Lønøy (2006). This study showed that neither trends can be observed between initial water saturation and porosity nor initially defined pore classes are useful in explaining the relationships between initial water saturation and porosity .The same observation is also valid for initial water saturation and permeability. There was not identified any single-phase flow property which correlates to the amount of initial water saturation in the core samples.

Remaining oil saturation (S_{orw}) was found to be influenced by amount of *flowing fraction* and trends are stronger within a given pore class. The pore class concept is useful when S_{orw} and flow fraction are compared and generally, samples with higher flowing fraction have lower remaining oil saturation. There was not found any relationship between S_{orw} and porosity, permeability, *cementation factor*, and *PSDI* for the selected samples. There seems to be a positive and general trend between S_{orw} and *tortuosity* for carbonate core samples. This may be explained due to this fact that more oil is trapped due to higher crookedness in flow path.

It is concluded that there are variations in waterflood efficiencies for the carbonate samples studied and these variations depend on the type of pore class and also single-phase flow properties. It was revealed that pore class concept is not dominant in explaining waterflood efficiencies for carbonate samples and single-phase flow properties.

Basic matrix properties such as *flowing fraction*, *dispersivity* and *formation resistivity factor* strongly influence oil recovery, and can to certain extent be used in predicting oil production by water flooding. Waterflood efficiencies have positive trend with *flowing fraction*, negative trend with F_R (or *tortuosity*), and *dispersivity*.

Oil recovery at the water-wet state versus *flowing fraction* shows a general trend which is pore type dependent. By knowing the pore type, in addition to the *flowing fraction*, oil recovery can be better estimated. The flowing fraction at S_{orw} has a more unique relation to oil recovery independent of the pore type.

Variations in initial water saturation was not found to be related to change in wettability (measured by AH-method) for carbonate samples while there was general decrease in S_{orw} for samples with less water-wetness.

It is revealed that the spontaneous imbibition process is not a good indicator of wettability and forced imbibition should also be considered both for wettability description and waterflood response for carbonate samples in this work. The results have shown that only very limited spontaneous imbibition is required to enhance waterflood efficiency

The distinction between *Tertiary* and *Cretaceous* chalk is necessary to improve the understanding of chalk properties like; single-phase flow properties, waterflood efficiency, spontaneous imbibition, and wettability. These results are in accordance with the classification by Lønøy (2006). Studies of the effect of wettability alteration on chalk (from water-wet to intermediate-wet behavior) showed only minor changes in total waterflood efficiency. In other words, the pore structure of chalk materials seems to be more important compared to wettability with respect oil recovery. Samples of chalky micro pore class shows have high recovery by water flooding compared to most other carbonate samples. This is explained by the facts that these chalk samples are characterized by low degree of mixing, high *flowing fraction*, narrow pore size distribution, and low *tortuosity*.

7.2. Further Work

Results of this study are based on limited amount of selected samples for each pore class and all pore classes defined for carbonates were not included. Thus, it is recommended to include more samples for each particular pore class, as well as, extension of the research followed in these studies to other pore classes.

In this study, the effect of heterogeneity on microscopic scale for the flow properties on macroscopic scale (core scale) was investigated. The representative elementary volume (*REV*) for each pore class is not known in this work. More investigations are required to select the proper scale which could be sufficient for obtaining average properties for these carbonate materials.

The effect of change in wettability behavior on oil recovery efficiency is limited to chalk samples and a few cores from other pore classes. It would be interesting to have a more extensive study the effect of wettability restoration from water-wet state to less water-wet state on interrelation between single-phase flow properties and recovery efficiency. A more elaborate study of wettability would also quantify the importance with respect to recovery by water flooding, especially compared to other petrophysical properties.

.

REFERENCES

- Adamson, A. W. (1982). *Physical Chemistry of Surfaces*, 4th edition, New York City, John Wiley and Sons
- Amott, E. (1959). "Observations Relating to the Wettability of Porous Rock." *Trans. AIME* **216**: 156-62.
- Amyx, J. W., Bass, D., and Whiting, R.L. (1960). *Petroleum Reservoir Engineering*, New York City, McGraw-Hill Book Co.
- Anderson, W. G. (1986a). "Wettability Literature Survey-Part 1: Rock/Oil/Brine Interactions and the Effects of Core Handling on Wettability." *JPT* **38** (10): 1125-44.
- Anderson, W. G. (1986b). "Wettability Literature Survey-Part 2: Wettability Measurement." *JPT* **38** (11): 1246-62.
- Anderson, W. G. (1986c). "Wettability Literature Survey-Part 3: The Effects of Wettability on the Electrical Properties of Porous Media " *JPT* **38**(12): 1371-78.
- Anderson, W. G. (1987a). "Wettability Literature Survey-Part 4: Effect of Wettability on Capillary Pressure." *JPT* **39**(10): 1283-1300.
- Anderson, W. G. (1987b). "Wettability Literature Survey Part 5: The Effects of Wettability on Relative Permeability." *JPT* **39**(11): 1453-68.
- Anderson, W. G. (1987c). "Wettability Literature Survey-Part 6: The Effects of Wettability on Water Flooding." *JPT* **39**(12): 1605-22.
- Archie, G. E. (1942). "The Electrical resistivity log as an aid in determining some reservoir characteristics" *Trans. AIME* **146**: 54-62.
- Archie, G. E. (1950). "Introduction to Petrophysics of Reservoir Rocks." *AAPG Bulletin* **34**(5):.941-63.
- Archie, G. E. (1952). "Classification of carbonate reservoir rocks and petrophysical considerations", *AAPG Bulletin*, V.36: 278-98.
- Arya, A., Hewett, T. A., Larson, R. G., and Lake, L. W. (1988). "Dispersion and Reservoir Heterogeneity." *SPE Reservoir Eng.*: 139-48.
- Ausbrooks, R., Hurley, N. F., May, A., and Neese, D. G. (2004). *Society of Petroleum Engineers, SPE*, 56506.
- Aziz, K. and Settari, A. (1979). *Petroleum Reservoir Simulation*. London and New York, Applied Science Publisher.
- Baker, L. E. (1977). "Effects of Dispersion and Dead-End Pore Volume in Miscible Flooding" *SPEJ* **17**(3): 219-27.

- Batycky, J. P., Maini, B. B., and Fisher, D. B., (1982). "Simulation of miscible displacement in full-diameter carbonates cores." *SPE Journal* **22**: 647–57.
- Bear, J. (1972). *Dynamics of Fluids in Porous Media*. New York, Diver Publications.
- Bentsen, R. G. and Anlie, J. (1977). "Using Parameter Estimation Techniques to Convert Centrifuge Data into a Capillary Pressure Curve." *Trans., AIME* **56**.
- Biggar, J. W. and D. R. Nielsen (1960). *J. Geophys. Res* **65**: 2887.
- Bissell, H. J. and G. V. Chilingar (1967). "Classification of sedimentary carbonate rocks. Carbonate Rocks: Origin, Occurrence and Classification" in G. V. Chilingar, H. J. Bissell and R. W. Fairbridge, *Development in Sedimentology.*, Amsterdam, Elsevier, : 68-87.
- Bloch, F. (1946). *Phys.Rev* **70**: p.406.
- Boneau, D. F. and Clampitt, R. L. (1977). "A Surfactant System for the Oil-Wet Sandstone of the North Burbank Unit." *JPT* **29**(5): 501-06.
- Bowers, M. C., Ehrlich, R., Howard, J. J., and Kenyon, W. E. (2004). *Society of Petroleum Engineers*, 26307.
- Brace, W.F., Orange, A. S., and Madden, T.R. (1965). "The Effect of Pressure on the Electrical Resistivity of Water-Saturated Crystalline Rocks." *J. of Geophys. Res.* **70** (22):5669-78.
- Brace, W. F. and Orange, A. S. (1968). "Further Studies of the Effects of Pressure on Electrical Resistivity of Rocks." *J. of Geophys. Res.* **73**(16): 5407-20.
- Brannan, G. O., and Von Gonten, W. D. (1973). "The Effect of Temperature on the Formation Resistivity Factor of Porous Media." *Trans., 14th SPWLA Annual Logging Symposium, Lafayette, LA*, (May 6-9), Paper U.
- Bretz, R.E., Specter, R. M., and Orr, Jr. F. M., (1988). "Effect of pore structure on miscible displacements in laboratory cores" *SPE* 15017.
- Brie A., J.D.L., and Nurmi R. D. (1985). "Effect of Spherical Pores on Sonic and Resistivity Measurements." SPWLA, 26th Ann. Logging Symp., Paper W., Houston, Texas, June 17-20: p.22.
- Brigham, W. E. (1974). "Mixing Equations in Short Laboratory Cores." *Trans., AIME, SPEJ* **257**: 91-99.
- Brigham, W. E., Reed, P.W., and Dew, J. N. (1961). " Experiments on Mixing During Miscible Displacement in Porous Media." *SPEJ* **1**(1):1-8.
- Brooks, R. H. and Corey, A. T. (1964). "Hydraulic Properties of Porous Media." Hydraulic Paper Number 3, Colorado State University.
- Brooks, R. H. and Corey, A. T. (1966). "Properties of Porous Media Affecting Fluid Flow." *Proc. Amer. Soc. Civ. Eng* **92**: 61-87
- Brown, H. W. (1951). "Capillary Pressure Investigations." *Trans. AIME* **192**: 67-74.

- Brown, R. J. S. and Fatt, I. (1956). "Measurements of Fractional Wettability of Oil Field Rocks by the Nuclear Magnetic Relaxation Method." *Trans. AIME* **207**: 262-64.
- Brownstein, K. R. and T., C. E. (1977). *Journal of Magnetic Resonance Series A* **26**: 17-24.
- Brownstein, K. R. and T., C. E. (1979). *Physical Review A* **19**: 2446-53.
- Buckley, S. E. and Leverett, M. C. (1942). "Mechanism of Fluid Displacement in Sands." *Trans. AIME* **146**: 107-16.
- Burdine, N. T. (1953). "Relative Permeability Calculations from Pore Size Distribution." *Trans., AIME* **198**: 71-78.
- Carr, M.B., Ehrlich, R., Bowers, M.C., and Howard, J.J., (1996). "Correlation of porosity types derived from NMR data and thin section image analysis in a carbonate reservoir." *Journal of Petroleum Science and Engineering* **14**: 115-31
- Chatzis, I. and Dullien, F.A.L. (1977). "Modeling pore structure by 2-D and 3-D networks with application to sandstones" *J. Can. Petroleum Technology* 1-12.
- Chatzis, I., Morrow, N. R., and Lim, H.T. (1983). "Magnitude and Detailed Structure of Residual Oil Saturation" *SPEJ* **23**(2): 311-26.
- Chatzis, I. and Morrow, N. R. (1984). "Correlation of Capillary Number Relationships for Sandstone" *SPE Journal* **24**(5): 555-62.
- Chierici, G. L. (1984). "Novel Relations for Drainage and Imbibition Relative Permeabilities." *SPEJ*: 275-76.
- Chilingar, G. V. and Yen, T.F. (1983). "Some Notes on Wettability and Relative Permeabilities of Carbonate Reservoir Rocks, II" *Energy Sources* **7**(1): 67-75.
- Chilingarian, G. V., S. J. Mazzullo, et al., Eds. (1992). *Carbonate Reservoir Characterization: A Geologic-Engineering Analysis, Part I*, New York, Elsevier.
- Choquette, P. W., and L. C. Pray (1970). "Geologic nomenclature and classification of porosity in sedimentary carbonates", *AAPG Bulletin*, **54**: 207-50.
- Clavier, C., Coates, G., and Dumanoir, J. (1984). "Theoretical and Experimental Bases for the Dual-Water Model for Interpretation of Shaly Sands." *Soc. of Petrol. Eng. J*, April: 153-68.
- Coats, K. H. and Smith, B. D. (1963). "Dead-End Pore Volume and Dispersion in porous Media." *Trans., AIME* **231**: 73-84.
- Coley, F. H., Marsden, S. S., and Calhoun, J.C. (1956). "A Study of the Effect of Wettability on the Behavior of Fluids in Synthetic Porous Media." *Prod. Monthly* **20**(8): 29-45.
- Corey, A. T. (1954). "The Interrelation between Gas and Oil Relative Permeabilities." *Prod. Monthly* **19**(1): 38-41.
- Corey, A. T. and Rathjens, C.H. (1956). "Effect of Stratification on Relative Permeability" *Trans. AIME* **8**(2): 69-71.

- Cornell, D. and Katz, D. L. (1953). "Flow of Gases through Consolidated Porous Media." *Ind. Eng. Chem.* **45**.
- Craig, F. F. (1971). *The Reservoir Engineering Aspects of Water Flooding*, Monograph Series, Richardson, TX **3**.
- Cuie, L. (1984). "Rock/Crude-Oil Interactions and Wettability: An Attempt to Understand Their Interrelation." *SPE* 13211.
- Dai, K. K. and Orr, F.M. Jr. (1987). "Prediction of CO₂ Flood Performance: Interaction of Phase Behavior with Microscopic Pore Structure Heterogeneity" *SPE* **2**(4): 531-42.
- Deans, H. A. (1963). "A Mathematical Model for Dispersion in the Direction of Flow in Porous Media." **228**(49).
- Delshad, M., MacAllister, D.J., Pope, G.A., and Rouse, B.A. (1985). "Multiphase Dispersion and Relative Permeability Experiments" *SPEJ* **25**(4): 524-34.
- Dixit, A. B., Buckley, J. S., McDougall, S. R., and Sorbie, K. S. (1998a). "Core Wettability: Should A_H Equal I_{USBM} ?" *SCA 9809, International Symposium of Special Core Analysis held in the Netherlands*.
- Dixit, A. B., McDougall, S. R., and Sorbie, K. S. (1998b). "Analysis of Relative Permeability Hysteresis Trends in Mixed-wet Porous Media Using Network Models." *SPE* 39656.
- Dixit, A. B., Buckley, J. S., McDougall, S. R., and Sorbie, K. S. (2000). "Empirical Measures of Wettability in Porous Media and the Relationship between them Derived from Pore-Scale Modeling." *Transport in Porous Media* **40**: 27-54.
- Djurrus, K., Lien, J.R., Skauge, A., and Sørland G.H. (2009). Pore Structure Variations in Carbonates. (in progress).
- Dolka, M. E. (1981). Effect of Temperature on Formation Resistivity of Some Saudi Reservoir Rocks. *SPE Middle East Oil Technical Conference and Exhibition*, Bahrain, March 9-12
- Donaldson, E. C., Thomas, R. D., and Lorenz, P. B. (1969). "Wettability Determination and Its Effect on Recovery Efficiency." *SPEJ* **9**(1): 13 - 20.
- Donaldson, E. C. (1980). "Equipment and Procedures for Fluid and Wettability Tests of Geological Materials." Bartlesville Energy Technology Center. Report DOE/BETC/IC-79/5.
- Dullien, F. A. L. (1992), *Porous Media Fluid Transport and Pore Structure*, 2nd ed. San Diego Academic Press, Inc.
- Dunham, R. J. (1962). "Classification of carbonate rocks according to their depositional texture", in W. E. Ham, ed., *Classification of Carbonate Rocks*: Tulsa. OK. *AAPG (Memoir 1)*: 108-21.
- Dunn, K. J., Bergman, D. J., and LaTorraca, G.A (2002). *Nuclear Magnetic Resonance - Petrophysical and Logging Applications*. Pergamon, Amsterdam.
- Embry, A. F. and J. E. Klovan (1971). "A late Devonian reef tract on northeastern Banks Island Northwest Territories", *Bulletin Canadian Petroleum Geologists*, **19**: 730-81.

- Fatt, I. (1956). "The Network Model of Porous Media" *Trans. AIME*, **207**: 144-81.
- Fatt, I. (1957). "Effect of Overburden and Reservoir Pressure on Electrical Logging Formation Factor." *AAPG Bulletin* **41**(11): 2456-66.
- Foley, I., Farooqui, S. A., and Kleinberg, R. L. (1996). *Journal of Magnetic Resonance Series A*: 95-104.
- Folk, R. L. (1959). "Practical petrographic classification of limestones", *AAPG*, **62**: 344-59.
- Folk, R. L. (1962). "Spectral subdivision of limestone types", in W. E. Ham, ed., *Classification of Carbonate Rocks*, *AAPG (Memoir 1)*: 62-84.
- Focke, J. W. and Munn, D. (1987). "Cementation Exponents in Middle Eastern Carbonate Reservoirs." *SPEFE*: 155-67.
- Geffen, T. M., Owens, W. W., Parrish, D. R. and Morse, R. A. (1951). "Experimental Investigation of Factors Affecting Laboratory Relative Permeability Measurements." *Trans. AIME* **192**: 99-110.
- Gelhar, L. W., A. Mantoglou, C. Welty, and K. R. Rehfeldt. (1985). A review of field-scale physical solute transport processes in saturated and unsaturated porous media. Palo Alto, California, Electric Power Research Institute EPRI.
- Gelhar, L. W., C. Welty, and K.R. Rehfeldt. (1992.). "A Critical Review of Data on Field-Scale Dispersion in Aquifers." *Water Resources Research* **28**(7): 1955–74.
- Glanville, C. R. (1959). "Laboratory Study Indicates Significant Effect of Pressure on Resistivity of Reservoir Rocks." *J. Pet. Tec.*: 20-26.
- Goddard, R. R. (1966). "Fluid Dispersion and Distribution in Porous Media Using the Frequency Response Method with a Radioactive Tracer." *Trans. AIME, SPEJ* **6**: 143 -52.
- Grane, F. E., Gardner, G.H.F (1961). "Measurements of transverse dispersion in granular media." *J. Chem. Eng.* **6**(2): 283– 87.
- Graue, A., Bognø, T., Moe, R.W., Baldwin, B.A., Spinler, E.A., Maloney, D., Tobola, D.P. (1997). "Impacts of Wettability on Capillary Pressure and Relative Permeability" **SCA-9907**, International Symposium of the Society of Core Analysts.
- Hall, A. C., Collins, S. H., and Melrose, J. C. (1983). "Stability of Aqueous Wetting Films in Athabasca Tar Sands." *SPEJ* **23**(2): 249-58.
- Hamon, G. (2000). "Field-Wide Variations of Wettability" *SPE* 63144.
- Hamon, G. (2003). "Two-Phase Flow Rock-Typing: Another Approach" **SCA 2003-13**, *International Symposium of the Society of Core Analysts*.
- Hamon, G. (2004). "Revisiting Ekofisk and Eldfisk wettability" *SPE* 90014.
- Hardman, R. F. P. (1983). Chalk hydrocarbon reservoirs of the North Sea –An introduction. Proceedings of the *JAPEC Chalk Seminar*, 15 December 1983.
- Hassler, G. L. and Brunner, E. (1945). "Measurement of Capillary Pressure in Small Cores." *Trans. AIME* **160**: 114-23.

- Helander, D. P. and Campbell, J. M. (1966). "The Effect of Pore Configuration, Pressure and Temperature on Rock Resistivity." *Trans., Seventh SPWLA Annual Logging Symposium*, Paper W.
- Honarpour, M., Koederitz, L., and Harvey, A. H. (1994). *Relative Permeability of Petroleum Reservoirs*. Roca Raton CRC Press.
- Howard, J. J., Kenyon, W. E., and Straley, C. (1993). *Society of Petroleum Engineers*, 20600.
- Jha, R. K. (2005). Pore level Investigation of dispersivity. Petroleum Department. Austin, the University of Texas at **Msc. Dissertation**
- Johnson, E. F., Bossler, D.P. and Naumann, V.O. (1959). "Calculation of Relative Permeability from Displacement Experiments." *Trans. AIME* **216**: 370-72.
- Johannesen, E. B., Graue, A., Baldwin, B.A., and Tobola, D.P. (2007a). "Establishing Mixed Wet Conditions in Chalk-Emphasis on Wettability Alteration and Oil Recovery" **SCA 2007-40**, *International Symposium of the Society of Core Analysts, Calgary, Canada, 10-12 September*.
- Johannesen, E. B., Graue, A. (2007b). "Systematic Investigation of Waterflood Reducing Residual Oil Saturations by Increasing Differential Pressures at Various Wettabilities" *SPE108593*
- Josendal, V. A., Sandiford, B. B., and Wilson, J. W. (1952). "Improved Multiphase Flow Studies Employing Radioactive Tracers." *Trans. AIME*.
- Kamath, J., Meyer, R.F. and Nakagawa, F.M. (2001). "Understanding Waterflood Residual Oil Saturation of Four Carbonate Rock Types." *Paper SPE 71505 presented at the SPE Annual Technical Conference and Exhibition, New Orleans, LA, 30 September-3 October*
- Kasraie, M., Farouq Ali, S.M. (1984). "Role of Immobile Phase Saturations in Tertiary Oil Recovery" *Paper SPE 12635 presented at SPE Enhanced Oil Recovery Symposium, 15-18 April, Tulsa, Oklahoma*
- Kenyon, W. E., Day, P.I, Straley, C., and Williem Sen, J. F. (1988). "A Three-Part Study of NMR Longitudinal Relaxation Properties of Water-Saturated Sandstones." *SPE Formation Evaluation*.
- Killins, C. R., Nielsen, R. F., and Calhoun, J. C. (1953). "Capillary Desaturation and Imbibition in Porous Rocks." *Producers Monthly* **18**(2): 30-39.
- Killough, J. E. (1976). "Reservoir Simulation with History-Dependent Saturation Functions." *SPEJ*.
- Kleinberg, R. L., Kenyon, W.E., and Mitra, P.P. (1994). *Magnetic Resonance Imaging* **12**:271-74.
- Korringa, J., SeEVERS, D. O., and Torrey, H. C. (1962). *Phys.Rev.* **127**:1143-48.
- Kovscek, A. R., Wonh, H., and Radke, C. J. (1993). "A pore-Level Scenario for the Development of Intermediate Wettability in Oil Reservoirs." *AICHE Journal* **39**(6): 1072-85.
- Lake, L. W. (1989). *Enhanced Oil Recovery*. New Jersey, Prentice-Hall.
- Langnes, G. L., Robertson, Jr., J. O, and Chilingarian, G. V. (1972). *Secondary Recovery and Carbonate Reservoirs*. New York, Elsevier.

- Leas, W. J., Jenks, L. H., and Russell, D. (1950). "Relative Permeability to Gas." *Trans. AIME* **189** 65-72.
- Leighton, M. W. and C. Pendexter (1962). "Carbonate rock types", in *Classification of Carbonate Rocks*, W. E. Ham., Amsterdam, AAPG. **Mem. 1**: 33-61.
- Leverett, M. C. (1941). "Capillary Behavior in Porous Solids." *Trans. AIME* **142**: 152-69.
- Levine, J. S. (1954). "Displacement experiments in a consolidated porous system." *Trans. AIME* **201**: 57-66.
- Lewis, M. G., Sharma, M. M., and Dunlap H. F. (1988). "Wettability and Stress Effect Saturation and Cementation Exponents." *SPWLA, 29th Ann. Logging Symp.* Paper K., June 5-8.
- Lomeland F., Ebeltoft, E. and Thomas, W. H. (2005). A New Versatile Relative Permeability Correlation. Rewired paper at the at the 2005 *International Symposium of the SCA*. Toronto, Canada: 21-25.
- Lomeland, F., and Ebeltoft, E. (2008). "A New Versatile Capillary Pressure Correlation." *Reviewed Proceeding of 22nd International Society of Core Analysis, held in Abu Dhabi, UAE, 29 Oct.-2 Nov.*
- Longeron, D. G., Argaud, M.J., and Feraud, J.P. (1989). "Effect of Overburden Pressure and the Nature and Microscopic Distribution of Fluids on Electrical Properties of Rock Samples." *SPEFE, Trans. AIME* **287**:194-202.
- Lønøy (2006). "Making Sense of Carbonate Pore Systems." *AAPG Bulletin* **90**(9): 1381-405
- Lucia, F. J. (1983). "Petrophysical Parameters Estimated from Visual Descriptions of Carbonate Rocks: a Field Classification of Carbonate Pore Space." *JPT*: 629-37.
- Lucia, F. J., and Conti, R. D. (1987). Rock Fabric, Permeability, and Log Relationships in an Upward-Shoaling, Vuggy Carbonate Sequence. The University of Texas at Austin, Geological Circular 87-5: p.22.
- Lucia, F. J. (1995). "Rock-fabric/petrophysical classification of carbonate pore space for reservoir characterization", *AAPG Bulletin*, **79**: 1275-1300.
- Lucia, F. J. (1999). *Carbonate Reservoir Characterization*, Berlin Heidelberg, Springer Verlag.
- Lyne, A., Varini, G., and Ghilardotti G. (1996). *Society of Petroleum Engineers*, 36852.
- Macleod, N., and 21 other authors (1997). "The Cretaceous-Tertiary Biotic Transition", *Journal of the geological Society (London)* **154**: 265-92.
- Makuch, D. S. (2005). "Longitudinal Dispersivity Data and Implications for Scaling Behavior." *Ground Water* **43**(3): 444-56.
- Matteson, A., Tomanic, J. P., Herron, M. M., Allen, D. F., and Kenyon, W. E. (2000). *SPE Reservoir Evaluation & Engineering* **3**:408-13.
- McCall, K. R., Johnson, D. L., and Guyer, R. A. (1991). *Physical Review* **B 44**:7344-55.

- McCall, K. R., Guyer, R. A., and Johnson, D. L. (1993). *Physical Review* **B 44**:7344-55.
- McDougall, S. R., and Sorbie, K.S. (1995). "The Impact of Wettability on Water flooding: Pore-Scale Simulation." *SPE Reservoir Eval. & Eng* **10**(3): 208-13.
- Meiboom, S. and Gill, D. (1958). *Review of Scientific Instruments* **29**: p.688-691.
- Melrose, J. C. (1982). "Interpretation of Mixed Wettability States in Reservoir Rocks." *SPE* 10971.
- Melrose, J. C. (1988). "Use of Water-Vapor Desorption Data in the Determination of Capillary Pressures at Low Water Saturations." *SPE Reservoir Engineering* **3**(3): 913-18.
- Moore, C. H. (2001). *Carbonate Reservoirs: Porosity Evolution and Diagenesis in a Sequence Stratigraphic Framework*, Amsterdam, Elsevier.
- Morrow, N. R. (1976). "Capillary pressure correlations for uniformly wetted porous media." *Journal of Canadian Petroleum Technology*, Oct.-Dec. **15**(4): 49-69.
- Morse, R. A., Terwilliger, P. L., and Yuster, S. T. (1947). "Relative Permeability Measurements on Small Core Samples." *Oil & Gas J.* **46**(16): 109-25.
- Mount, M. (1985). "Mixed siliciclastics and carbonate sediment: A proposed first-order textural and compositional classification", *Sedimentology*, **32**: 435-42.
- Muscatt, M. (1937). *The Flow of Homogenous Fluids through Porous Media*. New York, McGraw-Hill.
- O'Hanlon, M. E., Black, C.J.J., Webb, K.J., Bin-Daer, G., and El-Tawil, A. (1996). "Identifying the Controls on Waterflood Performance in a Giant Carbonate Reservoir" *SPE* 39206, *International Petroleum Exhibition and Conference, 13-16 October, Abu Dhabi, UAE*.
- Okasha, T. M., Funk, J.J., Al-Enezi, S.M. (2003). "Wettability and Relative Permeability of Lower Cretaceous Carbonate Rock Reservoir, Saudi Arabia" *SPE* 81484.
- Okasha, T. M., Funk, J.J., Al-Enezi, S.M., Al-Rashidi, H.N. (2004). "Fifty Years of Wettability Measurements in the Arab-D Carbonate" **SCA 2004-03**, *International Symposium of the Society of Core Analysts, Dhahran, Saudi Arabia*.
- Osoba, J. S., Richardson, J. G., Kerver, J. K., Hafford, J. A., and Blair, P. M. (1951). "Laboratory Measurements of Relative Permeability." *Trans. AIME* **191**: 47-56.
- Owens, W. W. and Archer, D. L. (1971). "The Effect of Rock Wettability on Oil-Water Relative Permeability Relationships." *JPT, Trans. AIME* **251**: 873-78.
- Perkins, J. F. and Johnson, O. C. (1963). "A Review of Diffusion and Dispersion in porous Media." *SPE Journal* **3**:70-84.
- Pettijohn, F. J. (1975). *Sedimentary Rocks*. New York, Harper & Row.
- Pickens, J. F., and G. E. Grisak. (1981). "Scale-Dependent Dispersion in a Stratified Granular Aquifer." *Water Resources Research* **17**(4): 1191-211.
- Pittman, E.D. (1992). "Relationship of Porosity and Permeability to Various Parameters Derived from Mercury Injection-Capillary Pressure Curves for Sandstone" *Bull. AAPG*, **76**: 191-98

- Pourmohammadi, S., Hetland, S., Spildo, K., and Skauge, A. (2007). "Fluid Flow Properties of Different Carbonate Pore Classes." *SPE/EAGE Reservoir Characterization and Simulation Symposium, SPE 111433*.
- Pourmohammadi, S., Hetland, S., Spildo, K. and Skauge, A. (2008a). "Does the Pore Class Concept for Carbonates Make Sense for Multi Phase Flow?" **SCA 2008-29**, *International Symposium of the Society of Core Analysts*, Abu Dhabi, UAE 29 October-2 November.
- Pourmohammadi, S., Hetland, S., Spildo, K., and Skauge, A. (2008b). "Impact of Petrophysical Properties on Water Flooding in Cretaceous and Tertiary Chalk" **SCA 2008-28**, *International Symposium of the Society of Core Analysts*, Abu Dhabi, UAE 29 October-2 November.
- Purcell, W. R. (1949). "Capillary Pressures - Their Measurement Using Mercury and the Calculation of Permeability There from." *Trans. AIME* **186**: 39-48.
- Rapoport, L. A. and Leas, W.J. (1953). "Properties of Linear Waterfloods." *Trans. AIME* **198**: 139-48.
- Raza, S. H., Treiber, L. E. and Archer, D. L. (1968). "Wettability of Reservoir Rocks and Its Evaluation." *Prod. Monthly* **37**(4): 82-87.
- Richardson, J. G., Kerver, J. K., Hafford, J. A. and Osoba, J. S. (1952) "Laboratory Determination of Relative Permeability." *Trans. AIME* **195**: 187-96.
- Rosales, C. P. (1982). "On the Relationship between Formation Resistivity Factor and Porosity." *Soc. of Petrol. Eng. J.*
- Rose, W. R. and Bruce, W. A. (1949). "Evaluation of Capillary Character in Petroleum Reservoir Rock." *Trans. AIME* **186**: 127-42.
- Salathiel, R. A. (1973). "Oil Recovery by Surface Film Drainage in Mixed-Wettability Rocks." *JPT; Trans. AIME* **255**.
- Salter, S. J., Mohanty, K.K. (1982). "Multiphase Flow in Porous Media: I. Macroscopic Observations and Modeling." *SPE* 11017
- Sanyal, S. K. (1972). "The Effect of Temperature on Electrical Resistivity of Porous Media." *Trans., 13th SPWLA Annual Logging Symposium*, Tulsa, (May 7-10), Paper U.
- Scholle, P. A. and D. S. Ulmer Scholle (1978). "A Color Guide to the Petrography of Carbonate Rocks: Grains, Texture, Porosity, and Diagenesis ", *AAPG (Memoir 77)*: Published by AAPG.
- Schumaker, L. L. (1981). *Spline Functions: Basic Theory*. Wiley & Sons, New York
- SENDRA Simulator Version 1.10, User Guide, Developed by International Research Institute of Stavanger (IRIS), Norway, 2008.
- Sharma, M. M. and Wunderlich, R.W. (1985). "The Alteration of Rock Properties Due to Interactions With Drilling Fluid Components." *SPE* 14302.

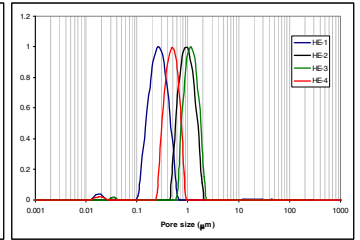
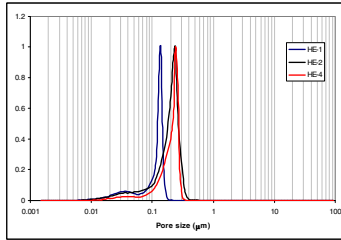
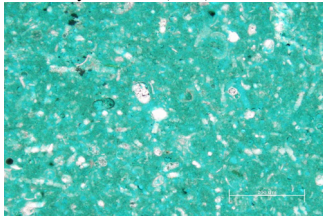
- Sigmund, P. M. and McCaffery, F.G. (1979). "An Improved Unsteady-State Procedure for Determining the Relative-Permeability Characteristics of Heterogeneous Porous Media." *SPE Journal* **19**(1): 15-28.
- Skauge, A., and Ottesen, B. (2002). "A Summary of Experimentally Derived Relative Permeability and Residual Saturation on North Sea Reservoir Cores" *SCA 2002-12, International Symposium of the Society of Core Analysts*
- Skauge, A., Spildo, K., Høiland, L., Vik, B., and Ottesen, B. (2004). "Experimental Evidence of Different Intermediate Wetting States." *SCA 04, International Symposium of Special Core Analysis held Abu Dhabi, UAE, 5-9 October.*
- Skauge, A., Vik, B., Pourmohammadi, S., and Spildo, K. (2006a). "Dispersion Measurements Used in Special Core Analysis of Carbonates" *SCA 2006-14, Society of Core Analysts, Trondheim, Norway 12-16 September*
- Skauge, A., Sørvik, A., Vik, B., and Spildo, K. (2006b). "Effect of Wettability on Oil Recovery from Carbonate Material Representing Different Pore Classes" *SCA 2006-01, International Symposium of the Society of Core Analysts, Trondheim, Norway 12-16 September*
- Skibitzke, H. E. and G. M. Robinson (1963). "Dispersion in ground water flowing through heterogeneous material." *U.S. Geological Survey Professional*, Paper 386.
- Skjæveland, S. M., Siqveland, L.M., Kjosavik, A., Hammervold, Thomas, W.L. and Virnovsky, G.A. (2000). "Capillary Pressure Correlation for Mixed-Wet Reservoirs." *SPE Reservoir Eval. & Eng* **3**(1).
- Slobod, R. L., Chambers, A., and Prehn, W. L. (1951). "Use of Centrifuge for Determining Connate Water, Residual Oil, and Capillary Pressure Curves of Small Core Samples." *Trans. AIME* **192**: 127-34
- Song, C., Miao, P., and Watson, A. T. (1992). "Characterization of Pore Structures Using NMR-Restricted Diffusion Measurements." *Spe*24812.
- Sorland, G. H., D. K., Lien, J. R., and Skauge, A. (2006). Absolute Pore Size Distributions from NMR. Proceedings at the International Symposium of the Society of Core Analysts (reviewed) 12-16 September, Trondheim, Norway.
- Spence, A. P., Watkins, R. W. (1980). "The Effect of Microscopic Core Heterogeneity on Miscible Flood Residual Oil Saturation" Paper *SPE* 9229-MS.
- Stalk up, F. I. (1970). "Displacement of oil by Solvent at High Water Saturation" *SPEJ* **10**(4): 337-48
- Standing, M. B. (1974). "Notes on Relative Permeability Relationships." Unpublished report, Division of Petroleum Engineering and Applied Geophysics, NTNU.
- Stegemeier, G. L. (1974). "Relationship of Trapped Oil Saturation to Petrophysical Properties of Porous Media." *SPE* 4745.

- Straley, C., Morriss, C. E., Kenyon, W. E., and Howard, J. J. (1991). NMR in partially saturated rocks: Laboratory insights on free fluid index and comparison with borehole logs. *SPWLA 32nd Annual Logging Symposium*.
- Sweeny, S. A., and Jennings, H.Y. (1960). "Effect of Wettability on the Electrical Resistivity of Carbonate Rock from a Petroleum Reservoir." *J. phys. Chem.*, **64**:551-553
- Taber, J. J. (1981). "Research on Enhanced Oil Recovery: Past, Present, and Future." Ed. D.O. Shah, Plenum Press, New York **13**.
- Taylor, G. (1953). "The Dispersion of Matter in Turbulent Flow through a pipe." *Proceedings of the Royal Society of London. Series A: Mathematical and Physical Sciences* **223**: 196-212.
- Terwilliger, E. L., Wisley, L. E., Hall, H. N., Bridges, E. M. and Morse, R. A. (1951). "An Experimental and Theoretical Investigation of Gravity Drainage Performance." *Trans. AIME* **1951**: 285-96
- Tie H. and Morrow, N.R. (2005). "Low-Flood-Rate Residual Saturations in Carbonate Rocks." *International Petroleum Technology Conference (IPTC)*, 21-23 November 2005, Doha, Qatar.
- Timur, A., Hemphkins, W. B., and Worthinton, A. E. (1972). "Porosity and Pressure Dependence of Formation Resistivity Factor for Sandstones." *Formation Evaluation Symposium, Canadian Well Logging Soc.*, Calgary, May 9-10.
- Torsæter, O. (1984), Experimental study of water imbibition in chalk from the Ekofisk Field. PhD dissertation
- Torsæter, O., and Abtahi, M. (2000). Experimental Reservoir Engineering: Laboratory Work Book. *Trondheim, Department of Petroleum Engineering and Applied Geophysics, NTNU*.
- Trantham, J. C., and Clampitt, R. L. (1977). "Determination of Oil Saturation After Water flooding in an Oil-Wet Reservoir The North Burbank Unit, Tract 97 Project." *JPT* **29** (5): 491-500.
- Treiber, L. E., and Owens, W. W. (1972). "A Laboratory Evaluation of the Wettability of Fifty Oil-Producing Reservoirs." *SPEJ* **12**(6): 531-40.
- UTCHEM-9.82.A three Dimensional Chemical Flood Simulator Developed by the University of Texas at Austin, July 2000
- Wardlaw, N. C. (1976). "Pore geometry of carbonate rocks as revealed by pore casts and capillary pressure" *AAPG* **60**: 245-47.
- Wardlaw, N. C., and Cassan, J.P. (1978). "Estimation of Recovery Efficiency by Visual Observation of Pore Systems in Reservoir Rocks" *J. Can. Petroleum Technology* **26**(4): 572-85.
- Waxman, M. H., and Smits, L. J. H. (1968). "Electrical Conductivities in Oil-Bearing Shale Sands." *Soc. of Petrol. Eng. J., Trans. AIME* **243**: 107-22.
- Waxman, M. H., and Thomas, E. C. (1974). "Electrical Conductivities in Shaly Sands-I. The Relation between Hydrocarbon Saturation and Resistivity Index; II, the Temperature Coefficient of Electrical I Conductivity." *JPT, Trans., AIME* **257**:213-225.
- Webb, K. J., Black, C.J.J., and Tjetland, G. (2005). "A Laboratory Study Investigating Methods for Improving Oil Recovery in Carbonates" *IPTC 10506*, held in Doha, Qatar, 21-23 Nov.

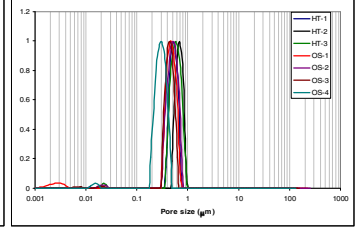
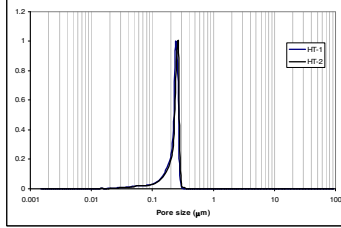
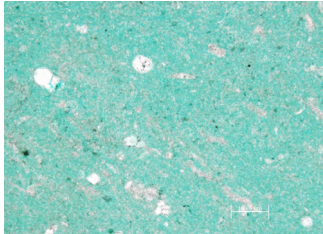
- Welge, H. J. (1952). "A Simplified Method for Computing Oil Recovery by Gas or Water Drive." *Trans. AIME* **195**: 91-98.
- Winsauer, W. O., Shearin H. M., Jr., Masson, P. H. and Williams, M. (1952). "Resistivity of Brine Saturated Sands in Relation to Pore Geometry." *AAPG Bulletin* **36**:253-277.
- Wyble, D. O. (1958). "Effect of Applied Pressure on the Conductivity, Porosity, and Permeability of Sandstones." *Trans. AIME* **213**:430-32.
- Wyllie, M. R. J., and Rose, W. D. (1950). "Some Theoretical Considerations Related to Quantitative Evaluation of Physical Characteristics of Reservoir Rock from Electrical Log Data." *Trans. AIME* **189**:105-18
- Wyllie, M. R. J., and Gardner, G. H. F (1958). "The Generalized Kozeny -Carman Equation." *World Oil*.

APPENDIX

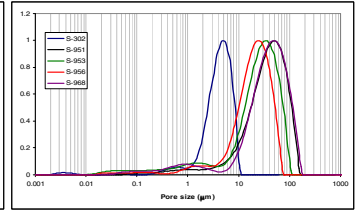
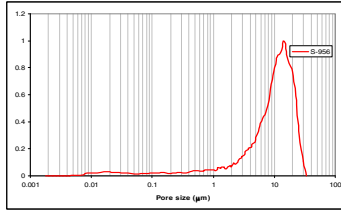
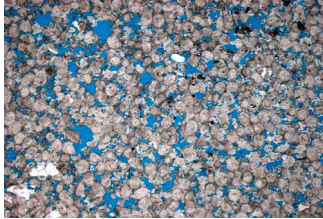
Tertiary Chalk (TC)



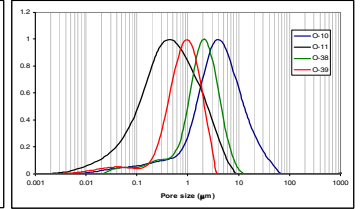
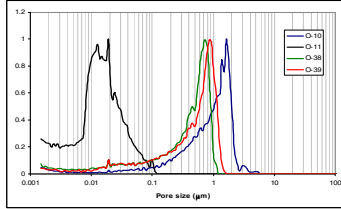
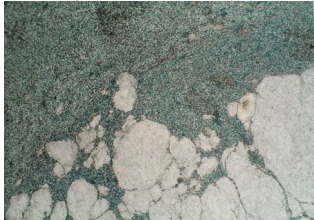
Cretaceous Chalk (CC)



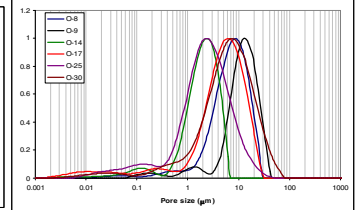
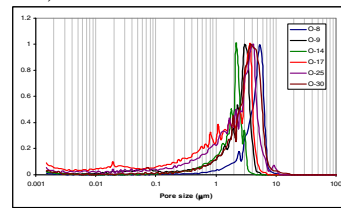
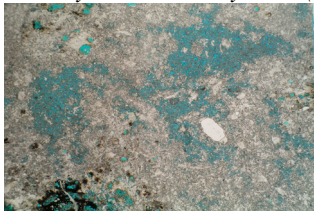
Interparticle Uniform Macro (IP-UMa)



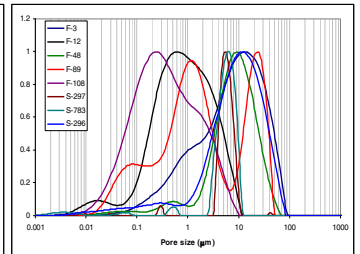
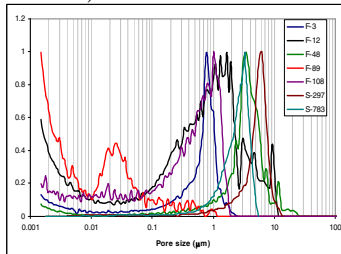
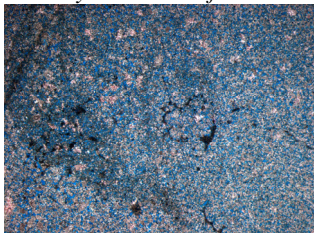
Intercrystalline Patchy Micro (IC-PMi)



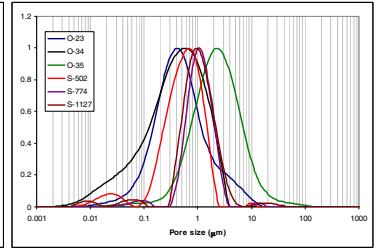
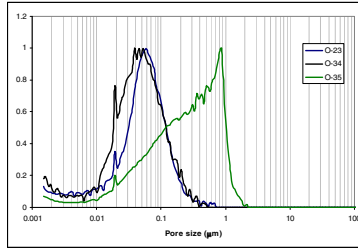
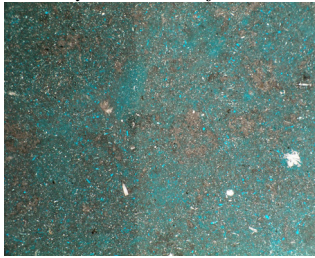
Intercrystalline Patchy Meso (IC-PMe)



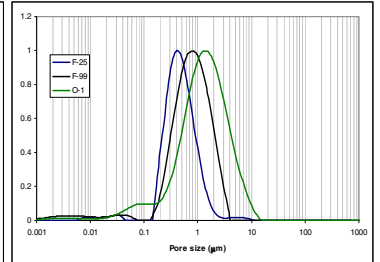
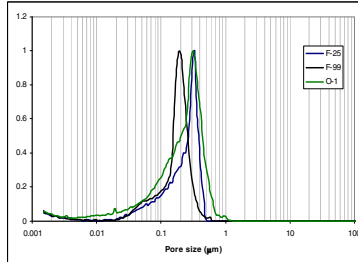
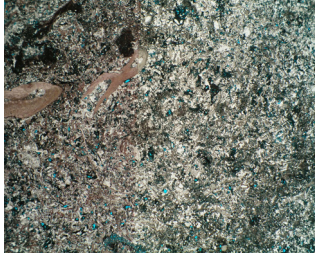
Intercrystalline Uniform Macro (IC-UMa)



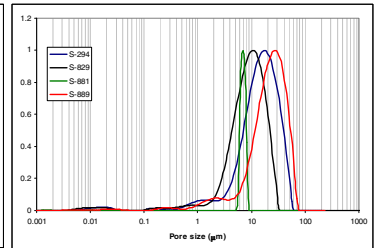
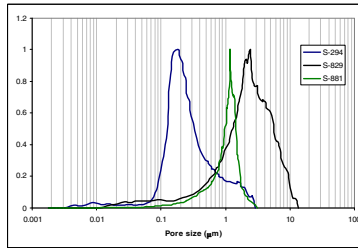
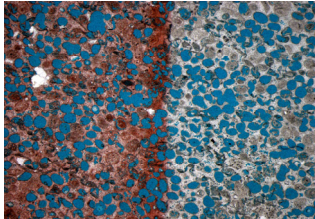
Intercrystalline Uniform Micro (IC-UMi)



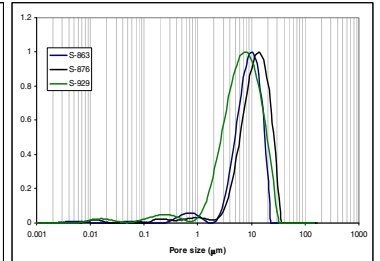
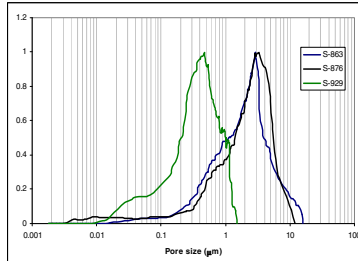
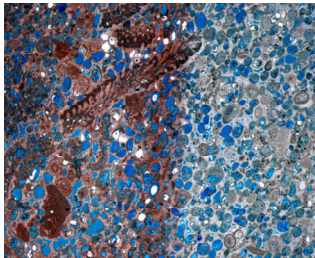
Moldic-Micro (M-Mi)



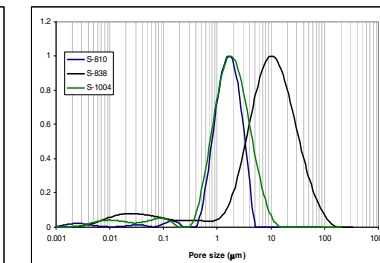
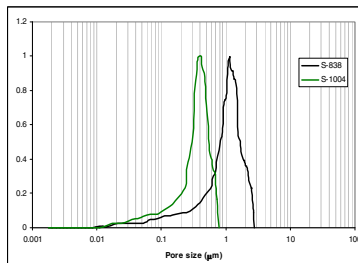
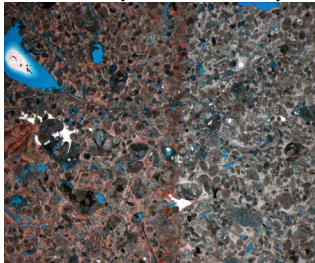
Moldic-Macro (M-Ma)



Interparticle Uniform Macro and Moldic-Macro



Interparticle Patchy Meso and Intercrystalline Patchy Meso



PAPERS

